Chapter 21

The Boundary Element Method for Damage Modeling

Chapter details

Chapter DOI:

https://doi.org/10.4322/978-65-86503-83-8.c21

Chapter suggested citation / reference style:

Peixoto, Rodrigo G., Chaves, Alisson P. (2022). "The Boundary Element Method for Damage Modeling". *In* Jorge, Ariosto B., et al. (Eds.) *Fundamental Concepts and Models for the Direct Problem*, Vol. II, UnB, Brasilia, DF, Brazil, pp. 809–880. Book series in Discrete Models, Inverse Methods, & Uncertainty Modeling in Structural Integrity.

P.S.: DOI may be included at the end of citation, for completeness.

Book details

Book: Fundamental Concepts and Models for the Direct Problem

Edited by: Jorge, Ariosto B., Anflor, Carla T. M., Gomes, Guilherme F., & Carneiro, Sergio H. S.

Volume II of Book Series in:

Discrete Models, Inverse Methods, & Uncertainty Modeling in Structural Integrity

Published by: UnB City: Brasilia, DF, Brazil Year: 2022

DOI: https://doi.org/10.4322/978-65-86503-83-8

The Boundary Element Method for Damage Modeling

Rodrigo G. Peixoto[1*] and Alisson P. Chaves[2]

[1]Department of Structural Engineering, Federal University of Minas Gerais, Brazil. E-mail: rgpeixoto@ufmg.br
[2]Department of Computation and Civil Construction, Federal Center of Technological Education of Minas Gerais, Timóteo-MG, Brazil. E-mail: alisson.chaves@cefetmg.br

*Corresponding author

Abstract

Materials physically non linear behaviour that arises when energy dissipation mechanisms occur, can be described by elastoplastic or elastic-degrading constitutive models. Such approaches can be summarized in a unified theoretical framework. The appearance of discontinuities in the strain field during inelastic loading with softening, and its transition until the emergence of jumps in the displacement fields can be analyzed with the Continuum Strong Discontinuity Approach (CSDA). These techniques, associated to the Implicit form of the Boundary Element Method (BEM) are discussed in this chapter, from the basic formulation concepts, to the numerical features and algorithms. The efficiency and versatility of the methodology can be observed through numerical simulation of typical plane state and three-dimensional analyzes.

Keywords: Boundary Element Method; damage modeling; strong discontinuity approach

1 Introduction

Analyses with the Boundary Element Method (BEM) are general and efficient when it makes use of algorithms capable to deal with independent constitutive modeling frameworks, which can be easily modified or expanded to encompass different material representations and particular behaviours, and also, to be evaluated with appropriated solution strategy.

The first developments of boundary integral equations for the treatment of elastoplastic materials may be attributed to Swedlow and Cruse [1971], Mendelson [1973] and Riccardella [1973]. Considering the incompressibility of the plastic strain tensor, Mukherjee [1977] verified some errors in the kernels involving inelastic fields for plane strain case and, later, Bui [1978] presented a corrected way to evaluate derivatives of the singular integrals involving such inelastic fields, introducing new free terms. Those results were then applied to the BEM by Telles and Brebbia [1979]. They used an explicit formulation, where the increment of the initial fields (plastic strains or its corresponding fictitious plastic stresses) explicitly appears in the non linear discretized equations and the equilibrium is achieved by a recursive procedure. Considering the proportional relationship

between stresses and elastic strains, Telles and Carrer [1991] proposed an implicit formulation, where the initial field increments are written in terms of total strains (actually, in the original work they used the fictitious elastic stresses related to total strains by the linear elastic Hooke's constitutive tensor), resulting in an accumulated equilibrium matrix equation, which is incrementally solved.

Some material behaviours, e.g., the quasi-brittle ones, requires the introduction of strain softening laws for a correct representation. A direct way to do this is to consider a plasticity model with yield limit degradation, as done by Lin et al. [2002] and Sládek et al. [2003]. The presence of strain softening results in a loss of objectiveness with respect to mesh refinements, as the solution tends to an infinitely small localization bandwidth with zero energy dissipation during failure. For that reason, in both works, a non-local procedure, based on the spatial averaging of the plastic multiplier, was also introduced. Another non-local plasticity model, based on a re-definition of the yield surface, including a dependency on the Laplacian of the plastic multiplier, was applied to the implicit formulation of the BEM by Benallal et al. [2002]. In that work, a complementary integral representation of the plastic multiplier was discretized and solved together (in a coupled way) to the incremental implicit equation.

Other constitutive models, such as continuum damage mechanics (CDM) based ones, have also been used with the BEM. CDM has been established to close the gap between classical continuum and fracture mechanics. In the BEM context, some works can be cited, such as Rajgelj et al. [1992], Herding and Kuhn [1996], García et al. [1999] and Botta et al. [2005]. Specifically, in the last work, the damage model presented by Comi and Perego [2001] was employed. As expected, they also reported mesh dependence when this model is locally applied and an averaging procedure of some strain invariants was introduced, regularizing the model.

Summarizing a large number of works devoted to damage modeling of material media, Carol et al. [1994] proposed a theoretical unification of elastic-degrading models based on a single loading function. In that reference, the authors developed a unified framework including a large range of damage models in analogy to the concepts and notations of classical plasticity. With this formalism, the two parameters required by the solution strategy mentioned above can be organized and numerically implemented in a completely independent way.

In the work of Simo et al. [1993], a new idea was introduced, based on the application of standard continuum constitutive models to unbounded strain fields, related to discontinuous displacements over a given surface (strong discontinuity surface). This methodology was latter called as continuum strong discontinuity approach (CSDA). Basically, a set of kinematic equations (in a regularized formulation) is used to describe displacements and strains at a discontinuity surface. Thus, applying this regularized kinematic on ordinary continuous constitutive models, the consistent discrete model obtained can relate traction with displacement jumps where the discontinuity is established.

The use of CSDA in the context of the BEM was firstly proposed in Manzoli and Venturini [2004] and Manzoli and Venturini [2007], who used the implicit BEM formulation for non linear analysis, and introduced discontinuity interfaces inside cells that dicretized the whole domain. This idea was extended in Manzoli et al. [2009] using an isotropic damage model and a tracking algorithm to generate cells automatically, in the direction of the crack path determined during the analyses. A further improvement was presented by Peixoto et al. [2017] and Peixoto et al. [2018], who sophisticated the non linear analysis, involving inelastic dissipation with softening in continuous media, bifurcation analysis and transition between weak and strong discontinuities.

The material failure process can also be modeled by a geometrical point of view using the fracture mechanics concepts, in which the singular character of the stress state at a crack tip is substituted by stress intensity factors, obtained from energetic considerations. This idea was notably well adapted for the BEM, in its dual formulation used by Portela et al. [1992], where distinct

integral equations are applied in each side of a discontinuous surface.

The Einstein's index notation is adopted for tensors algebra throughout the chapter. This chapter is divided in eleven sections. In the next section some fundamental equations for physically linear and non linear solid mechanics are reviewed. In Section 3, the integral equations considering initial strain fields, appropriate to deal with standard physically non linear problems, are presented. Following, in Section 4 presents a numerical counterpart of such equations, and a solution strategy with the required rearrangement for the implicit BEM formulation, and the control methods for non linear analyses. Some numerical examples of continuum non linear analysis of simple problems are presented in Section 5. Strain localization and material bifurcation analysis are discussed in Section 6, while in Section 7 the CSDA is presented, including the weak and strong discontinuity kinematics, the strong discontinuity analysis and variable bandwidth model. In Section 8 the boundary integral equations are reformulated for the consideration of discontinuous surface effects. Numerical features of the BEM formulation, regarding cell with embedded discontinuity and displacement jump evaluation are described in Section 9. Some the numerical examples of non linear problems with discontinuities are treated in Section 10, and Section 11 have some final remarks. Additionally, in Appendix A, elastoplastic and isotropic damage models are presented.

2 Basic Equations for Physically Non Linear Solid Mechanics

2.1 Linear Elasticity

Before presenting the physically non linear constitutive models, in which some energy dissipation phenomena take place, basic equations associated to conservative (elastic) deformation are firstly presented. Only small displacements are considered, such that a strain tensor can be defined from the gradient of the displacement field, configuring which is called as linear elasticity.

2.1.1 Cauchy stress tensor

Figure 1 represents a solid body Ω, delimited by a surface Γ.

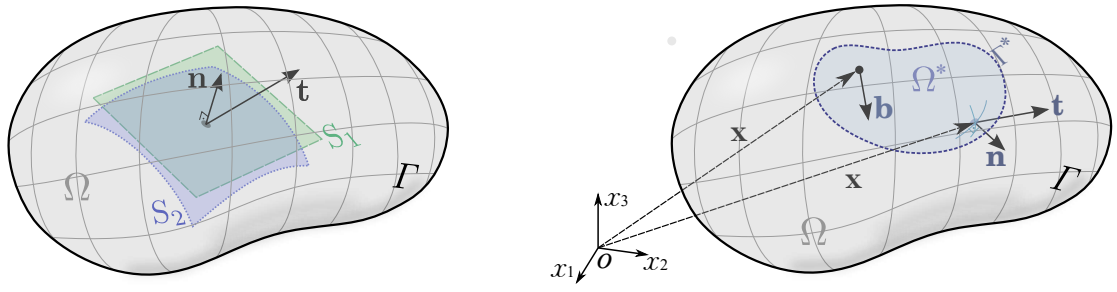

(a) (b)

Figure 1: A solid body Ω with boundary Γ – (a) Traction vector, (b) Arbitrary subdomain Ω^*

If the body is loaded, at any point of a given internal surface, say S_1 or S_2 (figure 1-a), a traction vector, $\mathbf{t}$ (units of force per area), can be defined as a function of the the unit normal vector, $\mathbf{n}$, to the surface at this point. The second order tensor that relate these vectors is called as Cauchy Stress Tensor, i.e.,

$$t_i = \sigma_{ij} n_j \tag{1}$$

Considering an arbitrary closed sub-domain, Ω^*, inside the body, as illustrated in Figure 1-b, and calling as $\mathbf{b}(\mathbf{x})$ the external forces (per volume unit) that act along the solid domain, the equilibrium condition can be expressed by

$$\oint_{\Gamma^*} t_i d\Gamma + \int_{\Omega^*} b_i d\Omega = \oint_{\Gamma^*} (\sigma_{ij} n_j) d\Gamma + \int_{\Omega^*} b_i d\Omega = \int_{\Omega^*} (\sigma_{ij,j} + b_i) d\Omega = 0$$

in which the surface integral was transformed to a volumetric one by applying the Divergence Theorem. Thus, from the arbitrariness of Ω^*, it is possible to conclude that, for any material point $\mathbf{x}$, the following equilibrium equation can be written

$$\sigma_{ij,j} + b_i = 0 \tag{2}$$

The Cauchy Stress Tensor is symmetric, i.e., $\sigma_{ij} = \sigma_{ji}$, which means that only six components are sufficient to describe the stress state at a given point. This property can be demonstrated by taking the angular momentum resultant of an arbitrary sub-domain, Ω^*, as developed below, making reference again to Figure 1-b.

$$\begin{aligned}
\oint_{\Gamma} (\mathbf{x} \times \mathbf{t}) d\Gamma + \int_{\Omega} (\mathbf{x} \times \mathbf{b}) d\Omega &= \oint_{\Gamma} (\varepsilon_{ijk} x_j \sigma_{kl} n_l) d\Gamma + \int_{\Omega} (\varepsilon_{ijk} x_j b_k) d\Omega = 0 \\
&= \int_{\Omega} (\varepsilon_{ijk} x_j \sigma_{kl})_{,l} \, d\Omega + \int_{\Omega} (\varepsilon_{ijk} x_j b_k) d\Omega = 0 \\
&= \int_{\Omega} (\varepsilon_{ijk} \underbrace{x_{j,l}}_{\delta_{jl}} \sigma_{kl}) d\Omega + \int_{\Omega} \big[\varepsilon_{ijk} x_j \underbrace{(\sigma_{kl,l} + b_k)}_{=0} \big] d\Omega = 0 \\
&= \int_{\Omega} (\varepsilon_{ijk} \sigma_{kj}) d\Omega = 0 \;\; \Rightarrow \varepsilon_{ijk} \sigma_{kj} = 0 \;\; \Rightarrow \sigma_{jk} = \sigma_{kj}
\end{aligned}$$

where δ_{ij} is the Kronecker delta and ε_{ijk} is the permutation operator, respectively defined by

$$\delta_{ij} = \begin{cases} 0 & \text{if} \quad i \neq j \\ 1 & \text{if} \quad i = j \end{cases} \tag{3}$$

and

$$\varepsilon_{ijk} = \begin{cases} 0 & \text{if there is repetition of, at least, two indexes} \\ -1 & \text{if} \quad (i,j,k) = (3,2,1) \text{ or } (1,3,2) \text{ or } (2,1,3) \\ +1 & \text{if} \quad (i,j,k) = (1,2,3) \text{ or } (3,1,2) \text{ or } (2,3,1) \end{cases} \tag{4}$$

Independently of the stress state in a given point, it is always possible to choose a coordinates system in which the stress tensor becomes diagonal, i.e., $\sigma_{ij} = 0$ if $i \neq j$. The directions of each axis of this system are called as principal directions and the normal stresses, action on perpendicular planes to these axis, are called as principal stresses. Evaluating such principal stress components is a typical eigenvalue problem, since the traction vector parallel a principal direction can be written as

$$t_i = \sigma_{ij} n_j = \lambda \delta_{ij} n_j \quad \Rightarrow \quad (\sigma_{ij} - \lambda \delta_{ij}) n_j = 0$$

where λ represents a scalar constant. For non-trivial solutions of this last equation,

$$\det(\sigma_{ij} - \lambda \delta_{ij}) = 0 \quad \Rightarrow \quad \lambda^3 - I_1 \lambda^2 - I_2 \lambda - I_3 = 0 \tag{5}$$

in which I_k are the stress tensor invariants, given by

$$I_1 = \sigma_{ii}, \quad I_2 = \frac{1}{2}(\sigma_{ij}\sigma_{ij} - I_1^2), \quad I_3 = \frac{1}{6}\varepsilon_{ijk}\varepsilon_{pqr}\sigma_{ip}\sigma_{jq}\sigma_{kr} \tag{6}$$

Equation (5) is the characteristic polynomial and its roots are the principal stress components.

2.1.2 Linear strain tensor

A displacement field, $\mathbf{u}(\mathbf{x})$, in a loaded solid body is represented in Figure 2.

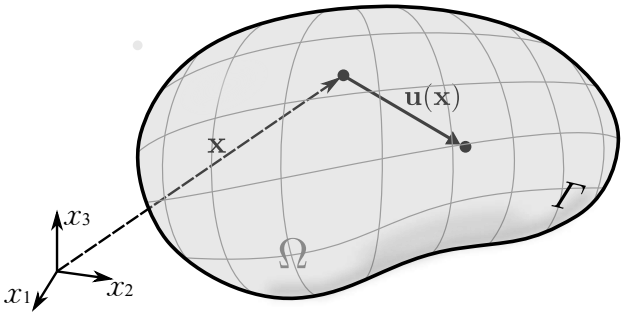

$x_i \rightarrow$ position of a given point in the initial (undeformed) configuration

$x_i + u_i \rightarrow$ position of the same point in a deformed configuration

$u_i \rightarrow$ displacement components, $u_i \equiv u_i(\mathbf{x})$

Figure 2: Displacements in a solid body

If the displacement field is such that its first order derivatives are sufficiently small, in order that the product of partial derivatives of $\mathbf{u}(\mathbf{x})$ become negligible, the strain field in the solid body can be described by linear strains, i.e., by the symmetric part of the displacement gradient tensor:

$$\epsilon_{ij} = \frac{1}{2}(u_{i,j} + u_{j,i}) \tag{7}$$

Although the displacements uniquely define the components of the strain tensor, the inverse problem, i.e., obtaining the displacements from a strain field, is not so straightforward. Since equation (7) is equivalent to six differential equations, the three components of u_i are not uniquely defined, unless additional conditions are imposed on the deformation components. Such conditions are defined by compatibility equations, which can be generically written in the form:

$$\epsilon_{ij,kl} + \epsilon_{kl,ij} - \epsilon_{ik,jl} - \epsilon_{jl,ik} = 0 \tag{8}$$

2.1.3 Hooke's Law

The strain field caused by a distributed stress state in a solid body depends on the material properties. In a conservative regime, the relation between strain and stress is known as Hooke's Law or linear elastic constitutive equation. Mathematically,

$$\sigma_{ij} = C_{ijkl}\epsilon_{kl} \tag{9}$$

where the fourth order tensor C_{ijkl} is the so-called constitutive tensor.

Considering an isotropic and homogeneous material, the expression of the constitutive tensor is

$$C_{ijkl} = \bar{\lambda}\delta_{ij}\delta_{kl} + \mu(\delta_{ik}\delta_{jl} + \delta_{il}\delta_{jk}) \tag{10}$$

where

$$\mu = \frac{E}{2(1+\nu)}, \qquad \bar{\lambda} = \frac{2\mu\bar{\nu}}{1-2\bar{\nu}}, \qquad \bar{\nu} = \begin{cases} \nu & \text{(3D or Plane Strain)} \\ \dfrac{\nu}{1+\nu} & \text{(Plane Stress)} \end{cases} \tag{11}$$

in which E represents the material Young's modulus and ν is the Poisson ratio.

An inverse of equation (9) can be written as

$$\epsilon_{ij} = C^{-1}_{ijkl}\sigma_{kl} \tag{12}$$

where

$$C^{-1}_{ijkl} = \frac{1}{2\mu}\left[\frac{1}{2}(\delta_{ik}\delta_{jl} + \delta_{il}\delta_{jk}) - \tilde{\nu}\delta_{ij}\delta_{kl}\right] \tag{13}$$

and

$$\tilde{\nu} = \begin{cases} \nu & \text{(Plane Strain)} \\ \dfrac{\nu}{1+\nu} & \text{(3D or Plane Stress)} \end{cases} \tag{14}$$

2.1.4 Navier Equation

Navier Equation represents the equilibrium condition rewritten in terms of the displacement field. It is obtained from the application of equation (7) into (9), followed by introducing the this result into equation (2), i.e.,

$$\sigma_{ij,j} + b_i = \frac{1}{2}C_{ijkl}(u_{k,lj} + u_{l,kj}) + b_i = 0$$

Then, applying equation (10) and considering the definition of the Kronecker delta (equation 3), the next result is achieved:

$$\frac{1}{2}\left[\bar{\lambda}(u_{k,ki} + u_{k,ki}) + \mu(u_{i,jj} + u_{j,ij}) + \mu(u_{j,ij} + u_{i,jj})\right] + b_i = 0$$

Finally, reorganizing,

$$\mu u_{i,jj} + (\bar{\lambda} + \mu)u_{j,ji} + b_i = 0 \tag{15}$$

which is the Navier Equation.

2.2 Kelvin Fundamental Solution

Lets consider now an infinite homogeneous and isotropic solid domain, loaded by punctual unit forces, namely $P_i = 1$, acting on a given point, $\boldsymbol{\xi}$, and directed at each cartesian direction, as illustrated in Figure 3. This problem is called as Kelvin fundamental problem of elasticity.

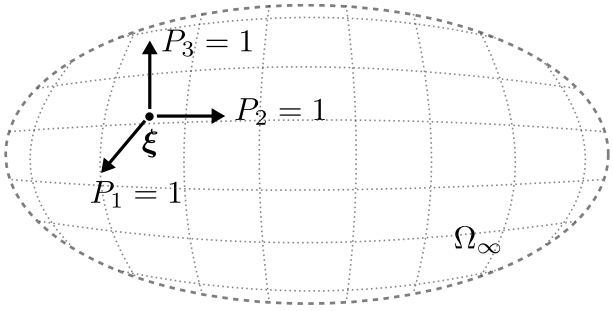

Figure 3: Infinite solid domain with punctual concentrated unit forces

To give a distributional character to concentrated loads, the Dirac delta function, $\delta(\mathbf{x}_0, \mathbf{x})$, might be used. Such function presents the following property:

$$\int_\Omega f(\mathbf{x})\delta(\mathbf{x}_0, \mathbf{x})d\Omega = f(\mathbf{x}_0) \tag{16}$$

Thus, in the case of the Kelvin fundamental problem, the body forces, previously defined, can be written as

$$b_i(\mathbf{x}) = \delta(\boldsymbol{\xi}, \mathbf{x})P_i \tag{17}$$

Substituting equation (17) into (15), and calling as $\mathbf{u}^*(\mathbf{x})$ the displacement field resulting from the Kelvin fundamental problem, one obtains

$$\mu u^*_{j,kk}(\mathbf{x}) + (\bar{\lambda}+\mu)u^*_{k,kj}(\mathbf{x}) + \delta(\boldsymbol{\xi},\mathbf{x})P_j = 0 \tag{18}$$

Among the different existing solution techniques for this problem, probably the most popular is the Galerkin vector formulation. This vector, G_i, is defined by the next expression:

$$u^*_j = G_{j,ii} - \left(\frac{\bar{\lambda}+\mu}{\bar{\lambda}+2\mu}\right)G_{i,ji} \tag{19}$$

Applying equation (19) to (18),

$$\mu G_{j,iikk} - \underbrace{\left[\mu\left(\frac{\bar{\lambda}+\mu}{\bar{\lambda}+2\mu}\right) - (\bar{\lambda}+\mu) + (\bar{\lambda}+\mu)\left(\frac{\bar{\lambda}+\mu}{\bar{\lambda}+2\mu}\right)\right]}_{=0} G_{i,jikk} + \delta(\boldsymbol{\xi},\mathbf{x})P_j = 0$$

Thus,

$$\mu G_{j,iikk} + \delta(\boldsymbol{\xi},\mathbf{x})P_j = 0 \tag{20}$$

Equations (20) can be transformed into a set of typical equations for scalar potential problems, by defining a vector F_i as the Laplacian of the Galerkin vector, i.e.,

$$F_j = G_{j,ii} \tag{21}$$

Substituting equation (21) into (20) gives

$$F_{j,kk} + \frac{1}{\mu}\delta(\boldsymbol{\xi},\mathbf{x})P_j = 0 \tag{22}$$

Consider now a sub-domain Ω', delimited by Γ', that encloses the source point of load application, $\boldsymbol{\xi}$, whereas $\boldsymbol{\xi} \notin \Gamma'$, as shown in Figure 4.

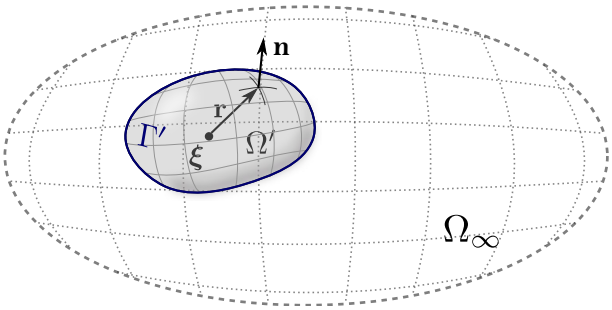

Figure 4: Sub-domain Ω' enclosing the source point in the Kelvin fundamental problem

Integrating equation (22) in this sob-domain,

$$\int_{\Omega'} F_{j,kk}d\Omega = -\frac{P_j}{\mu}\int_{\Omega'}\delta(\boldsymbol{\xi},\mathbf{x})d\Omega = -\frac{P_j}{\mu} \quad \Rightarrow \quad \oint_{\Gamma'} F_{j,k}n_k d\Gamma = -\frac{P_j}{\mu} \tag{23}$$

where equation (16) was applied and the integral at the left-hand side was transformed from Ω' to Γ' using the Divergence Theorem. In equation (23), n_k refer to the components of the unit normal vector on Γ', pointing outside to Ω'.

Note that equations (18) to (23) are valid for three dimensional and plane state problems, considering the appropriate definition of $\bar{\lambda}$ from equation (11) and that indexes vary only from 1 to 2. For convenience, in the next two subsections, each case is separately treated.

2.2.1 Three dimensional domains

For three dimensional domains, it is convenient to particularize Ω' by a sphere centred on the source point. Thus, defining an spherical coordinate system, $\{\hat{\mathbf{e}}_r, \hat{\mathbf{e}}_\theta, \hat{\mathbf{e}}_\phi\}$, with its origin at $\boldsymbol{\xi}$, the gradient of F_i can be written as

$$F_{j,k} \equiv F_{j,r}\hat{\mathbf{e}}_r + \frac{1}{r}F_{j,\theta}\hat{\mathbf{e}}_\theta + \frac{1}{r(\sin\theta)}F_{j,\phi}\hat{\mathbf{e}}_\phi \tag{24}$$

Noting that $\hat{\mathbf{e}}_r \equiv \mathbf{n}$, in such a way that $\hat{\mathbf{e}}_\theta \cdot \mathbf{n} = \hat{\mathbf{e}}_\phi \cdot \mathbf{n} = 0$, it is straightforward to conclude that the last two parcels of equation (24) result in null values when applied to equation (23). Thus,

$$\oint_{\Gamma'} F_{j,k}n_k d\Gamma = \int_0^{2\pi}\int_0^{\pi} F_{j,r}r^2(\sin\theta)d\phi d\theta = -\frac{P_j}{\mu} \quad \Rightarrow \quad F_{j,r} = -\frac{P_j}{4\pi\mu r^2}$$

Integrating this last result,

$$F_j = \frac{P_j}{4\pi\mu r} \tag{25}$$

It should be noted now that the sphere Ω' has been defined with an arbitrary size. Therefore, the radius r in the equation (25) can be interpreted as the distance between the source point, $\boldsymbol{\xi}$, and any field point, $\mathbf{x}$. Thus, one might write

$$r \equiv r(\boldsymbol{\xi}, \mathbf{x}) \tag{26}$$

for which the following properties are valid:

$$r_i = x_i - \xi_i \tag{27a}$$

$$r = (r_i r_i)^{1/2} \tag{27b}$$

$$r_{,i} \equiv r_{,i}\,\big|_{\mathbf{x}} = \frac{\partial r}{\partial x_i} = \frac{\partial r}{\partial r_j}\frac{\partial r_j}{\partial x_i} = \frac{r_j}{r}\delta_{ij} = \frac{r_i}{r} \tag{27c}$$

$$r_{,ij} \equiv r_{,ij}\,\big|_{\mathbf{x}} = \left(\frac{r_i}{r}\right)_{,j} = \frac{r_{i,j}}{r} - \frac{r_i}{r^2}r_{,j} = \frac{\delta_{ij}}{r} - \frac{r_{,i}\,r_{,j}}{r} \tag{27d}$$

Applying now equation (25) to (21),

$$G_{j,ii} = \frac{P_j}{4\pi\mu r} \tag{28}$$

and considering the radial symmetry of the Kelvin fundamental problem around $\boldsymbol{\xi}$, i.e., $G_i \equiv G_i(r)$ for the spherical coordinate system, it is possible to write

$$G_{j,ii} = \left(\frac{\partial G_j}{\partial r}r_{,i}\right)_{,i} = r_{,ii}\,\frac{\partial G_j}{\partial r} + \frac{\partial^2 G_j}{\partial r^2}\underbrace{(r_{,i}\,r_{,i})}_{=1} = r_{,ii}\,\frac{\partial G_j}{\partial r} + \frac{\partial^2 G_j}{\partial r^2} \tag{29}$$

Thus, from equations (27d), (28) and (29), the following set of non-homogeneous second order ordinary differential equations for the Galerkin vector components are obtained:

$$\frac{\partial^2 G_j}{\partial r^2} + \frac{2}{r}\frac{\partial G_j}{\partial r} = \frac{P_j}{4\pi\mu r} \tag{30}$$

Particular solutions for these equations are

$$G_j = \frac{P_j}{8\pi\mu}r \tag{31}$$

Finally, replacing equation (31) into (19) and taking into account the equations (11) and (27d), a displacement field is obtained, which is the solution of the problem represented by equation (18), i.e.,

$$u_j^*(\boldsymbol{\xi}, \mathbf{x}) = \frac{1}{16\pi\mu(1-\nu)r}[(3-4\nu)\delta_{ij} + r_{,i}\, r_{,j}\,]P_i \tag{32}$$

Equation (32) is the Kelvin fundamental solution to three dimensional problems. It should be noted that this equation gives the displacement component in direction j, at a field point, $\mathbf{x}$, caused by a concentrated force, given by unit components in each direction (once summation is implicit by repetition of i index and $P_i = 1$; $i = 1, 2, 3$) and applied at the source point, $\boldsymbol{\xi}$. Taking each component of P_i separately, we can write:

$$u_{ij}^*(\boldsymbol{\xi}, \mathbf{x}) = \frac{1}{16\pi\mu(1-\nu)r}[(3-4\nu)\delta_{ij} + r_{,i}\, r_{,j}\,] \tag{33}$$

Thus, tensor $u_{ij}^*(\boldsymbol{\xi}, \mathbf{x})$ represents the displacement in the direction j, at a field point, $\mathbf{x}$, caused by a unit concentrated force at a source point, $\boldsymbol{\xi}$, applied in the direction i.

2.2.2 Plane state problems

A similar idea might be adopted for two dimensional elastic domains, noting that now the indexes vary between 1 and 2 and that Γ' is particularized by a circumference centred on $\boldsymbol{\xi}$. Considering also a polar system of coordinates with origin at the source point, it is possible to write the gradient of F_i as

$$F_{j,k} \equiv F_{j,r}\hat{\mathbf{e}}_r + \frac{1}{r}F_{j,\theta}\hat{\mathbf{e}}_\theta \tag{34}$$

Thus, applying equation (34) to (23),

$$\oint_{\Gamma'} F_{j,k}n_k d\Gamma = \int_0^{2\pi} F_{j,r} r d\theta = -\frac{P_j}{\mu} \quad \Rightarrow \quad F_{j,r} = -\frac{P_j}{2\pi\mu r}$$

which leads to

$$F_j = -\frac{P_j}{2\pi\mu}\ln(r) \tag{35}$$

As in the three dimensional case, $r \equiv r(\boldsymbol{\xi}, \mathbf{x})$ is the distance of any field point, $\mathbf{x}$, from $\boldsymbol{\xi}$, in order that equations (26) and (27) remain valid for plane problems.

From equations (21) and (35),

$$G_{j,ii} = -\frac{P_j}{2\pi\mu}\ln(r) \tag{36}$$

Considering again the radial symmetry of the fundamental problem, equation (29) is also valid for two dimensional domains and, together with equations (27d) and (36), the following set of equations is obtained:

$$\frac{\partial^2 G_j}{\partial r^2} + \frac{1}{r}\frac{\partial G_j}{\partial r} = -\frac{P_j}{2\pi\mu}\ln(r) \tag{37}$$

which have as particular solutions,

$$G_j = \frac{P_j}{8\pi\mu}r^2 - \frac{P_j}{8\pi\mu}r^2\ln(r) \tag{38}$$

Applying equation (38) to (19) – note that the first parcel of equation (38) leads to rigid body motion, i.e., vanishes in this process – and taking into account equations (11) and (27d), the fundamental displacements can be written as

$$u_j^*(\boldsymbol{\xi}, \mathbf{x}) = \frac{-1}{8\pi\mu(1-\bar{\nu})}[(3-4\bar{\nu})\ln(r)\delta_{ij} - r_{,i}\, r_{,j}\,]P_i \tag{39}$$

Taking again each component separately,

$$u^*_{ij}(\boldsymbol{\xi}, \mathbf{x}) = \frac{-1}{8\pi\mu(1-\bar{\nu})}[(3-4\bar{\nu})\ln(r)\delta_{ij} - r_{,i}\, r_{,j}\,] \tag{40}$$

The same physical interpretation of this second order tensor, given for the three dimensional case, remains valid here.

2.3 Non Linear Constitutive Modeling

Equations presented in section 2.1 are restricted to conservative behaviour of elastic bodies. If any energy dissipation mechanism takes place, such relations needs to be reviewed. For example, the constitutive relation depicted in equation (9) needs to be rewritten by its rate form (since, when energy is dissipated, stress-strain relation becomes dependent from the load history) and the strain field is commonly decomposed into two parts, one elastic and other associated to the dissipative mechanism.

In this section, two classical approaches to represent the physically non linear behaviour of materials under non conservative loading are described, namely elastoplastic (EP) and elastic-degrading (ED) constitutive models, are described. Despite its differences, such approaches can be presented in a unified theoretical framework as shown in Peixoto et al. [2016]. This idea is used here.

Figure 5 shows the difference between ED and EP constitutive models. In the first case, if the body is unloaded after some energy dissipation, the stress-strain relation follows a secant trajectory returning to the initial unstrained configuration. Elastoplastic materials, however, presents a loading-unloading curve which is a straight segment with the same initial elastic slope, keeping a residual strain even after the total unload. It is clear that both are simplifications of the actual behaviour observed in experiments as shown in Figure 5-c, where both stiffness degradation and irreversible plastic strain take place.

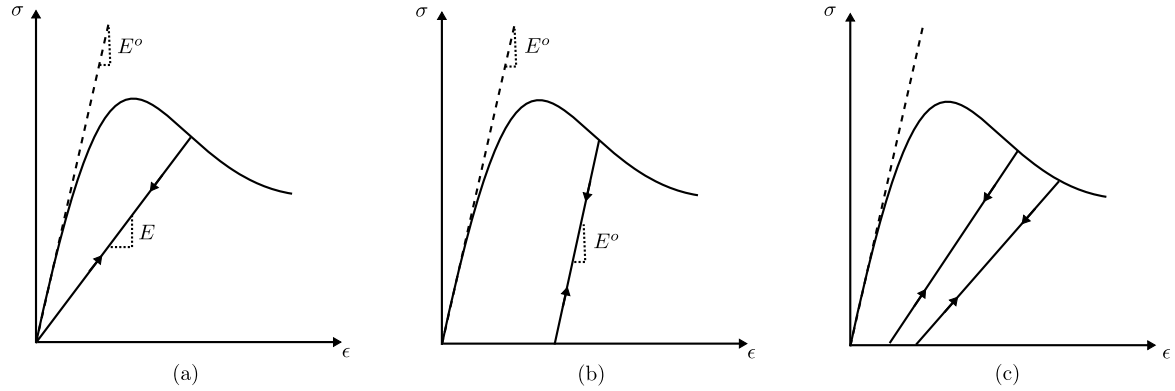

Figure 5: Non linear constitutive models: (a) Elastic-degrading material, (b) Elasto-plastic material, (c) Realistic behaviour

As will be seen in the next sections, the non linear solution algorithm only requires, during each iteration, the local evaluation of two parameters: the stresses, σ_{ij}, and the tangential stiffness operator, C^t_{ijkl}, relating incremental stresses and strains. How they are obtained is briefly described next. It is shown that the incremental governing equations have the same form in both constitutive models classes, regarding as the only difference the meaning of the inelastic strains and the presence of the secant stiffness tensor, C^s_{ijkl}, in ED equations, in place of the initial elastic stiffness tensor, C_{ijkl}, in EP equations.

2.3.1 Elastoplastic models

As a secant relationship is not defined a priori for EP models (see figure 5-b), a trial-return algorithm is required for numerical evaluation of the stress tensor as described, for example, in Simo and Hughes [1998].

Assuming a loading function that can be expressed as $F(\sigma_{ij}, \mathbf{q})$, where $\mathbf{q}$ is a vector of internal variables – which can be tensors of different orders – determining the current configuration of the elastic domain, the following rate equations can be defined:

$$\dot{\sigma}_{ij} = C_{ijkl}(\dot{\epsilon}_{kl} - \dot{\epsilon}^p_{kl}) \tag{41}$$

$$\dot{\epsilon}^p_{kl} = \dot{\lambda} m_{kl} \tag{42}$$

$$\dot{\mathbf{q}} = -\dot{\lambda}\mathbf{h} \tag{43}$$

$$\dot{F} = \left.\frac{\partial F}{\partial \sigma_{ij}}\right|_{\mathbf{q}} \dot{\sigma}_{ij} + \left.\frac{\partial F}{\partial \mathbf{q}}\right|_{\boldsymbol{\sigma}} : \dot{\mathbf{q}} = 0 \tag{44}$$

where equation (41) is the rate form of stress-strain relationship for elastoplastic materials, in which ϵ^p_{kl} is the plastic strain tensor, whose rate magnitude is defined by the plastic multiplier, $\dot{\lambda}$, and m_{kl} specifies its rate direction. The symbol (:) in the second term of equation (44) means tensors contraction and were used in function of the unspecified orders of internal variables in $\mathbf{q}$.

Equation (42) is called as plastic flow rule, while equation (43) is called as hardening-softening law and represents the evolution of the hardening-softening internal variables. Equation (44) is the linearised form of the consistency condition, meaning that during plastic loading the current stress state always remains on the current loading surface, commonly called as yield surface in elastoplastic theory.

Considering the set of internal variables, $\mathbf{q}$, as functions of the plastic strain, such as $\dot{\mathbf{q}} = (\partial \mathbf{q}/\partial \epsilon^p_{kl})\dot{\epsilon}^p_{kl}$, and using equation (42), one can rewrite equation (44) as

$$n_{ij}\dot{\sigma}_{ij} - H\dot{\lambda} = 0 \tag{45}$$

where,

$$\begin{cases} n_{ij} = \left.\dfrac{\partial F}{\partial \sigma_{ij}}\right|_{\lambda} \\ \\ H = -\left.\dfrac{\partial F}{\partial \lambda}\right|_{\boldsymbol{\sigma}} = -\left.\dfrac{\partial F}{\partial \mathbf{q}}\right|_{\boldsymbol{\sigma}} : \dfrac{\partial \mathbf{q}}{\partial \epsilon^p_{kl}} m_{kl} \end{cases} \tag{46}$$

The second-order tensor n_{ij}, involving derivatives of F for constant plastic strain ($\dot{\lambda} = \dot{\epsilon}^p_{kl} = 0$), has the geometrical meaning of the direction normal to the current loading surface, $F = 0$, in stress space, while the derivatives for constant stress, give the hardening-softening modulus H. For positive values of H (hardening), the loading surface expands in the stress space and, for negative values (softening), the loading surface contracts during plastic loading. If $H = 0$ (perfect plasticity), the loading surface is static. No kinematic effects, i.e., translation of loading surface, are considered here. The model is called associative if n_{ij} and m_{ij} are fully proportional. Loading/unloading conditions are determined by $\dot{\lambda} \geq 0$; $F \leq 0$; $\dot{\lambda}F = 0$ and $\dot{\lambda}\dot{F} = 0$.

Now, applying equations (41) and (42) to equation (45), the following expression for the plastic multiplier is obtained:

$$\dot{\lambda} = \frac{n_{ij} C_{ijkl} \dot{\epsilon}_{kl}}{H + n_{pq} C_{pqrs} m_{rs}} \tag{47}$$

Finally, the tangential stiffness operator is obtained by introducing equations (47) and (42) into equation (41), i.e.,

$$\dot{\sigma}_{ij} = C^t_{ijkl}\dot{\epsilon}_{kl}, \qquad C^t_{ijkl} = C_{ijkl} - \frac{C_{ijab}m_{ab}n_{cd}C_{cdkl}}{H + n_{pq}C_{pqrs}m_{rs}} \tag{48}$$

Equations (41) to 48 were defined in a stress-based formulation. Alternatively, a strain-based formulation can be developed beginning with a loading function defined in strain space, such as $\bar{F}(\epsilon_{ij}, \boldsymbol{\alpha})$, as detailed in Carol et al. [1994], and where $\boldsymbol{\alpha}$ represents the strain-like internal variables, thermodynamically conjugated to $\mathbf{q}$. Here, we are only interested in the result for the tangential stiffness operator, equivalent to equation (48), i.e.,

$$C^t_{ijkl} = C_{ijkl} + \frac{1}{\bar{H}}\bar{m}_{ij}\bar{n}_{kl} \tag{49}$$

where,

$$\begin{cases} \bar{m}_{ij} = -C_{ijkl}m_{kl} \\ \\ \bar{n}_{ij} = C_{ijkl}n_{kl} \\ \\ \bar{H} = H + n_{ij}C_{ijkl}m_{kl} \end{cases} \tag{50}$$

The equations presented in this subsection are particularized for the elastoplastic von Mises associative isotropic model in Appendix A.

2.3.2 Elastic-degrading models

In ED models, full unloading always leads to the original unstrained configuration, i.e., zero stresses with no permanent strains (see figure 5a), in opposition to classical EP models. For that reason, the next total stress-strain relationship can be formulated for ED models:

$$\sigma_{ij} = C^s_{ijkl}\epsilon_{kl} \tag{51}$$

where C^s_{ijkl} is the current secant stiffness tensor.

Taking the time derivative of equation (51), an expression for incremental stress can be obtained, i.e.,

$$\dot{\sigma}_{ij} = C^s_{ijkl}\dot{\epsilon}_{kl} + \dot{C}^s_{ijkl}\epsilon_{kl} \tag{52}$$

Each parcel of equation (52) is represented in the simplified uni-axial diagram of Figure 6, from which, one can conclude that

$$\dot{C}^s_{ijkl}\epsilon_{kl} = -C^s_{ijkl}\dot{\epsilon}^d_{kl} \tag{53}$$

where ϵ^d_{kl} is called as degrading strain, representing the inelastic part of total strain. It is important to note here that degrading strain of an ED model is intrinsically associated with the degradation of the secant stiffness.

Applying equation (53) to (52), the following result is obtained

$$\dot{\sigma}_{ij} = C^s_{ijkl}(\dot{\epsilon}_{kl} - \dot{\epsilon}^d_{kl}) \tag{54}$$

Now, it is convenient to define a degradation rule for the secant stiffness or, considering the stress-based formulation, for the secant compliance, i.e.,

$$\dot{C}^{s,-1}_{ijkl} = \dot{\lambda}M_{ijkl} \tag{55}$$

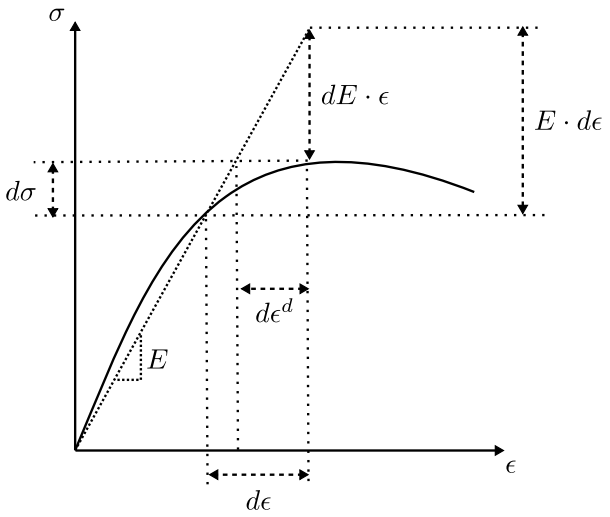

Figure 6: Representation of incremental stress and strain for elastic degrading models

where, in this new context, the multiplier, $\dot{\lambda}$, defines the magnitude and M_{ijkl}, the direction, of the rate of change of the secant compliance tensor.

For the unified framework proposed, it is necessary to write an evolution law for the degrading strains, in a similar way to the plastic flow rule of equation (42). This can be done by first taking the time derivative of the inverse of equation (51), substituting the incremental stresses by the right side of equation (54), to obtain

$$\dot{\epsilon}^d_{kl} = \dot{C}^{s,-1}_{klrs}\sigma_{rs} \tag{56}$$

and then introducing equation (55) to result in

$$\dot{\epsilon}^d_{kl} = \dot{\lambda} m_{kl}, \qquad m_{kl} = M_{klrs}\sigma_{rs} \tag{57}$$

Concepts of loading function and loading surface can be applied for ED models in a very similar manner as EP models, in such a way that the following expression for linearised consistency condition can be defined:

$$\dot{F}(\sigma_{ij}, \mathbf{q}) = n_{ij}\dot{\sigma}_{ij} - H\dot{\lambda} = 0 \quad \text{with} \quad n_{ij} = \left.\frac{\partial F}{\partial \sigma_{ij}}\right|_{\lambda} \quad \text{and} \quad H = -\left.\frac{\partial F}{\partial \lambda}\right|_{\boldsymbol{\sigma}} = -\left.\frac{\partial F}{\partial \mathbf{q}}\right|_{\boldsymbol{\sigma}} : \frac{\partial \mathbf{q}}{\partial \epsilon^d_{kl}} m_{kl} \tag{58}$$

where, in the ED context, the internal variables defines the current value of the compliance tensor, i.e., $C^{s,-1}_{ijkl} \equiv C^{s,-1}_{ijkl}(C^{-1}_{ijkl}, \mathbf{q})$, and a hardening-softening law, similar to equation (43), is postulated to describe the evolution of $\mathbf{q}$. Thus,

$$\dot{C}^{s,-1}_{ijkl} = \frac{\partial C^{s,-1}_{ijkl}}{\partial \mathbf{q}} : \dot{\mathbf{q}} = -\dot{\lambda}\left[\frac{\partial C^{s,-1}_{ijkl}}{\partial \mathbf{q}} : \mathbf{h}\right] \tag{59}$$

Comparing equations (55) and (59), one can conclude that

$$M_{ijkl} = -\frac{\partial C^{s,-1}_{ijkl}}{\partial \mathbf{q}} : \mathbf{h} \tag{60}$$

Now, noting the similarities between equations (41) to (46) and equations (54), (57) and (58), the same algebraic manipulations described in the last subsection can be repeated here, generating

expressions for the degrading multiplier and tangent stiffness, analogous to equations (47) and (48), i.e.,

$$\dot{\lambda} = \frac{n_{ij} C^s_{ijkl} \dot{\epsilon}_{kl}}{H + n_{pq} C^s_{pqrs} m_{rs}} \tag{61}$$

$$\dot{\sigma}_{ij} = C^t_{ijkl} \dot{\epsilon}_{kl}, \qquad C^t_{ijkl} = C^s_{ijkl} - \frac{C^s_{ijab} m_{ab} n_{cd} C^s_{cdkl}}{H + n_{pq} C^s_{pqrs} m_{rs}} \tag{62}$$

In the same way as mentioned for EP models, equations (51) to (62) were developed in a stress-based formulation. If this procedure is repeated beginning with a loading function defined in the strain space, $\bar{F}(\epsilon_{ij}, \boldsymbol{\alpha})$, the tangential stiffness operator takes the form:

$$C^t_{ijkl} = C^s_{ijkl} + \frac{1}{\bar{H}} \bar{m}_{ij} \bar{n}_{kl} \tag{63}$$

where,

$$\begin{cases} \bar{m}_{ij} = \bar{M}_{ijkl} \epsilon_{kl} = -C^s_{ijkl} m_{kl} \\ \\ \bar{M}_{ijkl} = \dfrac{\partial C^s_{ijkl}}{\partial \boldsymbol{\alpha}} : \dfrac{\partial \boldsymbol{\alpha}}{\partial \lambda} = -\dfrac{\partial C^s_{ijkl}}{\partial \boldsymbol{\alpha}} : \bar{\mathbf{h}} \\ \\ \bar{n}_{ij} = \left. \dfrac{\partial \bar{F}}{\partial \epsilon_{ij}} \right|_{\lambda} = C^s_{ijkl} n_{kl} \\ \\ \bar{H} = -\left. \dfrac{\partial \bar{F}}{\partial \lambda} \right|_{\boldsymbol{\epsilon}} = H + n_{ij} C^s_{ijkl} m_{kl} \end{cases} \tag{64}$$

The equations presented in this subsection are particularized for isotropic damage constitutive models in Appendix A.

Comparing equations (41), (48), (49) and (50) with equations (54), (62), (63) and (64), it is clear that the only differences are related to the definition of the inelastic part of total strains, ϵ^p_{ij} to EP models and ϵ^d_{ij} to ED models, and the presence of the secant stiffness tensor, C^s_{ijkl}, in ED equations, in place of the initial linear elastic constitutive tensor, C_{ijkl}, present in EP equations. For that reason, in a computational point of view, a large range of different constitutive models can be implemented in a completely independent way from the solution strategy described next. It is only necessary to appropriate define expressions for $\bar{n}_{ij}$, $\bar{m}_{ij}$ and $\bar{H}$, beyond a correct evaluation of stresses from a known strain state.

3 Boundary Integral Equations with Initial Fields

To develop the integral equations which constitute the basis of the BEM for inelastic solid mechanics, it is important to note that any point in a non linear equilibrium path can be defined, independently of the constitutive model, as a combination of two linear parts.

Consider, for example, the uni-axial equilibrium paths presented in Figure 7. In both cases, for an arbitrary strain state ϵ, the actual stress state which is given by a non linear constitutive model is represented by $\sigma(\epsilon)$. Additionally, a stress state evaluated using a purely linear elastic relationship for the same arbitrary strain state is given by $E^o \epsilon$, where E^o represents the initial elasticity modulus. Also, in both cases, the residual quantities ϵ^o and σ^o are defined as the difference between the actual and the purely elastic states. As is possible to note in Figure 7, and generalizing to a multi-axial solid domain, the total strain ϵ_{ij} and the actual stress $\sigma_{ij}(\epsilon_{ij})$ can be given by

$$\epsilon_{ij} = \epsilon^e_{ij} + \epsilon^o_{ij} \tag{65}$$

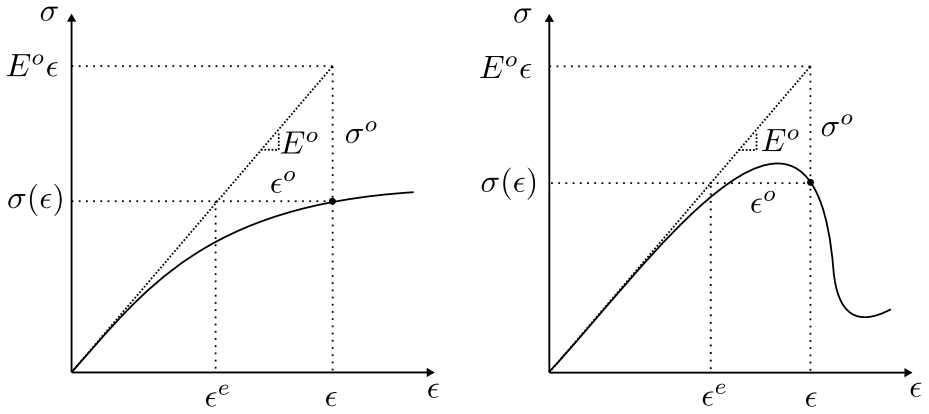

Figure 7: Relations between stress and strain for two distinct equilibrium paths

$$\sigma_{ij}(\epsilon_{ij}) = C_{ijkl}(\epsilon_{kl} - \epsilon^o_{kl}) = C_{ijkl}\epsilon_{kl} - \sigma^o_{ij} \tag{66}$$

Thus, the non linear integral equations in the BEM context are deduced considering the existence of an initial strain field ϵ^o_{ij}, or a corresponding initial stress field $\sigma^o_{ij} = C_{ijkl}\epsilon^o_{kl}$. For constitutive models based on plasticity theory, the initial strain hold the same value as the irreversible plastic strain ϵ^p_{ij} (see equation 41). However, these terms should not be the same when aiming for a more comprehensive non linear application of the method. For example, in the class of isotropic damage models described in Appendix A, where the secant tensor is given by $C^s_{ijkl} = (1-D)C_{ijkl}$ (see equation 244), the correspondence $\epsilon^o_{ij} = D\epsilon_{ij}$ can be verified from equation (51).

Such mentioned integral equations, that are relevant for physically non linear formulations of the BEM, can be obtained from a physical approach based on the Betti's Reciprocity Theorem or by an entirely numerical approach based on a generalization of the Method of Weighted Residuals. In the first case, the Kelvin's fundamental problem, described in Section 2.2, is used as auxiliary field, while in the second case, its solution is adopted as weighting function. A detailed derivation of these equations are easily found in many BEM textbooks, among which can be cited Telles [1983], Brebbia et al. [1984], Aliabadi [2002], Gao and Davies [2002]. Thus, such derivations are omitted here and only the final results (completely enough to implementation purposes) are presented.

Consider a solid domain Ω, delimited by boundary Γ, as previously illustrated in Figure 1, with an initial strain field distribution, ϵ^o_{ij}. The first relevant integral equation is the Somigliana's Identity, which gives the displacement vector at an internal point, $\boldsymbol{\xi}$ ($\boldsymbol{\xi} \in \Omega$ but $\boldsymbol{\xi} \notin \Gamma$), i.e.,

$$u_i(\boldsymbol{\xi}) = \int_\Gamma u^*_{ij}(\boldsymbol{\xi}, \mathbf{x}) t_j(\mathbf{x})\, d\Gamma - \int_\Gamma t^*_{ij}(\boldsymbol{\xi}, \mathbf{x}) u_j(\mathbf{x})\, d\Gamma + \int_\Omega u^*_{ij}(\boldsymbol{\xi}, \mathbf{x}) b_j(\mathbf{x})\, d\Omega + \int_\Omega \sigma^*_{ijk}(\boldsymbol{\xi}, \mathbf{x}) \epsilon^o_{jk}(\mathbf{x})\, d\Omega \tag{67}$$

where $u^*_{ij}(\boldsymbol{\xi}, \mathbf{x})$ refer to Kelvin's fundamental displacements, given in equations (33) and (40), respectively for three and two dimensional cases. In the same way, $t^*_{ij}(\boldsymbol{\xi}, \mathbf{x})$ represents the traction field on Γ and $\sigma^*_{ijk}(\boldsymbol{\xi}, \mathbf{x})$ is the Cauchy stress at any point of Ω, both associated to the Kelvin's fundamental solution. Remember that the first index of these tensors (i) refer to the direction of the concentrated force that act on the source point $\boldsymbol{\xi}$, while the other indexes (j or jk) designate the field components (displacement, traction or stress) that emerge at a field point $\mathbf{x}$. Expressions for t^*_{ij} and σ^*_{ijk} are presented further in section 3.1.

If the collocation point is taken as a boundary point, i.e., $\boldsymbol{\xi} \in \Gamma$, the fundamental solution second-order tensors introduce a weakly and a strongly singular character, respectively for the first and second integrals in equation (67). Similarly, the kernel of the domain integral involving the initial strain field becomes weakly singular. Thus, a correct deduction of the boundary dis-

placement integral equation requires, in this case, a limit process considering a radius of exclusion around the singular point, leading to the following expression:

$$c_{ij}(\boldsymbol{\xi})u_j(\boldsymbol{\xi}) = \int_\Gamma u^*_{ij}(\boldsymbol{\xi},\mathbf{x})t_j(\mathbf{x})\,d\Gamma - \cancel{\int_\Gamma} t^*_{ij}(\boldsymbol{\xi},\mathbf{x})u_j(\mathbf{x})\,d\Gamma + \int_\Omega u^*_{ij}(\boldsymbol{\xi},\mathbf{x})b_j(\mathbf{x})\,d\Omega + \int_\Omega \sigma^*_{ijk}(\boldsymbol{\xi},\mathbf{x})\epsilon^o_{jk}(\mathbf{x})\,d\Omega \tag{68}$$

where $c_{ij}(\boldsymbol{\xi})$ is a function of the boundary's geometry around the collocation point and the elastic properties of the material. Explicit forms for this free term is also presented further in this section.

The weakly singular integrals can be evaluated as improper integrals, since they are convergent in the conventional Riemann interpretation. Numerical solutions of these integrals, however, require special methods (other than standard Gauss-Legedre quadrature) to guarantee its accuracy. On the other hand, strongly singular integrals are bounded only in Cauchy Principal Value sense, as indicated by the crossed integral symbol, requiring more rigorous numerical methods in its evaluation. Such methods are always based in some kind of singularity elimination strategy.

Furthermore, internal strains can be obtained by taking the symmetric part of the gradient of equation (67), related to the source point (see equation 7, which is also valid for the total strain from equation 65), resulting in

$$\begin{aligned}\epsilon_{ij}(\boldsymbol{\xi}) = &\int_\Gamma u^*_{ijk}(\boldsymbol{\xi},\mathbf{x})t_k(\mathbf{x})\,d\Gamma - \int_\Gamma t^*_{ijk}(\boldsymbol{\xi},\mathbf{x})u_k(\mathbf{x})\,d\Gamma + \int_\Omega u^*_{ijk}(\boldsymbol{\xi},\mathbf{x})b_k(\mathbf{x})\,d\Gamma \\ &+ \cancel{\int_\Omega} \sigma^*_{ijkl}(\boldsymbol{\xi},\mathbf{x})\epsilon^o_{kl}(\mathbf{x})\,d\Omega + F^{\epsilon\epsilon}_{ijkl}\epsilon^o_{kl}(\boldsymbol{\xi})\end{aligned} \tag{69}$$

where the last domain integral have a strongly singular kernel when the collocation and field points coincide and, again, its evaluation exists only in the CPV sense. Tensors u^*_{ijk}, t^*_{ijk} and σ^*_{ijkl} are respectively obtained by taking the gradients of fundamental solutions u^*_{ij}, t^*_{ij} and σ^*_{ijk}, while $F^{\epsilon\epsilon}_{ijkl}$ is a free term, which existence was firstly verified by Bui [1978]. Explicit expressions for these parameters are also shown next.

3.1 Fields derived from Kelvin Fundamental Solution

From equations (33) and (40) – the Kelvin fundamental displacements, respectively, for three-dimensional and plane cases –, it is possible to obtain the associated strain and stress fields, at a given point $\mathbf{x}$, using equations (7) and (9). Moreover, the traction field on a surface oriented by a normal vector $\mathbf{n}$ at $\mathbf{x}$ can be obtained from equation (1). Explicitly, the following results are achieved.

Three-dimensional problems:

$$\epsilon^*_{ijk}(\boldsymbol{\xi},\mathbf{x}) \equiv \frac{1}{2}\left[u^*_{ij,k}\big|_{\mathbf{x}} + u^*_{ik,j}\big|_{\mathbf{x}}\right] = \frac{-1}{16\pi\mu(1-\nu)r^2}[(1-2\nu)(\delta_{ik}r_{,j} + \delta_{ij}r_{,k}) - \delta_{jk}r_{,i} + 3r_{,i}\,r_{,j}\,r_{,k}] \tag{70}$$

$$\sigma^*_{ijk}(\boldsymbol{\xi},\mathbf{x}) \equiv C_{jklm}\epsilon^*_{ilm}(\boldsymbol{\xi},\mathbf{x}) = \frac{-1}{8\pi(1-\nu)r^2}[(1-2\nu)(-\delta_{jk}r_{,i} + \delta_{ik}r_{,j} + \delta_{ij}r_{,k}) + 3r_{,i}\,r_{,j}\,r_{,k}] \tag{71}$$

$$t^*_{ij}(\boldsymbol{\xi},\mathbf{x}) \equiv \sigma^*_{ijk}(\boldsymbol{\xi},\mathbf{x})n_k(\mathbf{x}) = \frac{-1}{8\pi(1-\nu)r^2}\left\{\frac{\partial r}{\partial n}[(1-2\nu)\delta_{ij} + 3r_{,i}\,r_{,j}] - (1-2\nu)(n_j r_{,i} - n_i r_{,j})\right\} \tag{72}$$

Plane state problems:

$$\epsilon^*_{ijk}(\boldsymbol{\xi},\mathbf{x}) \equiv \frac{1}{2}\left[u^*_{ij,k}\big|_{\mathbf{x}} + u^*_{ik,j}\big|_{\mathbf{x}}\right] = \frac{-1}{8\pi\mu(1-\bar{\nu})r}[(1-2\bar{\nu})(\delta_{ik}r_{,j} + \delta_{ij}r_{,k}) - \delta_{jk}r_{,i} + 2r_{,i}\,r_{,j}\,r_{,k}] \tag{73}$$

$$\sigma^*_{ijk}(\boldsymbol{\xi},\mathbf{x}) \equiv C_{jklm}\epsilon^*_{ilm}(\boldsymbol{\xi},\mathbf{x}) = \frac{-1}{4\pi(1-\bar{\nu})r}[(1-2\bar{\nu})(-\delta_{jk}r_{,i}+\delta_{ik}r_{,j}+\delta_{ij}r_{,k}) + 2r_{,i}\,r_{,j}\,r_{,k}] \tag{74}$$

$$t^*_{ij}(\boldsymbol{\xi},\mathbf{x}) \equiv \sigma^*_{ijk}(\boldsymbol{\xi},\mathbf{x})n_k(\mathbf{x}) = \frac{-1}{4\pi(1-\bar{\nu})r}\left\{\frac{\partial r}{\partial n}[(1-2\bar{\nu})\delta_{ij}+2r_{,i}\,r_{,j}]-(1-2\bar{\nu})(n_j r_{,i}-n_i r_{,j})\right\} \tag{75}$$

In equations (72) and (75), the following result is valid:

$$\frac{\partial r}{\partial n} = \frac{r_i}{r}n_i = r_{,i}\,n_i \tag{76}$$

Note that results from equations (71) and (72) – or (74) and (75) – must be used in integral equations (67) and (68). Particularly for this second equation, the free term, $c_{ij}(\boldsymbol{\xi})$, still needs to be presented. Its deduction is intrinsically associated to the mentioned process of taking an augmented region around the source point (which is located at boundary Γ in this case), in order that only the final results are presented here, using Figure 8.

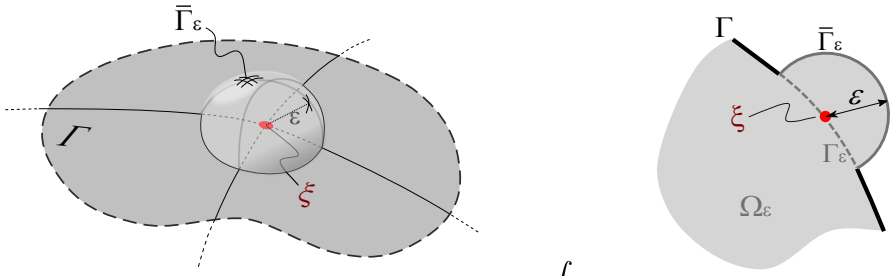

Figure 8: Expression for $c_{ij}(\boldsymbol{\xi})$ and the augmented region

Equation (69), on the other hand, is obtained by taking derivatives of equation (67), associated to the source point, $\boldsymbol{\xi}$. Thus, the parameters that appear in its integrals kernels are given by the next expressions.

Three-dimensional problems:

$$u^*_{ijk}(\boldsymbol{\xi},\mathbf{x}) \equiv \frac{1}{2}\left[u^*_{ik,j}\big|_{\boldsymbol{\xi}}+u^*_{jk,i}\big|_{\boldsymbol{\xi}}\right] = \frac{1}{16\pi\mu(1-\nu)r^2}[(1-2\nu)(\delta_{ik}r_{,j}+\delta_{jk}r_{,i})-\delta_{ij}r_{,k}+3r_{,i}\,r_{,j}\,r_{,k}] \tag{77}$$

$$\begin{aligned} t^*_{ijk}(\boldsymbol{\xi},\mathbf{x}) \equiv \frac{1}{2}\left[t^*_{ik,j}\big|_{\boldsymbol{\xi}} + t^*_{jk,i}\big|_{\boldsymbol{\xi}}\right] =& \frac{1}{8\pi(1-\nu)r^3}\Big\{(1-2\nu)[n_i\delta_{jk}+n_j\delta_{ik}-n_k\delta_{ij}+3r_{,i}\,r_{,j}\,n_k] \\ &+3\frac{\partial r}{\partial n}[\nu(r_{,j}\,\delta_{ik}+r_{,i}\,\delta_{jk})+r_{,k}\,\delta_{ij}-5r_{,i}\,r_{,j}\,r_{,k}] \\ &+3\nu(n_j r_{,i}\,r_{,k}+n_i r_{,j}\,r_{,k})\Big\} \end{aligned} \tag{78}$$

$$\begin{aligned} \sigma^*_{ijkl}(\boldsymbol{\xi},\mathbf{x}) \equiv \frac{1}{2}\left[\sigma^*_{ikl,j}\big|_{\boldsymbol{\xi}} + \sigma^*_{jkl,i}\big|_{\boldsymbol{\xi}}\right] =& \frac{1}{8\pi(1-\nu)r^3}\Big\{(1-2\nu)(\delta_{ik}\delta_{jl}+\delta_{jk}\delta_{il}-\delta_{ij}\delta_{kl}) \\ &+3\nu(\delta_{il}r_{,j}\,r_{,k}+\delta_{ik}r_{,j}\,r_{,l}+\delta_{jk}r_{,i}\,r_{,l}+\delta_{jl}r_{,i}\,r_{,k}) \\ &+3[(1-2\nu)\delta_{kl}r_{,i}\,r_{,j}+\delta_{ij}r_{,k}\,r_{,l}]-15r_{,i}\,r_{,j}\,r_{,k}\,r_{,l}\Big\} \end{aligned} \tag{79}$$

Plane state problems:

$$u^*_{ijk}(\boldsymbol{\xi},\mathbf{x}) \equiv \frac{1}{2}\left[u^*_{ik,j}\big|_{\boldsymbol{\xi}} + u^*_{jk,i}\big|_{\boldsymbol{\xi}}\right] = \frac{1}{8\pi\mu(1-\bar{\nu})r}[(1-2\bar{\nu})(\delta_{ik}r_{,j} + \delta_{jk}r_{,i}) - \delta_{ij}r_{,k} + 2r_{,i}\,r_{,j}\,r_{,k}] \tag{80}$$

$$\begin{aligned} t^*_{ijk}(\boldsymbol{\xi},\mathbf{x}) \equiv \frac{1}{2}\left[t^*_{ik,j}\big|_{\boldsymbol{\xi}} + t^*_{jk,i}\big|_{\boldsymbol{\xi}}\right] = &\frac{1}{4\pi(1-\bar{\nu})r^2}\Big\{(1-2\bar{\nu})[n_i\delta_{jk} + n_j\delta_{ik} - n_k\delta_{ij} \\ &+ 2r_{,i}\,r_{,j}\,n_k] + 2\frac{\partial r}{\partial n}[\bar{\nu}(r_{,j}\,\delta_{ik} + r_{,i}\,\delta_{jk}) + r_{,k}\,\delta_{ij} \\ &- 4r_{,i}\,r_{,j}\,r_{,k}] + 2\bar{\nu}(n_j r_{,i}\,r_{,k} + n_i r_{,j}\,r_{,k})\Big\} \end{aligned} \tag{81}$$

$$\begin{aligned} \sigma^*_{ijkl}(\boldsymbol{\xi},\mathbf{x}) \equiv \frac{1}{2}\left[\sigma^*_{ikl,j}\big|_{\boldsymbol{\xi}} + \sigma^*_{jkl,i}\big|_{\boldsymbol{\xi}}\right] = &\frac{1}{4\pi(1-\bar{\nu})r^2}\Big\{(1-2\bar{\nu})(\delta_{ik}\delta_{jl} + \delta_{jk}\delta_{il} - \delta_{ij}\delta_{kl}) \\ &+ 2\bar{\nu}(\delta_{il}r_{,j}\,r_{,k} + \delta_{ik}r_{,j}\,r_{,l} + \delta_{jk}r_{,i}\,r_{,l} + \delta_{jl}r_{,i}\,r_{,k}) \\ &+ 2[(1-2\bar{\nu})\delta_{kl}r_{,i}\,r_{,j} + \delta_{ij}r_{,k}\,r_{,l}] - 8r_{,i}\,r_{,j}\,r_{,k}\,r_{,l}\Big\} \end{aligned} \tag{82}$$

In equations (77) to (82), the following results were considered:

$$r_{,i}\,\big|_{\boldsymbol{\xi}} = \frac{\partial r}{\partial \xi_i} = \frac{\partial r}{\partial r_j}\frac{\partial r_j}{\partial \xi_i} = \frac{r_j}{r}(-\delta_{ij}) = -\frac{r_i}{r} = -r_{,i} \tag{83a}$$

$$\left(r_{,i}\,\big|_{\mathbf{x}}\right)_{,j}\big|_{\boldsymbol{\xi}} \equiv (r_{,i}\,)_{,j}\,\big|_{\boldsymbol{\xi}} = \left(\frac{r_i}{r}\right)_{,j}\Bigg|_{\boldsymbol{\xi}} = -\frac{\delta_{ij}}{r} + \frac{r_{,i}\,r_{,j}}{r} = -r_{,ij} \tag{83b}$$

Finally, the free terms $F^{\epsilon\epsilon}_{ijkl}$ are given by

$$F^{\epsilon\epsilon}_{ijkl} = \begin{cases} \dfrac{1}{15(1-\nu)}[(4-5\nu)(\delta_{ik}\delta_{jl} + \delta_{il}\delta_{jk}) - (1-5\nu)\delta_{ij}\delta_{kl}] & \text{(for 3D problems)} \\ \dfrac{1}{8(1-\bar{\nu})}[(3-4\bar{\nu})(\delta_{ik}\delta_{jl} + \delta_{il}\delta_{jk}) - (1-4\bar{\nu})\delta_{ij}\delta_{kl}] & \text{(for plane state problems)} \end{cases} \tag{84}$$

4 The Implicit BEM Formulation for Physically Non Linear Problems

Discrete versions of equations (67), (68) and (69), that are related to the BEM are presented in this section, followed by a re-organization of the matrices, according to the implicit formulation of the method. Moreover, the non linear solution strategy is described in detail.

The body forces, $b_i(\mathbf{x})$, are disregarded here, since it is negligible, when compared to boundary loads, or even, can be substituted by boundary tractions, for many types of problems.

4.1 Discrete equations

Obtaining the typical matrix equations of the BEM starts with the definition of a discrete set of source points (or collocation points), with a total of N points located on the boundary and M points internal to the domain, Ω. Next, the boundary, Γ, is divided into N_e boundary elements, while the region of the domain where inelastic dissipative effects occur is divided into N_c cells, as illustrated in Figure 9.

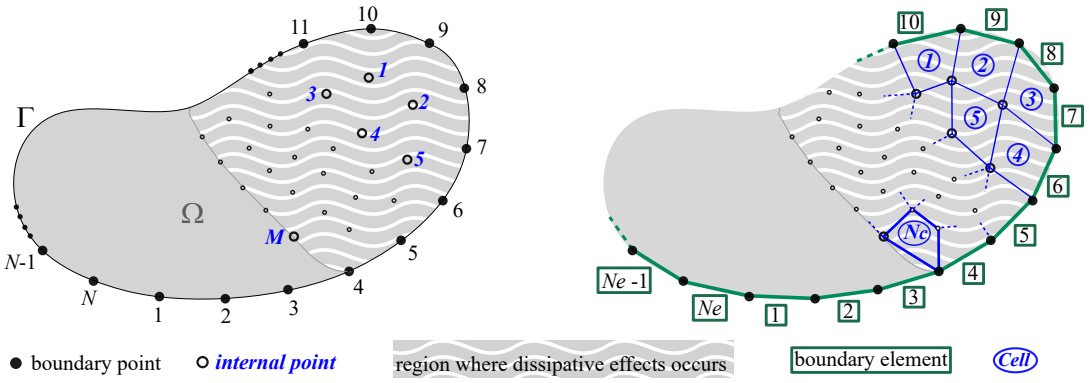

Figure 9: Plane solid with discrete division: points, elements and cells

In this way, equations (67), (68) and (69) can be rewritten in the following forms:

$$\dot{u}_i(\boldsymbol{\xi}^J) = \sum_{e=1}^{N_e} \int_{\Gamma_e} u^*_{ij}(\boldsymbol{\xi}^J, \mathbf{x}) \dot{t}_j(\mathbf{x}) d\Gamma - \sum_{e=1}^{N_e} \int_{\Gamma_e} t^*_{ij}(\boldsymbol{\xi}^J, \mathbf{x}) \dot{u}_j(\mathbf{x}) d\Gamma + \sum_{c=1}^{N_c} \int_{\Omega_c} \sigma^*_{ijk}(\boldsymbol{\xi}^J, \mathbf{x}) \dot{\epsilon}^o_{jk}(\mathbf{x}) d\Omega \tag{85}$$

$$c_{ij}(\boldsymbol{\xi}^I) \dot{u}_j(\boldsymbol{\xi}^I) = \sum_{e=1}^{N_e} \int_{\Gamma_e} u^*_{ij}(\boldsymbol{\xi}^I, \mathbf{x}) \dot{t}_j(\mathbf{x}) d\Gamma - \sum_{e=1}^{N_e} \int_{\Gamma_e} t^*_{ij}(\boldsymbol{\xi}^I, \mathbf{x}) \dot{u}_j(\mathbf{x}) d\Gamma + \sum_{c=1}^{N_c} \int_{\Omega_c} \sigma^*_{ijk}(\boldsymbol{\xi}^I, \mathbf{x}) \dot{\epsilon}^o_{jk}(\mathbf{x}) d\Omega \tag{86}$$

$$\dot{\epsilon}_{ij}(\boldsymbol{\xi}^J) = \sum_{e=1}^{N_e} \int_{\Gamma_e} u^*_{ijk}(\boldsymbol{\xi}^J, \mathbf{x}) \dot{t}_k(\mathbf{x}) d\Gamma - \sum_{e=1}^{N_e} \int_{\Gamma_e} t^*_{ijk}(\boldsymbol{\xi}^J, \mathbf{x}) \dot{u}_k(\mathbf{x}) d\Gamma + \sum_{c=1}^{N_c} \int_{\Omega_c} \sigma^*_{ijkl}(\boldsymbol{\xi}^J, \mathbf{x}) \dot{\epsilon}^o_{kl}(\mathbf{x}) d\Omega + F^{\epsilon\epsilon}_{ijkl} \dot{\epsilon}^o_{kl}(\boldsymbol{\xi}^J) \tag{87}$$

where $I = 1, \ldots, N$ e $J = 1, \ldots, M$. The domains of each boundary element and each cell are referenced, respectively, by Γ_e and Ω_c.

For the boundary elements, subparametric or isoparametric formulations are commonly used. Here, only the case of isoparametric elements is considered. In this kind of boundary elements, displacements, tractions and the geometry are approximated by the same interpolation functions over the collocation points. Thus, inside an element, it is possible to write:

$$x_j(\eta_k) \approx \sum_{\gamma=1}^{n_e} N_\gamma(\eta_k) x_j^\gamma \tag{88a}$$

$$\dot{u}_j(\mathbf{x}(\eta_k)) \approx \sum_{\gamma=1}^{n_e} N_\gamma(\eta_k) \dot{u}_j^\gamma \tag{88b}$$

$$\dot{t}_j(\mathbf{x}(\eta_k)) \approx \sum_{\gamma=1}^{n_e} N_\gamma(\eta_k) \dot{t}_j^\gamma \tag{88c}$$

where η_k ($\in [-1, +1]$) are parametric coordinates (k varies from 1 to 2 for 3D problems, while a single coordinate is necessary for boundary elements in plane problems – see Figure 10). Index γ is associated to the collocation points inside the element, $N^\gamma(\eta)$ are the interpolation functions and n_e represents the total number of collocation points in the element. In this way, x_j^γ, $\dot{u}_j^\gamma$ and

$\dot{t}_j^{\gamma}$ represent, respectively, the x_j coordinate, the u_j displacement component and the t_j traction component at the collocation point referenced by γ.

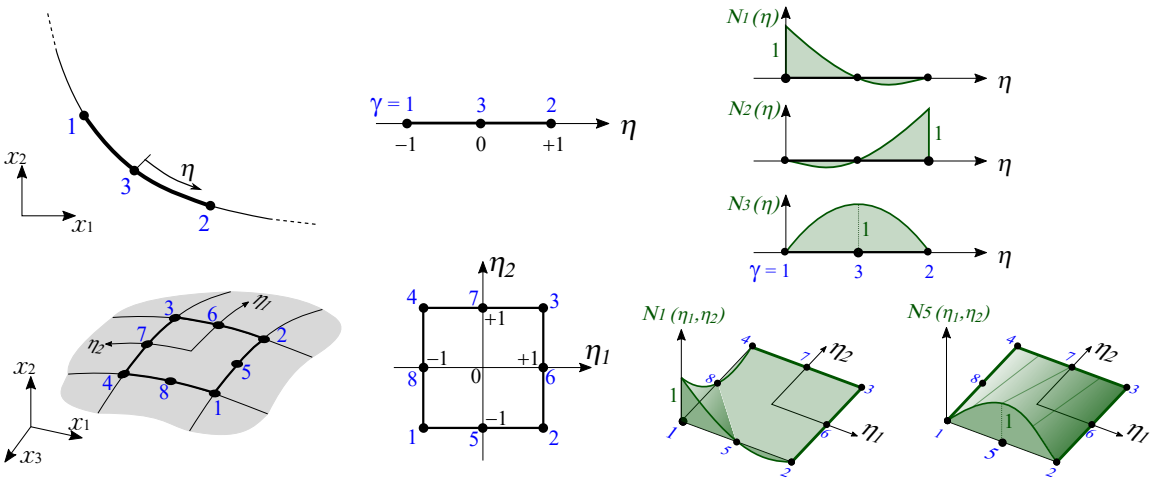

Figure 10: Linear and quadrilateral boundary elements, parametric coordinates, and quadratic interpolation functions

Equations (88b) and (88c) can be conveniently rewritten in the following matrix forms:

$$\{\dot{u}\} = [N(\eta_k)]\{\dot{u}^e\} \qquad \text{and} \qquad \{\dot{t}\} = [N(\eta_k)]\{\dot{t}^e\} \tag{89}$$

where, for three-dimensional problems,

$$\{\dot{u}\} = \begin{Bmatrix} \dot{u}_1(\mathbf{x}(\eta_1,\eta_2)) \\ \dot{u}_2(\mathbf{x}(\eta_1,\eta_2)) \\ \dot{u}_3(\mathbf{x}(\eta_1,\eta_2)) \end{Bmatrix}, \quad \{\dot{t}\} = \begin{Bmatrix} \dot{t}_1(\mathbf{x}(\eta_1,\eta_2)) \\ \dot{t}_2(\mathbf{x}(\eta_1,\eta_2)) \\ \dot{t}_3(\mathbf{x}(\eta_1,\eta_2)) \end{Bmatrix}$$

$$\{\dot{u}^e\} = \begin{Bmatrix} \dot{u}_1^1 & \dot{u}_2^1 & \dot{u}_3^1 & \cdots & \dot{u}_1^{n_e} & \dot{u}_2^{n_e} & \dot{u}_3^{n_e} \end{Bmatrix}^T, \quad \{\dot{t}^e\} = \begin{Bmatrix} \dot{t}_1^1 & \dot{t}_2^1 & \dot{t}_3^1 & \cdots & \dot{t}_1^{n_e} & \dot{t}_2^{n_e} & \dot{t}_3^{n_e} \end{Bmatrix}^T$$

$$[N(\eta_k)] = \begin{bmatrix} N_1(\eta_1,\eta_2) & 0 & 0 & \cdots & N_{n_e}(\eta_1,\eta_2) & 0 & 0 \\ 0 & N_1(\eta_1,\eta_2) & 0 & \cdots & 0 & N_{n_e}(\eta_1,\eta_2) & 0 \\ 0 & 0 & N_1(\eta_1,\eta_2) & \cdots & 0 & 0 & N_{n_e}(\eta_1,\eta_2) \end{bmatrix}$$

and, for plane problems,

$$\{\dot{u}\} = \begin{Bmatrix} \dot{u}_1(\mathbf{x}(\eta)) \\ \dot{u}_2(\mathbf{x}(\eta)) \end{Bmatrix}, \quad \{\dot{t}\} = \begin{Bmatrix} \dot{t}_1(\mathbf{x}(\eta)) \\ \dot{t}_2(\mathbf{x}(\eta)) \end{Bmatrix}$$

$$\{\dot{u}^e\} = \begin{Bmatrix} \dot{u}_1^1 & \dot{u}_2^1 & \cdots & \dot{u}_1^{n_e} & \dot{u}_2^{n_e} \end{Bmatrix}^T, \quad \{\dot{t}^e\} = \begin{Bmatrix} \dot{t}_1^1 & \dot{t}_2^1 & \cdots & \dot{t}_1^{n_e} & \dot{t}_2^{n_e} \end{Bmatrix}^T$$

$$[N(\eta_k)] = \begin{bmatrix} N_1(\eta) & 0 & \cdots & N_{n_e}(\eta) & 0 \\ 0 & N_1(\eta) & \cdots & 0 & N_{n_e}(\eta) \end{bmatrix}$$

Moreover, a boundary infinitesimal surface, $d\Gamma$, relates itself with the parametric coordinates by the next expression:

$$d\Gamma(\mathbf{x}(\eta_k)) = \mathcal{J}(\eta_k)\, d\eta_k \tag{90}$$

where, for three-dimensional problems, $d\eta_k \equiv d\eta_1\, d\eta_2$ and

$$\mathcal{J}(\eta_k) \equiv \mathcal{J}(\eta_1,\eta_2) = \sqrt{J_1^2 + J_2^2 + J_3^2}$$

with

$$J_1 = \frac{\partial x_2}{\partial \eta_1}\frac{\partial x_3}{\partial \eta_2} - \frac{\partial x_2}{\partial \eta_2}\frac{\partial x_3}{\partial \eta_1}, \quad J_2 = \frac{\partial x_3}{\partial \eta_1}\frac{\partial x_1}{\partial \eta_2} - \frac{\partial x_3}{\partial \eta_2}\frac{\partial x_1}{\partial \eta_1}, \quad J_3 = \frac{\partial x_1}{\partial \eta_1}\frac{\partial x_2}{\partial \eta_2} - \frac{\partial x_2}{\partial \eta_2}\frac{\partial x_1}{\partial \eta_1},$$

while, for plane state problems,

$$\mathcal{J}(\eta_k) \equiv \mathcal{J}(\eta) = \sqrt{J_1^2 + J_2^2}$$

with

$$J_1 = \frac{dx_1}{d\eta}, \quad J_1 = \frac{dx_2}{d\eta}.$$

In an analogous way, the initial strain field is interpolated inside each cell, i.e.,

$$\dot{\epsilon}^o_{ij}(\mathbf{x}(\eta_k)) \approx \sum_{\gamma=1}^{n_c} M_\gamma(\eta_k)\dot{\epsilon}^{o,\gamma}_{ij} \tag{91}$$

where, again, η_k ($\in [-1, +1]$), but now k varies between 1 and 3 for 3D problems and between 1 and 2 for 2D problems, as depicted in Figure 11. The interpolation functions, $M_\gamma(\eta)$, follow the same idea from the boundary elements, regarding the appropriate dimensions for each case. For example, considering also isoparametric cells, $M_\gamma(\eta)$ for a two-dimensional problem are exactly the same as $N_\gamma(\eta)$ for a three-dimensional one. Index n_c is associated to the number of collocation points in the cell.

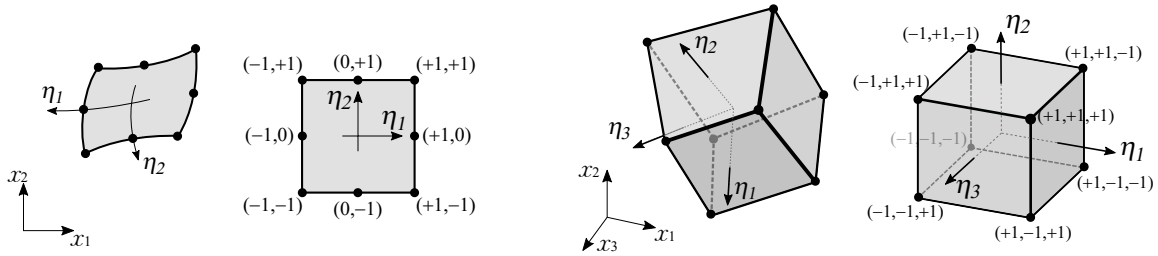

Figure 11: Quadrilateral and hexahedral cells, and parametric coordinates

In a matrix form, equation (91) is written as

$$\{\dot{\epsilon}^o\} = [M(\eta_k)]\{\dot{\epsilon}^{o,c}\} \tag{92}$$

where,

$$\{\dot{\epsilon}^o\} = \begin{Bmatrix} \dot{\epsilon}^o_{11}(\mathbf{x}(\eta_1,\eta_2,\eta_3)) \\ \dot{\epsilon}^o_{22}(\mathbf{x}(\eta_1,\eta_2,\eta_3)) \\ \dot{\epsilon}^o_{33}(\mathbf{x}(\eta_1,\eta_2,\eta_3)) \\ \dot{\epsilon}^o_{12}(\mathbf{x}(\eta_1,\eta_2,\eta_3)) \\ \dot{\epsilon}^o_{13}(\mathbf{x}(\eta_1,\eta_2,\eta_3)) \\ \dot{\epsilon}^o_{23}(\mathbf{x}(\eta_1,\eta_2,\eta_3)) \end{Bmatrix} \quad \text{(for 3D)}, \qquad \{\dot{\epsilon}^o\} = \begin{Bmatrix} \dot{\epsilon}^o_{11}(\mathbf{x}(\eta_1,\eta_2)) \\ \dot{\epsilon}^o_{22}(\mathbf{x}(\eta_1,\eta_2)) \\ \dot{\epsilon}^o_{12}(\mathbf{x}(\eta_1,\eta_2)) \end{Bmatrix} \quad \text{(for 2D)}$$

$$\{\dot{\epsilon}^{o,c}\} = \begin{Bmatrix} \{\dot{\epsilon}^{o,1}\} \\ \vdots \\ \{\dot{\epsilon}^{o,n_c}\} \end{Bmatrix}, \qquad \text{with} \qquad \{\dot{\epsilon}^{o,k}\} = \begin{Bmatrix} \dot{\epsilon}^{o,k}_{11} \\ \dot{\epsilon}^{o,k}_{22} \\ \dot{\epsilon}^{o,k}_{33} \\ \dot{\epsilon}^{o,k}_{12} \\ \dot{\epsilon}^{o,k}_{13} \\ \dot{\epsilon}^{o,k}_{23} \end{Bmatrix} \quad \text{(for 3D)}, \quad \begin{Bmatrix} \dot{\epsilon}^{o,k}_{11} \\ \dot{\epsilon}^{o,k}_{22} \\ \dot{\epsilon}^{o,k}_{12} \end{Bmatrix} \quad \text{(for 2D)}$$

$$[M(\eta_k)] = \begin{bmatrix} M_1(\eta_1,\eta_2,\eta_3)[I] & \cdots & M_{n_c}(\eta_1,\eta_2,\eta_3)[I] \end{bmatrix}, \quad [I] \rightarrow \begin{cases} \text{6x6 indentity matrix (for 3D)} \\ \text{3x3 indentity matrix (for 2D)} \end{cases}$$

As a matter of completeness, the geometry of a cell can be parametrized as

$$x_j(\mathbf{x}(\eta_k)) \approx \sum_{\gamma=1}^{n_c} M_\gamma(\eta_k) x_j^\gamma \tag{93}$$

from which is possible to obtain

$$d\Omega(\mathbf{x}(\eta_k)) = \bar{\mathcal{J}}(\eta_k)\, d\eta_k \tag{94}$$

4.1.1 Discrete form of Somigliana Identity

Considering an internal source point, integrals in equation (85) assume the following forms, after using equations (89), (90), (92) and (94):

$$\int_{\Gamma_e} u^*_{ij}(\boldsymbol{\xi}^J,\mathbf{x})\dot{t}_j(\mathbf{x})d\Gamma \approx \left(\int_{-1}^{+1} [u^*(\boldsymbol{\xi}^J,\eta_k)][N(\eta_k)]\mathcal{J}(\eta_k)\, d\eta_k \right)\{\dot{t}^e\} = [G_e^J]\{\dot{t}^e\} \tag{95}$$

$$\int_{\Gamma_e} t^*_{ij}(\boldsymbol{\xi}^J,\mathbf{x})\dot{u}_j(\mathbf{x})d\Gamma \approx \left(\int_{-1}^{+1} [t^*(\boldsymbol{\xi}^J,\eta_k)][N(\eta_k)]\mathcal{J}(\eta_k)\, d\eta_k \right)\{\dot{u}^e\} = [H_e^J]\{\dot{u}^e\} \tag{96}$$

$$\int_{\Omega_c} \sigma^*_{ijk}(\boldsymbol{\xi}^J,\mathbf{x})\dot{\epsilon}^o_{jk}(\mathbf{x})d\Omega \approx \left(\int_{-1}^{+1} [\sigma^*(\boldsymbol{\xi}^J,\eta_k)][M(\eta_k)]\bar{\mathcal{J}}(\eta_k)\, d\eta_k \right)\{\dot{\epsilon}^{o,c}\} = [Q_c^J]\{\dot{\epsilon}^{o,c}\} \tag{97}$$

where, for three-dimensional problems,

$$[u^*(\boldsymbol{\xi},\mathbf{x})] = \begin{bmatrix} u^*_{11}(\boldsymbol{\xi},\mathbf{x}) & u^*_{12}(\boldsymbol{\xi},\mathbf{x}) & u^*_{13}(\boldsymbol{\xi},\mathbf{x}) \\ u^*_{21}(\boldsymbol{\xi},\mathbf{x}) & u^*_{22}(\boldsymbol{\xi},\mathbf{x}) & u^*_{23}(\boldsymbol{\xi},\mathbf{x}) \\ u^*_{31}(\boldsymbol{\xi},\mathbf{x}) & u^*_{32}(\boldsymbol{\xi},\mathbf{x}) & u^*_{33}(\boldsymbol{\xi},\mathbf{x}) \end{bmatrix}, \qquad [t^*(\boldsymbol{\xi},\mathbf{x})] = \begin{bmatrix} t^*_{11}(\boldsymbol{\xi},\mathbf{x}) & t^*_{12}(\boldsymbol{\xi},\mathbf{x}) & t^*_{13}(\boldsymbol{\xi},\mathbf{x}) \\ t^*_{21}(\boldsymbol{\xi},\mathbf{x}) & t^*_{22}(\boldsymbol{\xi},\mathbf{x}) & t^*_{23}(\boldsymbol{\xi},\mathbf{x}) \\ t^*_{31}(\boldsymbol{\xi},\mathbf{x}) & t^*_{32}(\boldsymbol{\xi},\mathbf{x}) & t^*_{33}(\boldsymbol{\xi},\mathbf{x}) \end{bmatrix} \tag{98}$$

$$[\sigma^*(\boldsymbol{\xi},\mathbf{x})] = \begin{bmatrix} \sigma^*_{111}(\boldsymbol{\xi},\mathbf{x}) & \sigma^*_{122}(\boldsymbol{\xi},\mathbf{x}) & \sigma^*_{133}(\boldsymbol{\xi},\mathbf{x}) & 2\sigma^*_{112}(\boldsymbol{\xi},\mathbf{x}) & 2\sigma^*_{113}(\boldsymbol{\xi},\mathbf{x}) & 2\sigma^*_{123}(\boldsymbol{\xi},\mathbf{x}) \\ \sigma^*_{211}(\boldsymbol{\xi},\mathbf{x}) & \sigma^*_{222}(\boldsymbol{\xi},\mathbf{x}) & \sigma^*_{233}(\boldsymbol{\xi},\mathbf{x}) & 2\sigma^*_{212}(\boldsymbol{\xi},\mathbf{x}) & 2\sigma^*_{213}(\boldsymbol{\xi},\mathbf{x}) & 2\sigma^*_{223}(\boldsymbol{\xi},\mathbf{x}) \\ \sigma^*_{311}(\boldsymbol{\xi},\mathbf{x}) & \sigma^*_{322}(\boldsymbol{\xi},\mathbf{x}) & \sigma^*_{333}(\boldsymbol{\xi},\mathbf{x}) & 2\sigma^*_{312}(\boldsymbol{\xi},\mathbf{x}) & 2\sigma^*_{313}(\boldsymbol{\xi},\mathbf{x}) & 2\sigma^*_{323}(\boldsymbol{\xi},\mathbf{x}) \end{bmatrix} \tag{99}$$

and, for two-dimensional problems,

$$[u^*(\boldsymbol{\xi},\mathbf{x})] = \begin{bmatrix} u^*_{11}(\boldsymbol{\xi},\mathbf{x}) & u^*_{12}(\boldsymbol{\xi},\mathbf{x}) \\ u^*_{21}(\boldsymbol{\xi},\mathbf{x}) & u^*_{22}(\boldsymbol{\xi},\mathbf{x}) \end{bmatrix}, \qquad [t^*(\boldsymbol{\xi},\mathbf{x})] = \begin{bmatrix} t^*_{11}(\boldsymbol{\xi},\mathbf{x}) & t^*_{12}(\boldsymbol{\xi},\mathbf{x}) \\ t^*_{21}(\boldsymbol{\xi},\mathbf{x}) & t^*_{22}(\boldsymbol{\xi},\mathbf{x}) \end{bmatrix} \tag{100}$$

$$[\sigma^*(\boldsymbol{\xi},\mathbf{x})] = \begin{bmatrix} \sigma^*_{111}(\boldsymbol{\xi},\mathbf{x}) & \sigma^*_{122}(\boldsymbol{\xi},\mathbf{x}) & 2\sigma^*_{112}(\boldsymbol{\xi},\mathbf{x}) \\ \sigma^*_{211}(\boldsymbol{\xi},\mathbf{x}) & \sigma^*_{222}(\boldsymbol{\xi},\mathbf{x}) & 2\sigma^*_{212}(\boldsymbol{\xi},\mathbf{x}) \end{bmatrix} \tag{101}$$

In equations (99) and (101), the symmetry $\sigma^*_{ijk} = \sigma^*_{ikj}$ was used. Moreover, in equation (101), for the plane strain case, a fourth column might be added to contemplate terms σ^*_{i33}.

Also, note that, despite of the single integration symbol, integrals in equations (95) and (96) are in fact double integrals over the element domain, $(\eta_1,\eta_2) \rightarrow [-1,+1]\times[-1,+1]$, while integrals in equation (97) are triple integrals over the cell domain, for three-dimensional problems. On the other hand, for two-dimensional case, equations (95) and (96) refer to single integrals, while in equation (97) we have double integrals.

The left-hand-side term in equation (85), in turn, can be written as

$$\dot{u}_i(\boldsymbol{\xi}^J) \rightarrow \{\dot{u}^J\}, \quad \text{where} \quad \{\dot{u}^J\} = \begin{Bmatrix} \dot{u}_1(\boldsymbol{\xi}^J) \\ \dot{u}_2(\boldsymbol{\xi}^J) \\ \dot{u}_3(\boldsymbol{\xi}^J) \end{Bmatrix} \text{ (for 3D)}, \quad \begin{Bmatrix} \dot{u}_1(\boldsymbol{\xi}^J) \\ \dot{u}_2(\boldsymbol{\xi}^J) \end{Bmatrix} \text{ (for 2D)} \tag{102}$$

Thus, applying equation (85) to the complete set of internal points results in the following matrix expression, after introducing equations (95), (96), (97) and (102),

$$\bigcup_{J=1}^{M} (\{\dot{u}^J\}) = \bigcup_{J=1}^{M} \biguplus_{e=1}^{N_e} ([G_e^J]) \biguplus_{e=1}^{N_e} (\{\dot{t}^e\}) - \bigcup_{J=1}^{M} \bigcup_{e=1}^{N_e} ([H_e^J]) \bigcup_{e=1}^{N_e} (\{\dot{u}^e\}) + \bigcup_{J=1}^{M} \bigcup_{c=1}^{N_c} ([Q_c^J]) \bigcup_{c=1}^{N_c} (\{\dot{\epsilon}^{o,c}\}),$$

i.e.,

$$\{\dot{u}^\Omega\} = [G^u]\{\dot{t}\} - [H^u]\{\dot{u}\} + [Q^u]\{\dot{\epsilon}^o\} \tag{103}$$

where the superscript Ω in $\{\dot{u}^\Omega\}$ was adopted to indicate that the vector in question is formed by components referring to internal points. Symbols $\bigcup$ and $\biguplus$ are associated with the arrays' assembly forms. The first of them indicates that coefficients relative to the same geometric point are allocated in the same row or column of the matrix. The second indicates that coefficients referring to the interpolation points of two distinct elements, even if such points are geometrically coincident, are allocated in different lines or columns. The presence of only one symbol indicates the assembly of the lines of a vector. If two symbols are used, the first (or left) refers to the assembly of the rows and the second to the columns.

4.1.2 Discrete form of displacement boundary equation

Integrals in equation (86) differ from those of the equation (85) only by the location of the source point: in the former it is on the boundary, Γ. Therefore, equations (95) to (101) remain valid here, as long as the index J is replaced by I (questions concerning the degrees of singularity of the integral kernels are addressed further in this text). In this way, you can write, for a fixed source point on the boundary:

$$\int_{\Gamma_e} u_{ij}^*(\boldsymbol{\xi}^I, \mathbf{x}) \dot{t}_j(\mathbf{x}) d\Gamma \approx \left(\int_{-1}^{+1} [u^*(\boldsymbol{\xi}^I, \eta_k)][N(\eta_k)] \mathcal{J}(\eta_k)\, d\eta_k \right) \{\dot{t}^e\} = [G_e^I]\{\dot{t}^e\} \tag{104}$$

$$\int_{\Gamma_e} t_{ij}^*(\boldsymbol{\xi}^I, \mathbf{x}) \dot{u}_j(\mathbf{x}) d\Gamma \approx \left(\int_{-1}^{+1} [t^*(\boldsymbol{\xi}^I, \eta_k)][N(\eta_k)] \mathcal{J}(\eta_k)\, d\eta_k \right) \{\dot{u}^e\} = [H_e^I]\{\dot{u}^e\} \tag{105}$$

$$\int_{\Omega_c} \sigma_{ijk}^*(\boldsymbol{\xi}^I, \mathbf{x}) \dot{\epsilon}_{jk}^o(\mathbf{x}) d\Omega \approx \left(\int_{-1}^{+1} [\sigma^*(\boldsymbol{\xi}^I, \eta_k)][M(\eta_k)] \bar{\mathcal{J}}(\eta_k)\, d\eta_k \right) \{\dot{\epsilon}^{o,c}\} = [Q_c^I]\{\dot{\epsilon}^{o,c}\} \tag{106}$$

The free term at the left-hand-side in equation (86), on the other hand, assumes the following forms:

$$c_{ij}(\boldsymbol{\xi}^I) \rightarrow [C^I], \quad \text{where}$$

$$[C^I] = \begin{bmatrix} c_{11}(\boldsymbol{\xi}^I) & c_{12}(\boldsymbol{\xi}^I) & c_{13}(\boldsymbol{\xi}^I) \\ c_{21}(\boldsymbol{\xi}^I) & c_{22}(\boldsymbol{\xi}^I) & c_{23}(\boldsymbol{\xi}^I) \\ c_{31}(\boldsymbol{\xi}^I) & c_{32}(\boldsymbol{\xi}^I) & c_{33}(\boldsymbol{\xi}^I) \end{bmatrix} \text{ (3D)}, \quad [C^I] = \begin{bmatrix} c_{11}(\boldsymbol{\xi}^I) & c_{12}(\boldsymbol{\xi}^I) \\ c_{21}(\boldsymbol{\xi}^I) & c_{22}(\boldsymbol{\xi}^I) \end{bmatrix} \text{ (2D)} \tag{107}$$

Taking into account equations (104) to (107), the application of equation (86) to the set of collocation points localized on the boundary, $\boldsymbol{\xi}^I$, leads to

$$\bigcup_{I=1}^{N} \bigcup_{e=1}^{N_e} ([C^I] + [H_e^I]) \bigcup_{e=1}^{N_e} (\{\dot{u}^e\}) = \bigcup_{I=1}^{N} \biguplus_{e=1}^{N_e} ([G_e^I]) \biguplus_{e=1}^{N_e} (\{\dot{t}^e\}) + \bigcup_{I=1}^{N} \bigcup_{c=1}^{N_c} ([Q_c^I]) \bigcup_{c=1}^{N_c} (\{\dot{\epsilon}^{o,c}\}),$$

i.e.,

$$[H]\{\dot{u}\} = [G]\{\dot{t}\} + [Q]\{\dot{\epsilon}^o\} \tag{108}$$

4.1.3 Discrete form of internal strain boundary equation

Considering again a fixed internal collocation point, integrals in equation (87) take the following forms, after introduction of equations (89), (90), (92) and (94):

$$\int_{\Gamma_e} u^*_{ijk}(\boldsymbol{\xi}^J,\mathbf{x})\dot{t}_k(\mathbf{x})d\Gamma \approx \left(\int_{-1}^{1}[\nabla_{\boldsymbol{\xi}}u^*(\boldsymbol{\xi}^J,\eta_k)][N(\eta_k)]\mathcal{J}(\eta_k)d\eta_k\right)\{\dot{t}^e\} = [\bar{G}^J_e]\{\dot{t}^e\} \tag{109}$$

$$\int_{\Gamma_e} t^*_{ijk}(\boldsymbol{\xi}^J,\mathbf{x})\dot{u}_k(\mathbf{x})d\Gamma \approx \left(\int_{-1}^{1}[\nabla_{\boldsymbol{\xi}}t^*(\boldsymbol{\xi}^J,\eta_k)][N(\eta_k)]\mathcal{J}(\eta_k)d\eta_k\right)\{\dot{u}^e\} = [\bar{H}^J_e]\{\dot{u}^e\} \tag{110}$$

$$\int_{\Omega_c} \sigma^*_{ijkl}(\boldsymbol{\xi}^J,\mathbf{x})\dot{\epsilon}^o_{kl}(\mathbf{x})d\Omega \approx \left(\int_{-1}^{1}\int_{-1}^{1}[\nabla_{\boldsymbol{\xi}}\sigma^*(\boldsymbol{\xi}^J,\eta_k)][M(\eta_k)]\bar{\mathcal{J}}(\eta_k)d\eta_k\right)\{\dot{\epsilon}^{o,c}\} = [\bar{Q}^J_c]\{\dot{\epsilon}^{o,c}\} \tag{111}$$

where, for plane problems,

$$[\nabla_{\boldsymbol{\xi}}u^*(\boldsymbol{\xi},\mathbf{x})] = \begin{bmatrix} u^*_{111}(\boldsymbol{\xi},\mathbf{x}) & u^*_{112}(\boldsymbol{\xi},\mathbf{x}) \\ u^*_{221}(\boldsymbol{\xi},\mathbf{x}) & u^*_{222}(\boldsymbol{\xi},\mathbf{x}) \\ u^*_{121}(\boldsymbol{\xi},\mathbf{x}) & u^*_{122}(\boldsymbol{\xi},\mathbf{x}) \end{bmatrix}, \quad [\nabla_{\boldsymbol{\xi}}t^*(\boldsymbol{\xi},\mathbf{x})] = \begin{bmatrix} t^*_{111}(\boldsymbol{\xi},\mathbf{x}) & t^*_{112}(\boldsymbol{\xi},\mathbf{x}) \\ t^*_{221}(\boldsymbol{\xi},\mathbf{x}) & t^*_{222}(\boldsymbol{\xi},\mathbf{x}) \\ t^*_{121}(\boldsymbol{\xi},\mathbf{x}) & t^*_{122}(\boldsymbol{\xi},\mathbf{x}) \end{bmatrix} \tag{112}$$

$$[\nabla_{\boldsymbol{\xi}}\sigma^*(\boldsymbol{\xi},\mathbf{x})] = \begin{bmatrix} \sigma^*_{1111}(\boldsymbol{\xi},\mathbf{x}) & \sigma^*_{1122}(\boldsymbol{\xi},\mathbf{x}) & 2\sigma^*_{1112}(\boldsymbol{\xi},\mathbf{x}) \\ \sigma^*_{2211}(\boldsymbol{\xi},\mathbf{x}) & \sigma^*_{2222}(\boldsymbol{\xi},\mathbf{x}) & 2\sigma^*_{2212}(\boldsymbol{\xi},\mathbf{x}) \\ \sigma^*_{1211}(\boldsymbol{\xi},\mathbf{x}) & \sigma^*_{1222}(\boldsymbol{\xi},\mathbf{x}) & 2\sigma^*_{1212}(\boldsymbol{\xi},\mathbf{x}) \end{bmatrix} \tag{113}$$

Such matrices can be easily extended to three-dimensional problems.

In equation (113), the symmetry $\sigma^*_{ij12} = \sigma^*_{ij21}$ was considered and, again, a fourth column needs to be added for plane strain problems, to take into account terms σ^*_{ij33}.

Matrix forms for the left-hand side vector and for the last term in equation (87) are given, respectively, by

$$\dot{\epsilon}_{ij}(\boldsymbol{\xi}^J) \rightarrow \{\dot{\epsilon}^J\} \quad \text{where} \quad \{\dot{\epsilon}^J\} = \begin{Bmatrix} \dot{\epsilon}_{11}(\boldsymbol{\xi}^J) \\ \dot{\epsilon}_{22}(\boldsymbol{\xi}^J) \\ \dot{\epsilon}_{33}(\boldsymbol{\xi}^J) \\ \dot{\epsilon}_{12}(\boldsymbol{\xi}^J) \\ \dot{\epsilon}_{13}(\boldsymbol{\xi}^J) \\ \dot{\epsilon}_{23}(\boldsymbol{\xi}^J) \end{Bmatrix} \text{ (for 3D)}, \quad \{\dot{\epsilon}^J\} = \begin{Bmatrix} \dot{\epsilon}_{11}(\boldsymbol{\xi}^J) \\ \dot{\epsilon}_{22}(\boldsymbol{\xi}^J) \\ \dot{\epsilon}_{12}(\boldsymbol{\xi}^J) \end{Bmatrix} \text{ (for 2D)} \tag{114}$$

and

$$F^{\epsilon\epsilon}_{ijkl}\dot{\epsilon}^o_{kl}(\boldsymbol{\xi}^J) = \begin{bmatrix} F^{\epsilon\epsilon}_{1111} & F^{\epsilon\epsilon}_{1122} & 2F^{\epsilon\epsilon}_{1112} \\ F^{\epsilon\epsilon}_{2211} & F^{\epsilon\epsilon}_{2222} & 2F^{\epsilon\epsilon}_{2212} \\ F^{\epsilon\epsilon}_{1211} & F^{\epsilon\epsilon}_{1222} & 2F^{\epsilon\epsilon}_{1212} \end{bmatrix} \begin{Bmatrix} \dot{\epsilon}^o_{11}(\boldsymbol{\xi}^J) \\ \dot{\epsilon}^o_{22}(\boldsymbol{\xi}^J) \\ \dot{\epsilon}^o_{12}(\boldsymbol{\xi}^J) \end{Bmatrix} = [F^{\epsilon\epsilon,J}]\{\dot{\epsilon}^{o,J}\} \quad \text{(for 2D)} \tag{115}$$

where this last relation also can be easily extended to the 3D case.

Finally, considering the above equations and applying equation (87) to all internal collocation points, we obtain:

$$\bigcup_{J=1}^{M}(\{\dot{\epsilon}^J\}) = \bigcup_{J=1}^{M}\biguplus_{e=1}^{N_e}([\bar{G}^J_e])\biguplus_{e=1}^{N_e}(\{\dot{t}^e\}) - \bigcup_{J=1}^{M}\bigcup_{e=1}^{N_e}([\bar{H}^J_e])\bigcup_{e=1}^{N_e}(\{\dot{u}^e\}) + \bigcup_{J=1}^{M}\bigcup_{c=1}^{N_c}([\bar{Q}^J_c]+[F^{\epsilon\epsilon,J}])\bigcup_{c=1}^{N_c}(\{\dot{\epsilon}^{o,c}\}),$$

i.e.,

$$\{\dot{\epsilon}\} = [G^\epsilon]\{\dot{t}\} - [H^\epsilon]\{\dot{u}\} + [Q^\epsilon]\{\dot{\epsilon}^o\} \tag{116}$$

4.1.4 Integrals numerical treatment

The integrals of the discrete equations (85), (86) and (87) are usually performed numerically, through the boundary elements and cells. For plane problems the integrals are line integrals on the boundary and area integrals at the domain, while for three-dimensional problems the integrals are area integrals on the boundary and volume integrals at the domain. The nature of the kernel, and the relative position of the collocation point with respect to the element on which the integration is being performed, defines if the type of the integral, that can be classified as regular or singular. The technique to solve those integrals are chosen accordingly.

Regular Integrals and Nearly Singular Integrals

Integrals are considered regular when the collocation point do not coincides with an element point. The regular integrals are performed through standard Gauss quadrature. For computational efficiency it is possible to choose the number of integration points according to a fixed tolerance error (e.g. 10^{-3}), therefore, it varies according to the distance from the collocation point to the element where integration is being carried out. Criterium proposed by Eberwien et al. [2005] present the number of integration points according to the line integral kernel singularity. This criterion can be extended for area and volume integrals.

When the collocation point is close to the element under consideration, the integral is said to be nearly singular, and special treatment is required as the integrand varies sharply. The element subdivision technique is an efficient approach for dealing with these integrals. A simple way is to subdivide the element into equal subintervals, as presented in Beer et al. [2008], where the number of subdivision is determined in order to preserve the integration accuracy. This technique can be extended for area and volume integrals aswell.

Singular Integrals

Singular integral occurs when the collocation point lies within the element being integrated. They are classified as weakly singular integrals when the singularity of the kernel is of order $O(ln(1/r))$ for two-dimensional problems or $O(1/r)$ for three-dimensional problems. The integrals in equations (95) and (104) are possibly in this case. On the other hand, if the singularity of the integral kernel is of order $O(1/r)$ for two-dimensional problems or $O(1/r^2)$ for three-dimensional problems, they are classified as strongly singular integrals, and are considered in the Cauchy principal value sense. This might be the case for the integrals in equations (96), (105), (106) and (109). Finally, integrals with kernel of high singularity order, i.e., $O(1/r^2)$ for two-dimensional or $O(1/r^3)$ for three-dimensional problems, respectively, are said to be hypersingular integrals, considered as Hadamard principal value sense. Equations (110) and (111) may carry this type of integrals.

For two-dimensional problems boundary elements (one dimension) the weakly singular integrals can be evaluated using a logarithmic Gauss quadrature, as presented by Huang [1993], while for the the strongly singular integrals the technique proposed by Guiggiani and Casalini [1987] is usual.

The treatment of integrals for cells in two-dimensional problems and the boundary elements in three-dimensional problems are similar (area integrals). Weakly singular integrals can be performed through a variable transformation by an element subdivision technique proposed by Lachat and Watson [1976], while for the strongly singular integrals Guiggiani and Gigante [1990] presented an efficient technique.

The volume weakly singular integrals in three-dimensional cells can also be performed using the cell subdivision technique proposed by Lachat and Watson [1976]. Strongly singular integrals cam be evaluated using the technique proposed by Gao and Davies [2000], where the integral can

be divided in two parts, in such way that the first part is weakly singular and can be integrated by the technique previously mentioned, whilst the second part, with the strong singularity, is evaluated semi-analytically.

Direct evaluation of CPV integrals in the free-therm c_{ij}, present in equation (86) (see figure 8), can be avoided by using the rigid body motion concept. Similarly, the use of the so called stress recovery technique may dispense the direct evaluation of hypersingular integrals, for the assessment of strains and stresses on the boundary. These well known approaches are detailed in Beer et al. [2008] and Gao and Davies [2002].

4.2 Solution strategy

The matrix equations obtained in section 4.1 can be algebraically manipulated in order to generate a single non linear equation, typical of the implicit BEM formulation, developed by Telles and Carrer [1991]. Such equation is first obtained in the present section, followed by its the solution strategy, presented in Peixoto et al. [2016], which has the advantage of encapsulate different control methods in a single computational framework.

Considering the essential and natural boundary conditions, equations (103), (108) and (116) can be respectively reorganized in the next forms:

$$\{\dot{u}^{\Omega}\} = [A^u]\{\dot{x}\} + [B^u]\{\dot{y}\} + [Q^u]\{\dot{\epsilon}^o\} \tag{117}$$

$$[A]\{\dot{x}\} = [B]\{\dot{y}\} + [Q]\{\dot{\epsilon}^o\} \tag{118}$$

$$\{\dot{\epsilon}\} = [A^{\epsilon}]\{\dot{x}\} + [B^{\epsilon}]\{\dot{y}\} + [Q^{\epsilon}]\{\dot{\epsilon}^o\} \tag{119}$$

where, in $\{\dot{y}\}$ the prescribed values on the boundary are grouped, coming from $\{\dot{\hat{u}}\}$ or $\{\dot{t}\}$, while the vector $\{\dot{x}\}$ contains the unknown components of these fields. Matrices referenced by $[A]$ and $[B]$, on the other hand, are composed by coefficients from those referenced by $[H]$ and $[G]$. In reality, computationally speaking, the matrix equations are already assembled directly in these last forms, without the need to go through a rearrangement step.

Solving for $\{\dot{x}\}$ in equation (118), we obtain

$$\{\dot{x}\} = [N]\{\dot{y}\} + [M]\{\dot{\epsilon}^o\} \tag{120}$$

where

$$[N] = [A]^{-1}[B]; \quad [M] = [A]^{-1}[Q] \tag{121}$$

Thus, applying equation (120) into (117) and (119), the following results are respectively ontained:

$$\{\dot{u}^{\Omega}\} = [N^u]\{\dot{y}\} + [M^u]\{\dot{\epsilon}^o\} \tag{122}$$

$$\{\dot{\epsilon}\} = [N^{\epsilon}]\{\dot{y}\} + [M^{\epsilon}]\{\dot{\epsilon}^o\} \tag{123}$$

where

$$[N^u] = [A^u][A]^{-1}[B] + [B^u]; \quad [M^u] = [A^u][A]^{-1}[Q] + [Q^u] \tag{124}$$

$$[N^{\epsilon}] = [A^{\epsilon}][A]^{-1}[B] + [B^{\epsilon}]; \quad [M^{\epsilon}] = [A^{\epsilon}][A]^{-1}[Q] + [Q^{\epsilon}] \tag{125}$$

For rate independent constitutive models (as the ones presented in Appendix A), the time derivatives can be substituted by finite increments, i.e., $\dot{(\cdot)} = \Delta(\cdot) \equiv (\cdot)_i - (\cdot)_{i-1}$, where i is an incremental index. In this way, for the i-th increment of the the prescribed loads, $\{y\}$, equations (120), (122) and (123) can be rewritten as

$$\{x\}^i = \lambda^i[N]\{y\} + [M]\{\epsilon^o\}^i \tag{126}$$

$$\{u^{\Omega}\}^i = \lambda^i [N^u]\{y\} + [M^u]\{\epsilon^o\}^i \tag{127}$$

$$\{\epsilon\}^i = \lambda^i [N^\epsilon]\{y\} + [M^\epsilon]\{\epsilon^o\}^i \tag{128}$$

where the parameter λ^i, known as load factor, is a cumulative scalar quantity that defines the amount of external load is necessary, at each increment, to guarantee the mechanical equilibrium.

From equation (128), it is possible to define an equilibrium vector in function of strain and the load factor, $\{Q\}^i \equiv \{Q(\epsilon^i, \lambda^i)\}$, introducing also equation (66), i.e.,

$$\{Q\}^i = \lambda^i [N^\epsilon]\{y\} + [M^\epsilon]\big(\{\epsilon\}^i - [C]^{-1}\{\sigma(\epsilon)\}^i\big) - \{\epsilon\}^i = \{0\} \tag{129}$$

where $[C]$ represents the quasi-diagonal linear elastic constitutive matrix, referring to the set of internal collocation points.

Vector $\{\sigma(\epsilon)\}$ refers to the stress field obtained from a given strain state, according with the constitutive model adopted.

The fact that the initial fields, ϵ^o_{ij}, do not appear explicitly in the equation (129) justifies the naming of implicit formulation originally adopted by Telles and Carrer [1991]. Normally, this equation is solved by Newton's method, based on its linearization in relation to the total strain vector, together with a specific equation that adequately establishes the increase in external loads. On the other hand, in the solution strategy presented in Peixoto et al. [2016], which is based on the ideas of Batoz and Dhatt [1979] and Yang and Shieh [1990], the load factor is treated as an additional variable of $\{Q\}^i$ and the linearization procedure must be performed taking this into account. In this way, the algorithm becomes generic enough to adopt different control methods for non linear analysis. The description of this strategy begins, rewriting equation 129 as follows:

$$\{Q\}^i = \lambda^i \{P\} - \{F\}^i = \{0\} \tag{130}$$

where

$$\{P\} = [N^\epsilon]\{y\} \tag{131}$$

$$\{F\}^i = \{\epsilon\}^i - [M^\epsilon]\big(\{\epsilon\}^i - [C]^{-1}\{\sigma(\epsilon)\}^i\big) \tag{132}$$

Thus, linearizing equation (130), i.e.,

$$\{Q\}^i_{j-1} + \left[\frac{\partial\{Q\}}{\partial\{\epsilon\}}\right]^i_{j-1}\{\delta\epsilon\}^i_j + \left[\frac{\partial\{Q\}}{\partial\lambda}\right]^i_{j-1}\delta\lambda^i_j \approx \{0\} \tag{133}$$

where j is an iterative index and $\delta(\cdot)^i_j = (\cdot)^i_j - (\cdot)^i_{j-1}$, the following result is obtained:

$$[D]^i_{j-1}\{\delta\epsilon\}^i_j = \delta\lambda^i_j\{P\} + \{Q\}^i_{j-1} \tag{134}$$

in which

$$[D]^i_{j-1} = \left[[I] - [M^\epsilon][C]^{-1}\left([C] - \left[\frac{\partial\sigma}{\partial\epsilon}\right]^i_{j-1}\right)\right] \tag{135}$$

where $[I]$ is an identity matrix and $\left[\frac{\partial\sigma}{\partial\epsilon}\right]$ is assembled from the tangent operator of the constitutive model, C^t_{ijkl}, particularized by equations (49) or (63), respectively, for elastoplastic or elastic-degrading constitutive models.

The iterative strain vector in equation (134), $\{\delta\epsilon\}^i_j$, can be dismembered in the following parcels:

$$\{\delta\epsilon\}^i_j = \delta\lambda^i_j\{\epsilon^P\}^i_j + \{\delta\epsilon^Q\}^i_j \tag{136}$$

where vector $\{\epsilon^P\}^i_j$ corresponds to the solution associated to the external load $\{P\}$, while $\{\delta\epsilon^Q\}^i_j$ is associated to the residual, $\{Q\}^i_{j-1}$, i.e.,

$$[D]^i_{j-1}\{\epsilon^P\}^i_j = \{P\} \tag{137}$$

$$[D]^i_{j-1}\{\delta\epsilon^Q\}^i_j = \{Q\}^i_{j-1} \tag{138}$$

Thus, in a given iteration, equations (137) and (138) can be solved independently and the correction of strains is obtained by equation (136), after evaluation of $\delta\lambda^i_j$, through a chosen control method. This sequence of activities is further systematized in section 4.2.1. Before that, expressions for the iterative corrections of vectors containing the boundary unknowns and the internal displacements, i.e., $\{\delta x\}^i_j$ and $\{\delta u^\Omega\}^i_j$, are shown. The same idea of breaking up equation (134) is followed and such expressions are important for application to the different control methods, listed in section 4.2.2.

Considering equations (126) and (128), it is possible to write

$$\{\delta x\}^i_j = \{x\}^i_j - \{x\}^i_{j-1} = \delta\lambda^i_j[N]\{y\} + [M]\{\delta\epsilon^o\}^i_j \tag{139}$$

$$\{\delta\epsilon\}^i_j = \{\epsilon\}^i_j - \{\epsilon\}^i_{j-1} = \delta\lambda^i_j[N^\epsilon]\{y\} + [M^\epsilon]\{\delta\epsilon^o\}^i_j \tag{140}$$

Isolating vector $\{\delta\epsilon^\varphi\}^i_j$ in equation (140) and substituting the result into the last term of equation (139), after application of equations (131), (136) and (137), the next result is obtained:

$$\{\delta x\}^i_j = \delta\lambda^i_j\{x^P\}^i_j + \{\delta x^Q\}^i_j \tag{141}$$

where

$$\{x^P\}^i_j = [N]\{y\} + [M][M^\epsilon]^{-1}\big([I] - [D]^i_{j-1}\big)\{\epsilon^P\}^i_j \tag{142}$$

$$\{\delta x^Q\}^i_j = [M][M^\epsilon]^{-1}\{\delta\epsilon^Q\}^i_j \tag{143}$$

Similarly, starting from equation (127), one can show that

$$\{\delta u^\Omega\}^i_j = \delta\lambda^i_j\{u^{\Omega,P}\}^i_j + \{\delta u^{\Omega,Q}\}^i_j \tag{144}$$

where

$$\{u^{\Omega,P}\}^i_j = [N^u]\{y\} + [M^u][M^\epsilon]^{-1}\big([I] - [D]^i_{j-1}\big)\{\epsilon^P\}^i_j \tag{145}$$

$$\{\delta u^{\Omega,Q}\}^i_j = [M^u][M^\epsilon]^{-1}\{\delta\epsilon^Q\}^i_j \tag{146}$$

4.2.1 Non linear algorithm

The above equations, can be organized in a systematic procedure as described below.

i. Evaluate $\{P\}$, using equation (131), and initialize $i = 0$;

ii. $i = i + 1$, $j = 0$;

iii. Se $i >$ maximum number of increments $\Rightarrow$ STOP;

iv. $\{Q\}^i_j = \{0\}$, $\{F\}^i_j = \{0\}$;

v. $j = j + 1$;

vi. Se $j >$ maximum number of iterations $\Rightarrow$ STOP;

vii. Mount matrix $[D]^i_{j-1}$, from equation (135);

viii. Solve equations (137) and (138) for $\{\epsilon^P\}^i_j$ e $\{\delta\epsilon^Q\}^i_j$;

ix. Evaluate $\{x^P\}^i_j$, $\{\delta x^Q\}^i_j$, $\{u^{\Omega,P}\}^i_j$ e $\{\delta u^{\Omega,Q}\}^i_j$, using equations (142), (143), (145) and (146);

x. Evaluate $\delta\lambda_j^i$, from a chosen control method (see section 4.2.2);

xi. Mount $\{\delta\epsilon\}_j^i$, $\{\delta x\}_j^i$ e $\{\delta u^\Omega\}_j^i$, using equations (136), (141) and (144);

xii. Actualize λ_j^i, $\{\hat{\epsilon}\}_j^i$, $\{x\}_j^i$ and $\{\hat{u}^\Omega\}_j^i$, using $(\cdot)_j^i = (\cdot)_{j-1}^i + \delta(\cdot)_j^i$;

xiii. Mount $\{F\}_j^i$, from equation (132);

xiv. Evaluate $\{Q\}_j^i = \lambda_j^i\{P\} - \{F\}_j^i$ (equation 130);

xv. Verify convergence:

If $\dfrac{\parallel \{Q\}_j^i \parallel}{\parallel \lambda_j^i\{P\} \parallel} <$ Tolerance, return to step (ii) for the next load increment, else, return to step (v) for a new iteration.

4.2.2 Control methods

The most prominent advantage of the approach described above is its generality, especially for being able to work with different control methods.

Control methods are equations which determine the load factor increment, $\delta\lambda_j^i$, at each iteration. Depending mainly on the material behaviour, a specific control method has its advantages and its limitations or disadvantages. For this reason, a great number of them were developed and some are summarized in table 1.

Table 1: Types of control methods.

Control method	$\delta\lambda_j$ for $j = 1$	$\delta\lambda_j$ for $j > 1$
Load control	constant	$\delta\lambda_j = 0$
Direct displacement	$\dfrac{\delta U_1^k}{U_1^{P,k}}$	$-\dfrac{\delta U_j^{Q,k}}{U_j^{P,k}}$
Arc length	$\pm\dfrac{\Delta S}{\sqrt{\{U^P\}_1^T\{U^P\}_1}}$	$-\dfrac{\{\Delta U\}_1^T\{\delta U^Q\}_j}{\{\Delta U\}_1^T\{U^P\}_j}$
Generalized displacement	$\delta\lambda_1^1\sqrt{\dfrac{\{U^P\}_1^{1,T}\{U^P\}_1^1}{\{U^P\}_1^{i-1,T}\{U^P\}_1^{i-1}}}$	$-\dfrac{\{U^P\}_1^{i-1,T}\{U^Q\}_j^i}{\{U^P\}_1^{i-1,T}\{U^P\}_j^{i-1}}$
Strain control	$\dfrac{\Delta e}{\{C^\Omega\}^T\{\epsilon^P\}_1}$	$-\dfrac{\{C^\Omega\}^T\{\delta\epsilon^Q\}_j}{\{C^\Omega\}^T\{\epsilon^P\}_j}$

Herein the vector $\{U\}$ stands for a simple collection of all displacements values at boundary and domain collocation points which, when not prescribed, are evaluated at each iteration, and has the following increment decomposition:

$$\{\delta U\}_j = \delta\lambda_j\{U^P\}_j + \{\delta U^Q\}_j \tag{147}$$

where index j stands for an iteration in an increment i, which has been omitted for clearer presentation.

In the standard load control method, the load factor is pre-defined at the beginning of the increment and no variations are made during the iterative procedure. As is well known, this method inevitably results in non-convergence when the material exhibits softening behaviour. In the direct

displacement control method, as developed by Batoz and Dhatt [1979], a specific displacement component (of a specific point), identified by the superscript k in table 1, is selected to be controlled. If this component is correctly chosen, the divergence problem in softening behaviour can be solved, however, instabilities may occur if a snap-back trajectory is present in the equilibrium path. For that reason, arc-length methods, where a combination of displacement components and load factor increments is controlled, were developed. In expressions for this method, ΔS is the constant which limits the increment advance and $\{\Delta U\}_j$ means the cumulative displacements in the current increment, until iteration j. Usually, two different variations of arc-length control can be adopted. In the first, as used by Riks [1972] and Riks [1979], the iterative correction trajectory is always orthogonal to the first tangent of the increment, as represented in column for $j > 1$ in table 1. In the second variation, proposed by Crisfield [1981] and Crisfield [1983], a cylindrical trajectory is taken from the solution of a quadratic equation. With the intention to automatize the size of the incremental step, Yang and Shieh [1990], introduced the generalized displacement method, which relates two successive incremental steps, designated by i and $i-1$ in the expressions presented in table 1.

For some problems, it seems to be more efficient to control a linear combination of some strain components of a limited region of the domain. Thus, the strain control method, developed by Chen and Schreyer [1990], can be used as an alternative. In the equations of table 1, Δe is a scalar value which limits the mentioned linear combination and $\{C^{\Omega}\}$ is the weight vector which determines the influence of each strain component.

5 Examples of Continuum Non Linear Problems

In this section the numerical analyses of three-dimensional and plane problems, involving elastoplastic and continuum damage models, performed with the presented formulation and algorithm, are presented. The results are compared to those obtained experimentally or analytically. For all examples, the control method adopted to drive the incremental-iterative procedure in the non linear analyses, considered a convergence tolerance of 10^{-4}.

In the first and second examples, the von Mises elastoplastic model is applied to a perforated strip with linear hardening and a pressurized thick cylinder, respectively. For the third example, the isotropic constitutive models of Simo and Ju [1987] and Oliver et al. [1990] were applied with an exponential damage evolution law for the analysis of a three-point bending beam. Three-dimensional and plane analysis were performed in all examples.

5.1 Example 1: perforated strip

In this example the case of a perforated strip under uniaxial tension is analyzed. Reference results where obtained experimentally by Theocaris and Marketos [1964] using the aluminum alloy $57S$, who assume the Mises yield criterion to be the most suitable and accepted as governing the mode of nucleation and evolution of plastic enclaves for such material. The geometry of this thin plate is presented in Figure 12, were the geometric parameters are $h = 18$ mm, $r = 5$ mm and thickness 1 mm.

The elastoplastic von Mises associative constitutive model, as detailed in Appendix A.1, is used with the Young's modulus $E = 70$ GPa, the Poisson's ratio $\nu = 0.2$, the initial yield limit $\sigma_Y = 243$ MPa and a linear hardening law with $H = 0.032E$. The tensile load is taken to be $\sigma = 0.47\sigma_Y$.

Due to the symmetry, only a quarter of the plane problem is discretized, following the analysis presented in Aliabadi [2002]. Only part of the domain, where dissipative effects are probable to occur, need to be discretized.

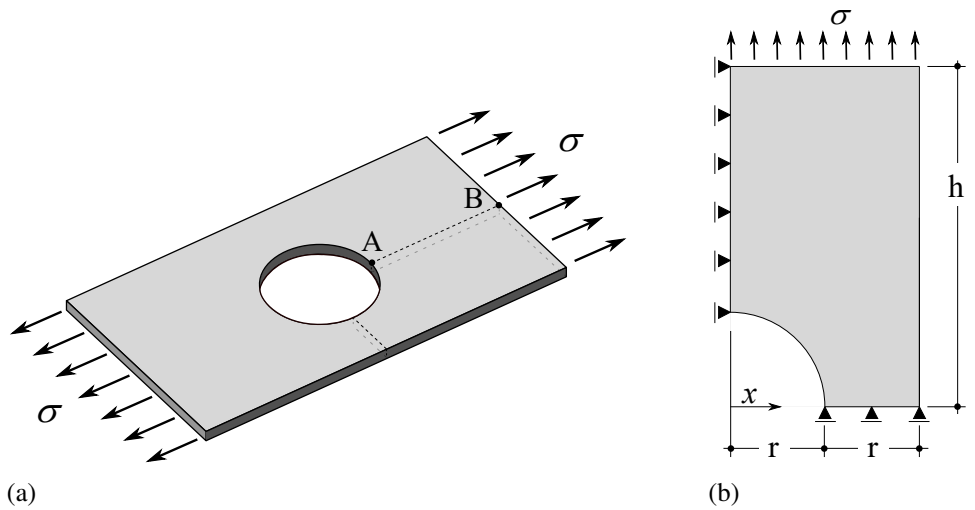

Figure 12: Example 1 – Perforated strip; (a) Geometry and load, (b) Plane model dimensions

Plane stress was considered in bidimensional analysis, where the analysis were performed with two different meshes: a coarse one (Mesh 1) with 32 quadratic boundary elements and 16 quadratic quadrilateral cells, and a fine one (Mesh 2) with 64 linear boundary elements and 64 linear quadrilateral cells. Also, the analysis where performed with three-dimensional model. In this case, due to the symmetry, only one eight of the problem was discretized in other two meshes: a coarse one (Mesh 3) with 448 linear quadrilateral boundary elements and 64 constant hexahedral cells, and a fine one (Mesh 4) with 1664 boundary elements and 256 cells. The used meshes can be seen in Figure 13.

In both analysis, the usual load control was adopt, with a total of 50 load steps. Experimental and numerical results are plotted in Figure 14. Additionally, in Figure 15 stress-displacement plots obtained for the refined meshes (Mesh 2 and Mesh4) are shown for some key positions on the strip, together with FEM results presented by Aliabadi [2002].

5.2 Example 2: pressurized thick cylinder

This example presents a steel thick cylinder subjected to internal pressure. The internal and external radius were taken as 100 mm and 200 mm, respectively. Due to the symmetry of the problem, only one quarter of a section is modelled. The problem is considered under plain strain conditions. For three-dimensional analysis, the transversal section planes have displacements restricted in the longitudinal direction, in order to make the analysis under a plane strain condition. The solid modelled also consider one quarter of a section, with width 5.0 mm. Figure 16 illustrates the geometry, load and support conditions.

Again, the elastoplastic von Mises associative constitutive model was adopted, with the Young's modulus $E = 210$ GPa, the Poisson's ratio $\nu = 0.3$ and the yield limit $\sigma_Y = 240$ MPa. Perfect plasticity were considered, with hardening parameter $H = 0$. The internal pressure was taken to be $\sigma = 180$ MPa. An analytical solution for this problem, performed by Hill [1950], is presented in de Souza Neto et al. [2006].

Two different meshes were analysed under plane strain conditions. The coarse mesh (Mesh 1) has 24 quadratic boundary elements and 32 quadratic internal cells, while the (Mesh 2) has 48 quadratic boundary elements and 128 quadratic cells. The mesh used in the three-dimensional analysis (Mesh 3) has 648 linear quadrilateral boundary elements and 288 hexahedral constant

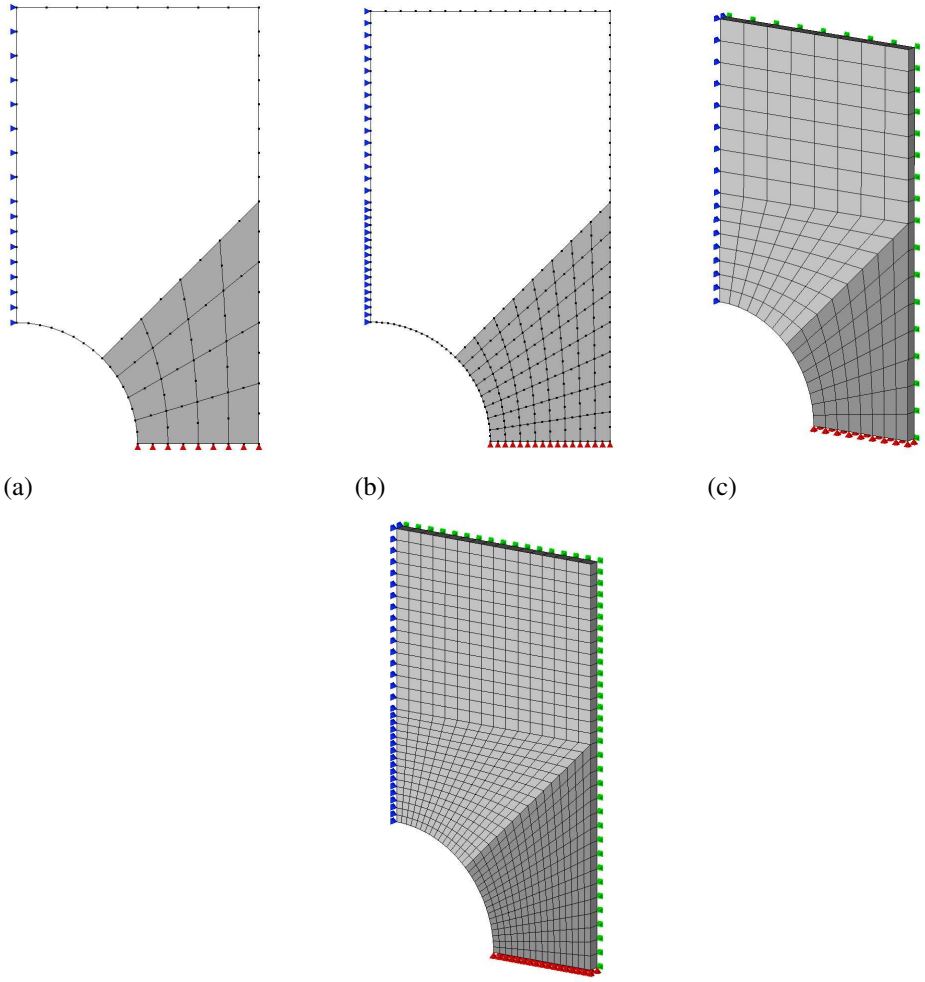

Figure 13: Example 1 – Meshes considered in the analyses; (a) Mesh 1, (b) Mesh 2, (c) Mesh 3, (d) Mesh 4

cells. A total of 30 steps, with load control, were used in the whole cases. Figure17 illustrates the the refereed meshes.

The results achieved for hoop and radial stresses components, together with the analytical solution are plotted in Figures 18 and 19 respectively.

5.3 Example 3: three point bending

The three point bending of a notched concrete beam, experimentally treated by Petersson [1981], is addressed in this example. The problem geometry, load and supports are depicted in Figure 20. The geometrical parameters were taken as $l = 1000$ mm, $h = 200$ mm, $a = 100$ mm and $w = 20$ mm. A width $t = 50$ mm was considered for the beam.

To represent the concrete softening behaviour, the isotropic constitutive models of Simo and Ju [1987] and Oliver et al. [1990] were applied with an exponential damage evolution law of the form

$$D(\phi) = 1 - \left[\frac{\kappa_o}{\phi}\right] e^{-b(\phi-\kappa_o)}, \quad \text{with} \quad \kappa_o = \frac{f_t}{\sqrt{E}} \quad \text{and} \quad b = \frac{h f_t}{G_f \sqrt{E}} \tag{148}$$

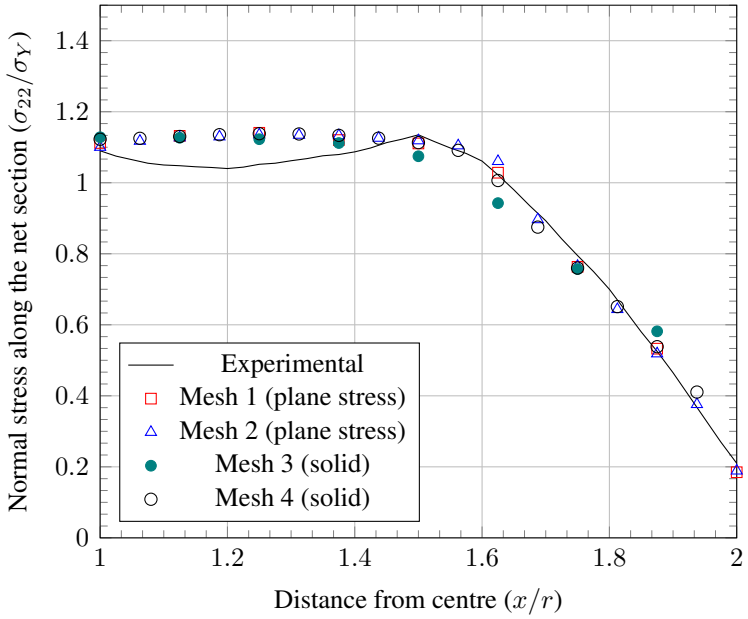

Figure 14: Example 1 – Computed stresses on net section of the plate for a load of $0.47\sigma_Y$, and the experimental reference [Theocaris and Marketos, 1964].

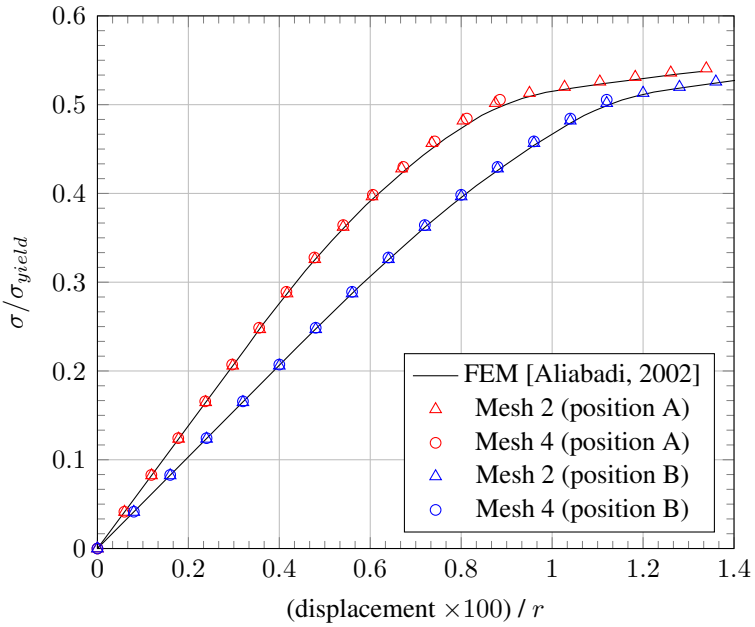

Figure 15: Example 1 – Displacements at positions A and B (from Figure 12)

where f_t is the uni-axial tensile strength, G_f is the fracture energy, h is a material's characteristic length and E is the Young's modulus. For concrete mechanical properties, the following values were adopted: $f_t = 3.33$ MPa, $G_f = 0.124$ N/mm, $h = 30$ mm and $E = 30$ GPa and Poisson's ratio $\nu = 0.20$.

Only the domain's region around the expected area to be damaged was discretized by cells. For the plane stress analysis a total of 100 constant internal cells were employed, while the boundary was divided in 392 linear elements. For the three-dimensional analysis, the mesh has 952 quadri-

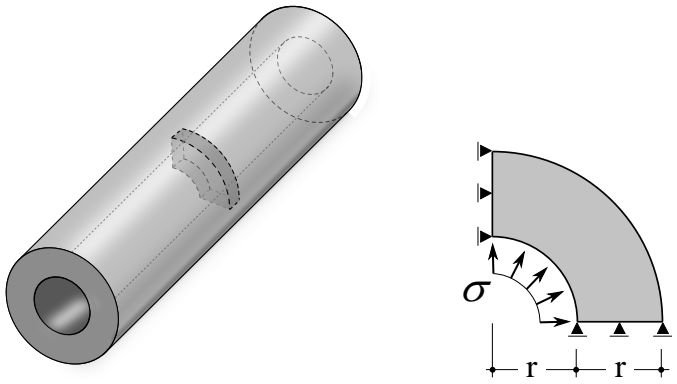

(a) (b)

Figure 16: Example 2 – Pressurized thick cilinder; (a) Geometry, (b) Plane model dimensions and supports

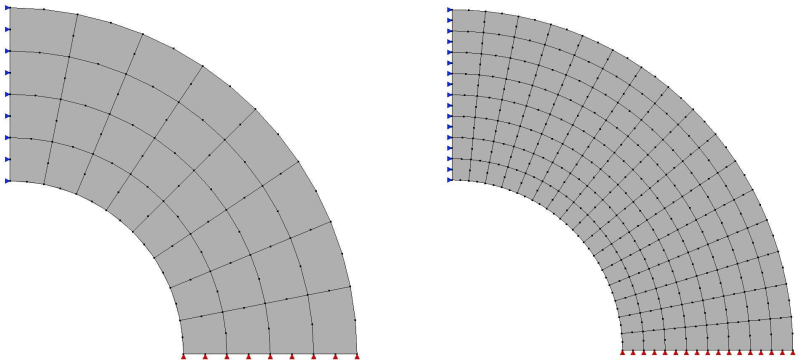

(a)
Mesh1

(b)
Mesh2

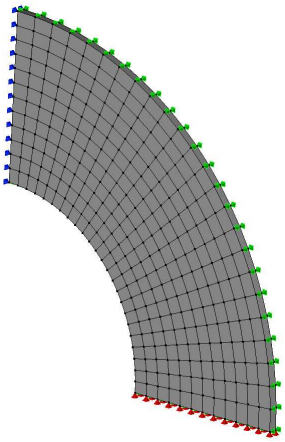

(c)
Mesh3

Figure 17: Example 2 – Meshes considered in the analyses

lateral quadratic elements and 36 hexahedral constant cells. Figure 21 illustrates these meshes. The analyses were performed by controlling the vertical displacement of a loaded element node.

A comparison between the models results and Petersson's experimental envelopment is pre-

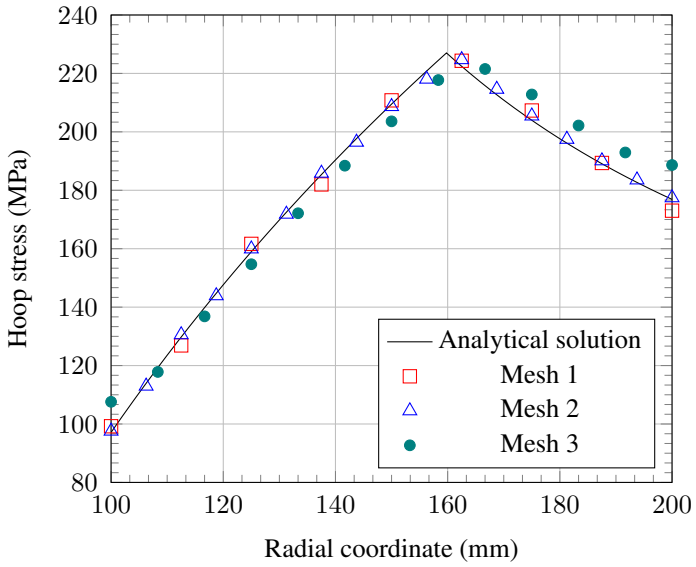

Figure 18: Example 2 – Computed circumferential stress distribution in the pressurized cylinder along the radial coordinate, and the analytical solution [de Souza Neto et al., 2006].

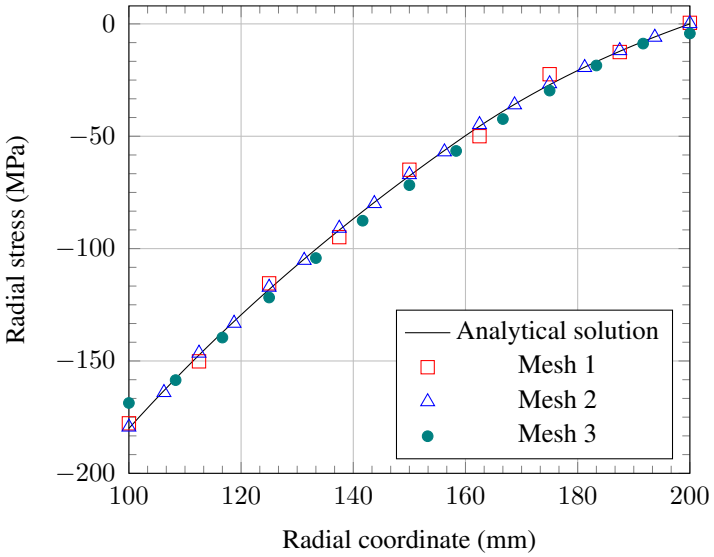

Figure 19: Example 2 – Computed radial stress distribution in the pressurized cylinder along the radial coordinate, and the analytical solution [de Souza Neto et al., 2006].

sented in Figure 22.

Since the region close to the applied load is subjected to compressive stress states, spurious damage evolution is verified for Simo and Ju [1987] model, leading to a premature loss of structural strength. However, for the Oliver et al. [1990] model, where the equivalent strain norm involves only positive strain components, as detailed in Appendix A.2, such problem is overcome and a good agreement between the numerical and experimental results is obtained.

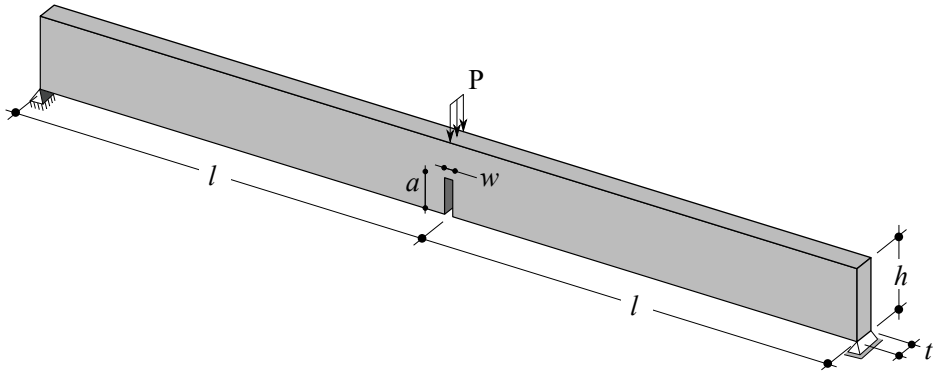

Figure 20: Example 3 – Three point bending of a concrete notched beam: geometry, load and supports.

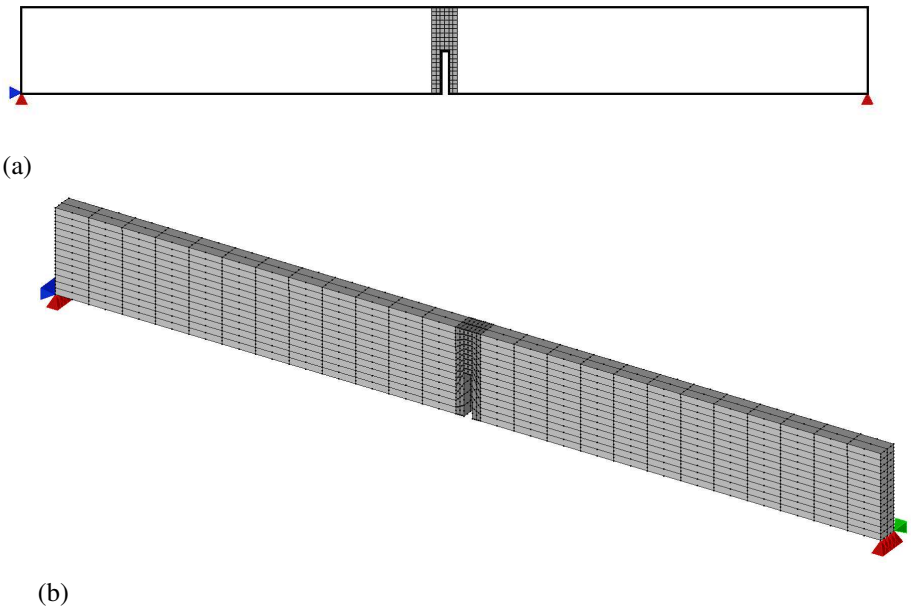

(a)

(b)

Figure 21: Example 3 – Meshes considered in the analyses (a) plane stress and (b) three-dimensional

6 Strain Localization and Material Bifurcation Analysis

This section addresses the necessary conditions for the occurrence of discontinuous bifurcation in material media that present softening laws in their continuous (or macroscopic) constitutive formulation. By bifurcation, we mean the instant of inelastic loading at which the strain field is no longer continuous, which does not necessarily correspond to the appearance of discontinuities in the displacement field. In this case, there is the emergence of the so-called weak discontinuity surfaces. From there, strain localization bands (regions of high strain values) can be formed, delimited by such surfaces.

Strain localization in homogeneous media with softening is associated with the loss of the elliptical character of the set of differential equations and, consequently, the boundary value problem becomes ill-defined. As a result, the solution is no longer unique and, in numerical analyses, a lack of objectivity in relation to mesh refining is verified, since the most stable solution corresponds to

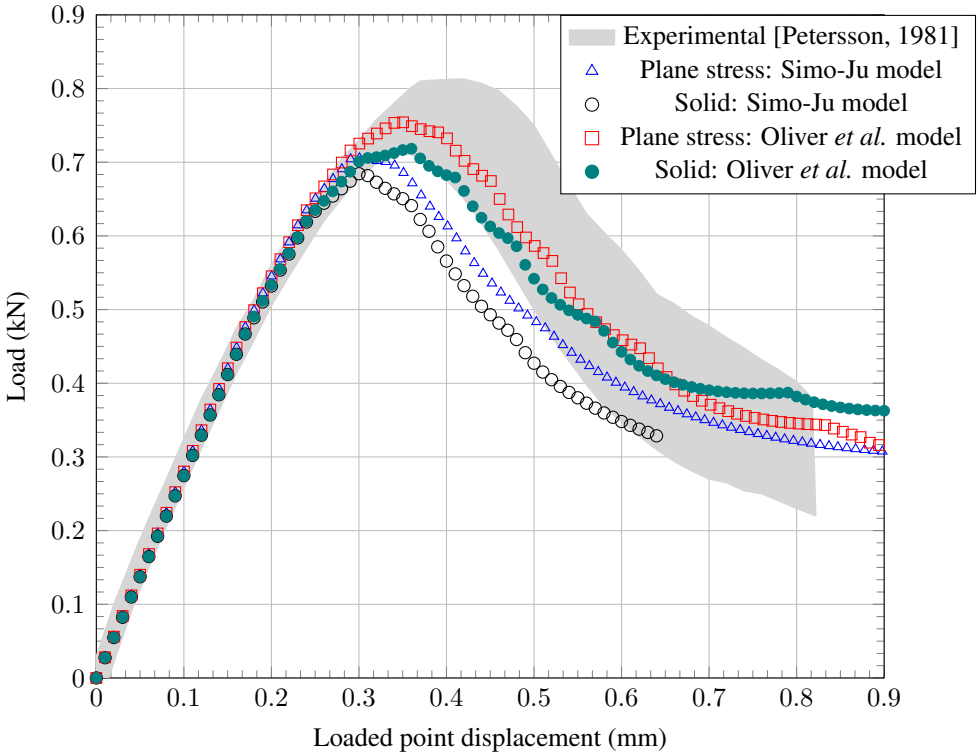

Figure 22: Example 3 – Results for vertical displacement of the loaded point: numerical BEM analyses and experimental.

a zero-thickness localization band without energy dissipation during failure.

In general, bifurcation does not coincide with the beginning of the inelastic regime. Normally, from a macroscopic point of view, it is preceded by a dissipation phase in a continuous medium. Thus, based on a valid mathematical formalism for time-independent constitutive models, the necessary conditions for the appearance of strain localization are established in the following.

It starts by assuming a homogeneous three-dimensional solid domain Ω, subject to a uniform state of small deformations ϵ_{ij}. We then look for the necessary conditions so that the rate of the strain field, $\dot{\epsilon}_{ij}$, can become discontinuous on two surfaces that delimit a band $\Omega_b \subset \Omega$, as indicated in Figure 23. It is also assumed that the two surfaces have parallel tangent planes at the point under analysis, so that a single orthonormal basis $\{\mathbf{n}, \mathbf{p}, \mathbf{q}\}$ can be established, where $\mathbf{n}$ is the unit vector normal to these planes.

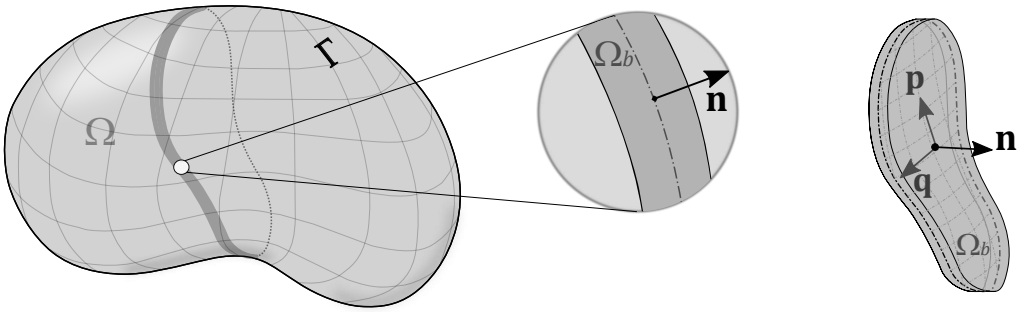

Figure 23: Solid domain with strain localization band

Considering now that the displacement rate, $\dot{u}_i$, remains continuous on the two surfaces, we

have:

$$[\![\partial_{\mathbf{q}} \dot{u}_i]\!] = [\![\dot{u}_{i,j}]\!] q_j = 0 \tag{149a}$$

$$[\![\partial_{\mathbf{p}} \dot{u}_i]\!] = [\![\dot{u}_{i,j}]\!] p_j = 0 \tag{149b}$$

where $[\![\cdot]\!]$ represents the difference between the values of field $(\cdot)$, in and out of the localization band, while $\partial_{\mathbf{q}}(\cdot)$ and $\partial_{\mathbf{p}}(\cdot)$ are the directional derivatives of $(\cdot)$, respectively in the directions of $\mathbf{q}$ and $\mathbf{p}$.

From equations (149), to occur discontinuity in the strain rate, one must have:

$$[\![\dot{u}_{i,j}]\!] n_j = \dot{\alpha} m_i \neq 0 \;\; \Rightarrow \;\; [\![\dot{u}_{i,j}]\!] = \dot{\alpha} m_i n_j \tag{150}$$

where $\dot{\alpha}$ is a scalar corresponding to the magnitude of the jump in the velocity field and m_i is a unit vector referring to the direction of this jump. It can also be noted that the angle between the vectors n_i and m_i determines the failure mode, which can vary from simple opening, when they are parallel (mode I), to pure shear, when they are perpendicular to each other (mode II). For intermediate angles, there are so-called mixed modes.

As a consequence of equation (150), the strain rate must satisfy the following compatibility equation:

$$[\![\dot{\epsilon}_{ij}]\!] = \frac{1}{2}([\![\dot{u}_{i,j}]\!] + [\![\dot{u}_{j,i}]\!]) = \frac{1}{2}(m_i n_j + m_j n_i)\dot{\alpha} \tag{151}$$

On the other hand, the equilibrium condition states that tractions, as well as their rates, must be continuous on surfaces of weak discontinuity, i.e.,

$$[\![\dot{\sigma}_{ij} n_j]\!] = [\![\dot{\sigma}_{ij}]\!] n_j = 0 \tag{152}$$

Thus, remembering that stress and strain rates are related to each other by a tangential operator – see equations (48) and (62) –, introduction of equation (151) into (152) gives

$$(n_i C^{t,\Omega_b}_{ijkl} n_l)\dot{\alpha} m_k = n_i (C^{t,\Omega\setminus\Omega_b}_{ijkl} - C^{t,\Omega_b}_{ijkl}) \dot{\epsilon}^{\Omega\setminus\Omega_b}_{kl} \tag{153}$$

where $C^{t,\Omega\setminus\Omega_b}_{ijkl}$ and $\epsilon^{\Omega\setminus\Omega_b}_{kl}$ represent, respectively, the tangent stiffness operator and strain field outside the strain localization band, while C^{t,Ω_b}_{ijkl} is the tangent operator inside it.

At this point, one can differentiate between discontinuous bifurcation, when, in fact, $C^{t,\Omega_b}_{ijkl} \neq C^{t,\Omega\setminus\Omega_b}_{ijkl}$, and continuous bifurcation, when the constitutive tangent tensors inside and outside the localization band are the same. In the latter case, equation (153) takes the form:

$$(n_i C^{t}_{ijkl} n_l) m_k = Q_{jk} m_k = 0 \tag{154}$$

where Q_{jk} is called the localization tensor or acoustic tensor. This second term is adopted for historical reasons, since in elastic problems, the eigenvalues of this tensor, divided by the specific mass of the material, are associated with the propagation speeds of waves in the solid medium [van der Giessen and de Borst, 1998].

Rice and Rudnicki [1980] showed that the continuous bifurcation condition corresponds to a limiting case of the discontinuous one, with a tendency to occur firstly during inelastic loading. Thus, equation (154) can be understood as the most unfavourable case for the occurrence of discontinuous bifurcation and can be adopted as a necessary condition for the beginning of strain localization.

It should also be noted that the trivial solution of the equation (154), $m_k = 0$, corresponds to $[\![\dot{\epsilon}_{ij}]\!] = 0$ and therefore the localization will start only when Q_{jk} is singular, i.e., the bifurcation condition becomes:

$$\det(Q_{jk}) = \det(n_i C^{t}_{ijkl} n_l) = 0 \tag{155}$$

In a general way, solution of equation (155) is associated to a optimization problem of find, between all possible directions that satisfy the singularity condition (if exists at least one), the n_i that gives the maximum softening modulus, H. However, for some cases, a closed set of equations can be analytically obtained. For example, considering an isotropic damage model with particular parameters defined in Oliver et al. [2006], detailed in Appendix A, a critical softening modulus and the associated band orientation can be obtained for plane problems, as described by Peixoto et al. [2018]. On the other hand, for associative elastoplastic models, closed solutions can be found in Oliver et al. [1999].

7 The Continuum Strong Discontinuity Approach

In the previous section, the necessary conditions for bifurcation, i.e., the appearance of discontinuities in the strain field during inelastic loading with softening, were established. It is now a subsequent step, referring to the transition between these discontinuities, called weak, and the emergence of jumps in the displacement field, known as strong discontinuities. Such a transition can be interpreted as a model with a localization band of variable thickness. When standard continuous constitutive models are employed together with these discontinuous kinematics, in order to represent dissipative effects, we have the so-called Continuum Strong Discontinuity Approach (CSDA), which is the scope of the present section.

Firstly, a kinematic formulation, valid for weak and strong discontinuities, is presented. Next, the Strong Discontinuity Analysis where, from the imposition of equilibrium conditions on the discontinuous surface, cohesive constitutive model is obtained – which relates tractions to displacement jumps – associated with the original continuous constitutive model, is addressed. As a consequence of this analysis, the necessary conditions for the establishment of the strong discontinuity are obtained, in addition to a reinterpretation of the softening modulus of the continuous constitutive model to make it compatible with the discrete model. Finally, the numerical aspects that define the variable bandwidth model are presented.

7.1 Weak and Strong Discontinuity Kinematics

Kinematic equations involving weak and strong discontinuities are presented in this section, followed by the establishment of a regularized formulation capable of treating the two cases in a single set of equations, as developed by Oliver et al. [1998, 1999].

7.1.1 Weak discontinuity kinematics

Referring to Figure 24a, a two-dimensional domain Ω is assumed, where the material points are designated by $\mathbf{x}$. We also consider a curvilinear coordinate system, $\{\chi, \upsilon, \zeta\}$, so that $\zeta = 0$ defines a surface $\mathcal{S}$, entirely contained into a localization band, Ω_b. The boundaries of this band are also formed by surfaces of a fixed coordinate ζ, i.e., $\mathcal{S}^-(\zeta = \zeta^-)$ and $\mathcal{S}^+(\zeta = \zeta^+)$, which allows to define its thickness as a function of only $(\chi, \upsilon) : h(\chi, \upsilon)$. The surface $\mathcal{S}$ divides the domain into two parts, Ω^- and Ω^+, and defines a unit vector n_i, normal to $\mathcal{S}$ and directed to Ω^+.

Being $\{\hat{\mathbf{e}}_\chi, \hat{\mathbf{e}}_\upsilon, \hat{\mathbf{e}}_\zeta\}$ the orthonormal basis associated with the curvilinear coordinates and defining by $r_\chi(\chi, \upsilon, \zeta)$, $r_\upsilon(\chi, \upsilon, \zeta)$ and $r_\zeta(\chi, \upsilon, \zeta)$ their corresponding scale factors, such that $ds_\chi = r_\chi d\chi$, $ds_\upsilon = r_\upsilon d\upsilon$ and $ds_\zeta = r_\zeta d\zeta$ are the arc lengths, respectively along χ, υ and ζ, one can write $h(\chi, \upsilon) = r_\zeta(\chi, \upsilon, 0)(\zeta^+ - \zeta^-)$. It should also be noted that, for points located on $\mathcal{S}$, the unit vector $\hat{\mathbf{e}}_\zeta$ coincides with the normal n_i.

Assuming now the following velocity field in Ω:

$$\dot{u}_i(\mathbf{x}, t) = \dot{\bar{u}}_i(\mathbf{x}, t) + \mathcal{H}_{\Omega_b}(\mathbf{x}, t)[\![\dot{u}_i]\!](\mathbf{x}, t) \tag{156}$$

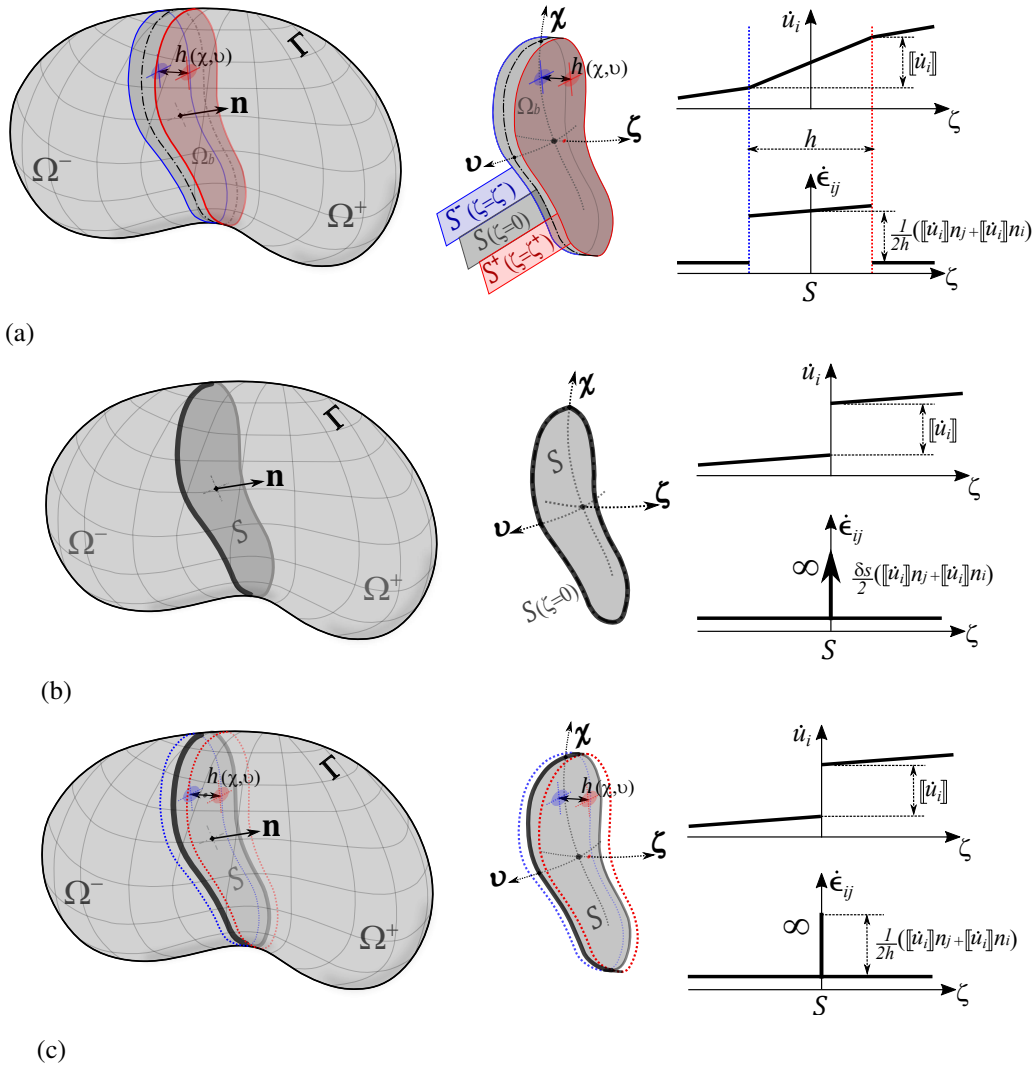

Figure 24: Kinematics with discontinuities: (a) weak discontinuity, (b) strong discontinuity, (c) regularized formulation

where t represents time, $\bar{u}(\mathbf{x},t)$ and $[\![u_i]\!](\mathbf{x},t)$ are displacement fields $\mathcal{C}^0$-continuous and $\mathcal{H}_{\Omega_b}(\mathbf{x},t) = \mathcal{H}_{\Omega_b}(\zeta,t)$ is a ramp function, given by:

$$\mathcal{H}_{\Omega_b} = \begin{cases} 0, & \text{para } \mathbf{x} \in \Omega^-\backslash\Omega_b \\ 1, & \text{para } \mathbf{x} \in \Omega^+\backslash\Omega_b \\ \dfrac{\zeta-\zeta^-}{\zeta^+-\zeta^-}, & \text{para } \mathbf{x} \in \Omega_b \end{cases} \tag{157}$$

where $a\backslash b$ means the part of a excluding b, i.e., $a\backslash b = a - (a \cap b)$.

It can be seen that $\mathcal{H}_{\Omega_b}$ represents a unit jump between the surfaces $\mathcal{S}^-$ and $\mathcal{S}^+$, since, for the same coordinate χ, $\{[\![\mathcal{H}_{\Omega_b}]\!] = \mathcal{H}_{\Omega_b}(\zeta^+,t) - \mathcal{H}_{\Omega_b}(\zeta^-,t) = 1\ \forall(\chi,\upsilon)\}$. Its gradient, in curvilinear coordinates and written in an extended form, is given by:

$$\begin{aligned} &\mathcal{H}_{\Omega_b,i} = \frac{1}{r_\zeta}\frac{\partial H_{\Omega_b}}{\partial\zeta}\hat{\mathbf{e}}_\zeta + \frac{1}{r_\chi}\frac{\partial H_{\Omega_b}}{\partial\chi}\hat{\mathbf{e}}_\chi + \frac{1}{r_\upsilon}\frac{\partial H_{\Omega_b}}{\partial\upsilon}\hat{\mathbf{e}}_\upsilon = \mu_{\Omega_b}\frac{1}{h_\zeta}\hat{\mathbf{e}}_\zeta \\ &h_\zeta(\chi,\upsilon,\zeta) = r_\zeta(\chi,\upsilon,\zeta)(\zeta^+-\zeta^-) \\ &h_\zeta(\chi,\upsilon,0) = r_\zeta(\chi,\upsilon,0)(\zeta^+-\zeta^-) = h(\chi,\upsilon) \end{aligned} \tag{158}$$

where μ_{Ω_b} is a collocation function in Ω_b, i.e., $\{\mu_{\Omega_b}(\mathbf{x}) = 1 \text{ if } \mathbf{x} \in \Omega_b \text{ and } \mu_{\Omega_b}(\mathbf{x}) = 0 \text{ if } \mathbf{x} \notin \Omega_b\}$.

Thus, taking the symmetrical part of the gradient of equation (156) and making use of equation (158), the following field of infinitesimal strain rates is obtained:

$$\dot{\epsilon}_{ij}(\mathbf{x},t) = \frac{1}{2}(\dot{\tilde{u}}_{i,j} + \dot{\tilde{u}}_{j,i}) + \frac{\mathcal{H}_{\Omega_b}}{2}([\![\dot{u}_{i,j}]\!] + [\![\dot{u}_{j,i}]\!]) + \frac{\mu_{\Omega_b}}{2h_\zeta}([\![\dot{u}_i]\!]\hat{e}_j^\zeta + [\![\dot{u}_j]\!]\hat{e}_i^\zeta) \tag{159}$$

where $\hat{e}_i^\zeta$ refer to the projections of $\hat{\mathbf{e}}_\zeta$ in the original cartesian coordinate system.

Note that the first two terms on the right hand side in equation (159) represent a continuous portion of the strain field, while the last one, as indicated in Figure 24a, has non-zero values only in the (localization) band Ω_b, characterizing strain discontinuities on the surfaces $\mathcal{S}^-$ and $\mathcal{S}^+$.

7.1.2 Strong discontinuity kinematics

Strong discontinuity kinematics can be defined as a limiting case of weak discontinuity kinematics when the strain localization band tends towards the surface $\mathcal{S}$, i.e., towards a band of zero thickness, as represented in the Figure 24b. Thus, as $\zeta^- \to 0$ and $\zeta^+ \to 0$ simultaneously, the ramp function of equation (157) collapses into the Heaviside (step) function, given by:

$$\mathcal{H}_{\mathcal{S}}(\mathbf{x}) = \begin{cases} 0, & \text{to } \mathbf{x} \in \Omega^- \\ 1, & \text{to } \mathbf{x} \in \Omega^+ \end{cases} \tag{160}$$

Thus, the displacement rate field takes the form:

$$\dot{u}_i(\mathbf{x},t) = \dot{\tilde{u}}_i(\mathbf{x},t) + \mathcal{H}_{\mathcal{S}}(\mathbf{x})[\![\dot{u}_i]\!](\mathbf{x},t) \tag{161}$$

i.e., becoming discontinuous on $\mathcal{S}$. In this case, function $[\![u_i]\!](\mathbf{x},t)$ represents the magnitude of the jump components in the displacement field over the strong discontinuity surface.

The infinitesimal strain rate field, compatible with the equation 161, is, in turn, written as:

$$\dot{\epsilon}_{ij}(\mathbf{x},t) = \frac{1}{2}(\dot{\tilde{u}}_{i,j} + \dot{\tilde{u}}_{j,i}) + \frac{\mathcal{H}_{\mathcal{S}}}{2}([\![\dot{u}_{i,j}]\!] + [\![\dot{u}_{j,i}]\!]) + \frac{\delta_{\mathcal{S}}}{2}([\![\dot{u}_i]\!]n_j + [\![\dot{u}_j]\!]n_i) \tag{162}$$

where $\delta_{\mathcal{S}}$ is the Dirac delta function over the surface $\mathcal{S}$.

It can be seen that the first two terms on the right in the equation (162) correspond to a parcel containing, at most, finite discontinuities, while the last term becomes infinite over $\mathcal{S}$.

7.1.3 Regularized kinematics

Now, a regularized formulation of kinematics with discontinuities, capable of representing both cases (weak and strong discontinuities) through a single set of equations, is presented. Such formulation will prove useful, later, in the development of a numerical model with variable localization bandwidth.

From the Figure 24c, the displacement and strain fields are written in the following forms:

$$\dot{u}_i(\mathbf{x},t) = \dot{\tilde{u}}_i(\mathbf{x},t) + \mathcal{H}_{\mathcal{S}}(\mathbf{x})[\![\dot{u}_i]\!](\mathbf{x},t) \tag{163}$$

$$\dot{\epsilon}_{ij}(\mathbf{x},t) = \underbrace{\frac{1}{2}(\dot{\tilde{u}}_{i,j} + \dot{\tilde{u}}_{j,i}) + \frac{\mathcal{H}_{\mathcal{S}}}{2}([\![\dot{u}_{i,j}]\!] + [\![\dot{u}_{j,i}]\!])}_{\dot{\tilde{\epsilon}}_{ij} \text{ (finite)}} + \underbrace{\frac{\mu_{\mathcal{S}}}{2h(\zeta)}([\![\dot{u}_i]\!]n_j + [\![\dot{u}_j]\!]n_i)}_{\text{infinity when } h(\zeta)\to 0} \tag{164}$$

where $\mu_{\mathcal{S}}$ is a collocation function over $\mathcal{S}$, i.e., $\{\mu_{\mathcal{S}}(\mathbf{x}) = 1 \text{ if } \mathbf{x} \in \mathcal{S} \text{ and } \mu_{\mathcal{S}}(\mathbf{x}) = 0 \text{ if } \mathbf{x} \notin \mathcal{S}\}$.

When the bandwidth, $h(\zeta)$, approaches zero, $\left(\frac{\mu_{\mathcal{S}}}{2h(\zeta)}\right) \rightarrow \delta_{\mathcal{S}}$, and equations (163) and (164) become equivalent to equations (161) and (162). In this way, the kinematics of strong discontinuities is completely recovered.

On the other hand, since $h(\zeta) = h_{\zeta}(\chi, \upsilon, 0)$ and n_i corresponds to $\hat{\mathbf{e}}_{\zeta}$ in $\mathcal{S}$, the strain rate of equation (164) represents its correspondent in the presence of weak discontinuities (equation 159), provided that the localization band thickness is sufficiently small. It should be noted, however, that in this case, $h(\zeta) \neq 0$, and the fields of equations (163) and (164) are not compatible, in the sense that $\dot{\epsilon}_{ij} \neq \frac{1}{2}(\dot{u}_{i,j} + \dot{u}_{j,i})$. Compatibility is achieved only when $h(\zeta) \rightarrow 0$.

As will be discussed later, a variable bandwidth model can be adopted, characterized by the evolution of the strain localization band, from a finite thickness h, defined at the bifurcation instant, t_B, to a null thickness , numerically characterized by a small constant k, representing the regime with strong discontinuity, that begins at time t_{SD}. In this way, the state of total strains for an instant of time after the start of the strong discontinuity regime, i.e., $t \geqslant t_{SD}$, can be obtained from time integration of equation (164), i.e.,

$$\begin{aligned}\epsilon_{ij}(\mathbf{x},t)|_{t\geqslant t_{SD}} &= \underbrace{\int_0^t \dot{\bar{\epsilon}}_{ij}dt + \frac{\mu_{\mathcal{S}}}{2}\int_{t_B}^{t_{SD}} \frac{1}{h}([\![\dot{u}_i]\!]n_j + [\![\dot{u}_j]\!]n_i)dt}_{\bar{\epsilon}_{ij}} + \frac{\mu_{\mathcal{S}}}{2}\int_{t_{SD}}^{t} \frac{1}{h}([\![\dot{u}_i]\!]n_j + [\![\dot{u}_j]\!]n_i)dt \\ &= \underbrace{\bar{\epsilon}_{ij}}_{\text{finite for } h\equiv k\rightarrow 0} + \underbrace{\mu_{\mathcal{S}}\frac{1}{2h}(\Delta[\![u_i]\!]n_j + \Delta[\![u_j]\!]n_i)}_{\text{infinity for } h\equiv k\rightarrow 0}\end{aligned} \tag{165}$$

where $\Delta[\![u_i]\!] = [\![u_i]\!](\mathbf{x},t) - [\![u_i]\!](\mathbf{x},t_{SD})$ is the increment in the displacement jump during the strong discontinuity regime and the material character of the discontinuous surface, i.e., $\dot{n}_i = 0$, was adopted.

7.2 The Strong Discontinuity Analysis

The objective of Strong Discontinuity Analysis (SDA) is to identify the necessary conditions for continuous constitutive models to be compatible with the kinematics represented by the equation (165). As a starting point, it should be noted that the continuity of traction (and its rate), through the interface $\mathcal{S}$, is a necessary condition for meeting the equilibrium equations, i.e.,

$$t_i(\mathbf{x},t) = \sigma_{ij}^{\Omega\backslash\mathcal{S}}(\mathbf{x},t)n_j(\mathbf{x}) = \sigma_{ij}^{\mathcal{S}}(\mathbf{x},t)n_j(\mathbf{x}) \tag{166a}$$

$$\dot{t}_i(\mathbf{x},t) = \dot{\sigma}_{ij}^{\Omega\backslash\mathcal{S}}(\mathbf{x},t)n_j(\mathbf{x}) = \dot{\sigma}_{ij}^{\mathcal{S}}(\mathbf{x},t)n_j(\mathbf{x}) \tag{166b}$$

where $\sigma_{ij}^{\mathcal{S}}$ are the stress components at a point on $\mathcal{S}$, while $\sigma_{ij}^{\Omega\backslash\mathcal{S}}$ are the stress components of an infinitesimally close point localized, however, at $\Omega\backslash\mathcal{S}$.

Thus, it is verified that, as the strains are finite in $\Omega\backslash\mathcal{S}$ (ϵ_{ij}= $\bar{\epsilon}_{ij}$), the components $\sigma_{ij}^{\Omega\backslash\mathcal{S}}$ will also be, as will t_i ($t_i = \sigma_{ij}^{\Omega\backslash\mathcal{S}}n_j$). The same arguments are valid for equation (166b). On the other hand, it should be noted that $\sigma_{ij}^{\mathcal{S}}$ and $\dot{\sigma}_{ij}^{\mathcal{S}}$ must also be finite , although $\epsilon_{ij}^{\mathcal{S}}$ and $\dot{\epsilon}_{ij}^{\mathcal{S}}$ are not, so that the physical sense of the stress field is preserved.

As previously mentioned, the SDA establishes a discrete constitutive model, which relates traction to jumps in displacements on $\mathcal{S}$, associated with the continuum one. It also leads to a reinterpretation of the original model's softening modulus, causing it to be rewritten as a function of its counterpart in the discrete model (called discrete or intrinsic softening modulus). Therefore, such an analysis must be carried out in the light of a specific continuous model. Thus, for now on, the discussion is particularized for the isotropic damage model (see Appendix A.2), with the

particular parameters defined by Oliver et al. [2006]. Such a model can be summarized by the following set of equations:

$$\text{Free energy:} \quad \psi(\epsilon_{ij}, r) = [1 - D(r)]\psi_o(\epsilon_{ij}), \quad \psi_o(\epsilon_{ij}) = \frac{1}{2}\epsilon_{ij} C_{ijkl} \epsilon_{kl} \tag{167a}$$

$$\text{Constitutive equation:} \quad \sigma_{ij} = \frac{\partial \psi(\epsilon_{ij}, r)}{\partial \epsilon_{ij}} = (1 - D) C_{ijkl} \epsilon_{kl} = C^s_{ijkl} \epsilon_{kl} \tag{167b}$$

$$\text{Damage variable:} \quad D \equiv D(r) = 1 - \frac{q(r)}{r}, \quad D \in [0, 1] \tag{167c}$$

$$\text{Internal variable evolution law:} \quad \dot{r} = \dot{\lambda}, \quad \begin{cases} r \in [r_o, \infty), \\ r_o = r|_{t=0} = \frac{f_t}{\sqrt{E}} \end{cases} \tag{167d}$$

$$\text{Damage criterion:} \quad \bar{F}(\epsilon_{ij}, r) \equiv \phi - r = \sqrt{\epsilon^+_{ij} C_{ijkl} \epsilon_{kl}} - r \tag{167e}$$

$$\text{Loading–unloading conditions:} \quad \bar{F} \leqslant 0, \quad \dot{\lambda} \geqslant 0, \quad \dot{\lambda}\bar{F} = 0, \quad \dot{\lambda}\dot{\bar{F}} = 0 \tag{167f}$$

$$\text{Softening law:} \quad \dot{q} = H(r)\dot{r}, \quad (H = q'(r) \leqslant 0), \quad \begin{cases} q \in [0, r_o], \\ q|_{t=0} = r_o \end{cases} \tag{167g}$$

In equation (167d), f_t refer to the material's tensile strength.

A detailed application of SDA to this model, which is shown by Oliver [2000], leads to the following correspondent discrete model:

$$\text{Free energy:} \quad \hat{\psi}(\Delta[\![u_i]\!], \omega) = [1 - \omega(\Delta\alpha)]\hat{\psi}_o(\Delta[\![u_i]\!]), \quad \hat{\psi}_o(\Delta[\![u_i]\!]) = \frac{1}{2}\Delta[\![u_i]\!] Q^e_{ij} \Delta[\![u_j]\!] \tag{168a}$$

$$\text{Constitutive equation:} \quad t_i = \frac{\partial \hat{\psi}(\Delta[\![u_i]\!], \omega)}{\partial(\Delta[\![u_i]\!])} = (1 - \omega) Q^e_{ij} \Delta[\![u_j]\!] = Q^s_{ij} \Delta[\![u_j]\!] \tag{168b}$$

$$\text{Damage variable:} \quad \omega \equiv \omega(\Delta\alpha) = 1 - \frac{q^*(\Delta\alpha)}{\Delta\alpha}, \quad \omega \in (-\infty, 1] \tag{168c}$$

$$\text{Internal variable evolution law:} \quad \omega \equiv \omega(\Delta\alpha) = 1 - \frac{q^*(\Delta\alpha)}{\Delta\alpha}, \quad \omega \in (-\infty, 1] \tag{168d}$$

$$\text{Damage criterion:} \quad \bar{G}(\Delta[\![u_i]\!], \Delta\alpha) \equiv \tau_{\Delta[\![u]\!]} - \Delta\alpha = \sqrt{\Delta[\![u_i]\!] Q^e_{ij} \Delta[\![u_j]\!]} - \Delta\alpha \tag{168e}$$

$$\text{Loading–unloading conditions:} \quad \bar{G} \leqslant 0, \quad \dot{\lambda}^* \geqslant 0, \quad \dot{\lambda}^*\bar{G} = 0, \quad \dot{\lambda}^*\dot{\bar{G}} = 0 \tag{168f}$$

$$\text{Softening law:} \quad \dot{q}^* = H^*\dot{\alpha}, \ (H^* = (1/h)H < 0), \quad \begin{cases} q^* \in [0, q_{SD}], \\ q^*|_{t=t_{SD}} = q_{SD} \end{cases} \tag{168g}$$

In the above equations, ω is the discrete damage variable, analogous to the continuum variable D; t_i is the traction vector over the discontinuity surface; Q^e_{ij} is the elastic localization tensor, given by $Q^e_{ij} = n_k C_{kijl} n_l$; q^* and α are the discrete internal variables, analogous respectively to q and r ($\Delta\alpha$ meaning the cumulative variation in α since the beginning of the strong discontinuity regime); and H^* is the discrete softening modulus, which value is obtained from the analysis of the power expended in the strong discontinuity regime as described later.

Particularly, deduction of equations (168b) and (168f) are detailed here, since they lead to the mentioned reinterpretation of the softening modulus, which is a key point in the compatibility between discontinuous kinematics and the continuous constitutive model.

From equations (167b), (167c) and (165), the stress tensor for a point on $\mathcal{S}$ is given by:

$$\sigma^{\mathcal{S}}_{ij} = \frac{q_{\mathcal{S}}}{r_{\mathcal{S}}} C_{ijkl} \left[\bar{\epsilon}_{kl} + \frac{1}{2h}(\Delta[\![u_k]\!] n_l + \Delta[\![u_l]\!] n_k) \right] \tag{169}$$

Assuming that this point is in the strong discontinuity regime, that is, $t > t_{SD} \Rightarrow h \equiv k \to 0$, we have from equation (166a) that

$$\begin{aligned} t_j = n_i \sigma_{ij}^{\mathcal{S}} &= \lim_{h\to 0} \left\{ \frac{q_{\mathcal{S}}}{r_{\mathcal{S}}} n_i C_{ijkl} \left[\bar{\epsilon}_{kl} + \frac{1}{2h} (\Delta[\![u_k]\!] n_l + \Delta[\![u_l]\!] n_k) \right] \right\} \\ &= \lim_{h\to 0} \left(\frac{1}{h r_{\mathcal{S}}} \right) q_{\mathcal{S}} \underbrace{(n_i C_{ijkl} n_l)}_{Q^e_{jk}} \Delta[\![u_k]\!] \\ &= \lim_{h\to 0} \left(\frac{1}{h r_{\mathcal{S}}} \right) q_{\mathcal{S}} Q^e_{jk} \Delta[\![u_k]\!] \end{aligned} \tag{170}$$

Since Q^e_{jk} is a positive definite tensor, for $\Delta[\![u_i]\!] \neq 0$, the term $q_{\mathcal{S}} Q^e_{jk} \Delta[\![u_k]\!]$ must be finite and non-zero. Thus, for the traction vector to also remain finite, as argued earlier, one must have:

$$\lim_{h\to 0} (h r_{\mathcal{S}}) \neq 0 \quad \text{if} \quad \Delta[\![u_k]\!] \neq 0 \tag{171}$$

In order for this condition to be fully satisfied, the following structure is assumed for the evolution of the internal variable of strain-type at points on the discontinuous surface:

$$\dot{r}_{\mathcal{S}} = \frac{1}{h} \dot{\alpha} \;\; \forall t \geqslant t_B; \quad \alpha|_{t=t_B} = 0 \tag{172}$$

where α is the discrete internal variable that appears in equations (168), considered finite (as well as $\dot{\alpha}$).

Equation (172) can be integrated up to an instant $t \geqslant t_{SD}$, resulting in

$$\begin{aligned} r_{\mathcal{S}} = \int_0^t \dot{r}_{\mathcal{S}} dt &= \underbrace{r_B + \int_{t_B}^{t_{SD}} \frac{1}{h(\tau)} \dot{\alpha}(\tau) d\tau}_{:= r_{SD}} + \int_{t_{SD}}^{t} \underbrace{\frac{1}{h(\tau)}}_{h \equiv k} \dot{\alpha}(\tau) d\tau \\ &= r_{SD} + \frac{1}{k} \int_{t_{SD}}^{t} \dot{\alpha}(\tau) d\tau = r_{SD} + \frac{1}{k} \Delta\alpha \end{aligned} \tag{173}$$

where $\Delta\alpha = \alpha|_t - \alpha|_{t_{SD}}$ and $r_B = r_{\mathcal{S}}|_{t=t_B}$.

Note now that the term r_{SD}, defined in the equation (173), for $t \geqslant t_{SD}$ satisfies the condition:

$$\lim_{h\to 0} (h r_{SD}) = \lim_{k\to 0} (k r_{SD}) = \lim_{k\to 0} \left[k r_B + \int_{t_B}^{t_{SD}} \frac{k}{h(\tau)} \dot{\alpha}(\tau) d\tau \right] = 0 \tag{174}$$

Thus, applying equation (173) to (171) and taking into account the result of the equation (174), we obtain:

$$\lim_{h\to 0} (h r_{\mathcal{S}}) = \lim_{h\to 0} (h r_{SD} + \Delta\alpha) = \Delta\alpha \neq 0 \tag{175}$$

which demonstrates that the evolution law proposed in equation (172) is consistent with the condition pointed out in equation (171) and makes equation (170) compatible with $\Delta[\![u_i]\!] \neq 0$.

Finally, replacing the equation (175) in equation (170), results in

$$t_i = \frac{q_{\mathcal{S}}}{\Delta\alpha} Q^e_{ij} \Delta[\![u_j]\!]; \quad \forall t \geqslant t_{SD}$$

which corresponds to equation (168b), i.e., the discrete constitutive equation, relating surface forces in $\mathcal{S}$ to increments in the jump of displacements.

Moreover, applying the equation(172) to (167g), the following expression is obtained for the evolution of stress-type internal variable, in points over $\mathcal{S}$:

$$\dot{q}_{\mathcal{S}} = H\dot{r}_{\mathcal{S}} = H\frac{1}{h}\dot{\alpha} \tag{176}$$

Since $\dot{q}_{\mathcal{S}}$ and $\dot{\alpha}$ are, by definition, finite quantities, we have that the term $\lim_{h\to 0}(H/h)$ must also assume finite values. Thus, the following relation is expected:

$$H = hH^*; \quad \forall t > t_B \tag{177}$$

where $H^* < 0$ is defined as finite and is called, as already said, as discrete or intrinsic softening modulus.

Equation (177) refers to the mentioned reinterpretation of the softening modulus of the continuous constitutive model. When $h \to 0$, the law of softening assumes the distributive character highlighted in the original work of Simo et al. [1993], since $H^* \to \delta_S H$. On the other hand, in the structure considered here, where h assumes finite values during the regime with weak discontinuities, equation (177) can be considered an appropriate extension to the variable band model.

Now, substituting the equation (177) into (176), we obtain:

$$\dot{q}_{\mathcal{S}} = H^*\dot{\alpha}$$

which corresponds to equation (168g).

7.2.1 Strong discontinuity conditions

Applying equation (165) to (167b) leads to the following result for points over $\mathcal{S}$ in the strong discontinuity regime:

$$\begin{aligned}
\sigma_{ij}^{\mathcal{S}} = \frac{q_{\mathcal{S}}}{r_{\mathcal{S}}} C_{ijkl}\epsilon_{kl}^{\mathcal{S}} &= \lim_{h\to 0}\left\{\frac{q_{\mathcal{S}}}{r_{SD} + \frac{1}{h}\Delta\alpha} C_{ijkl}\left[\bar{\epsilon}_{kl} + \frac{1}{2h}(\Delta[\![u_k]\!]n_l + \Delta[\![u_l]\!]n_k)\right]\right\} \\
&= \lim_{h\to 0}\left\{\frac{q_{\mathcal{S}}}{hr_{SD} + \Delta\alpha} C_{ijkl}\left[h\bar{\epsilon}_{kl} + \frac{1}{2}(\Delta[\![u_k]\!]n_l + \Delta[\![u_l]\!]n_k)\right]\right\} \\
&= \frac{q_{\mathcal{S}}}{\Delta\alpha} C_{ijkl}\left[\frac{1}{2}(\Delta[\![u_k]\!]n_l + \Delta[\![u_l]\!]n_k)\right]
\end{aligned} \tag{178}$$

where equations (167c) and (173) were also used. In this way, one can write:

$$\frac{1}{2}(\Delta[\![u_i]\!]n_j + \Delta[\![u_j]\!]n_i) = \frac{\Delta\alpha}{q_{\mathcal{S}}} C_{ijkl}^{-1}\sigma_{kl}^{\mathcal{S}} = \frac{\Delta\alpha}{q_{\mathcal{S}}}\epsilon_{ij}^{\mathcal{S},ef} \tag{179}$$

where $\epsilon_{ij}^{ef} := C_{ijkl}^{-1}\sigma_{kl} = (1-D)\epsilon_{ij}$ is the so-called effective strain. The finite character of $\sigma_{ij}^{\mathcal{S}}$ makes $\epsilon_{ij}^{\mathcal{S},ef}$ also to be limited.

Equation (179) is called the strong discontinuity equation and can be seen as a set of six algebraic equations (due to symmetry), relating the stress components, $\sigma_{ij}^{\mathcal{S}}$, (or of effective deformation, $\epsilon_{ij}^{\mathcal{S},ef}$) to the components of the jumps in the displacements, $\Delta[\![u_i]\!]$. Three of them are, in fact, the discrete constitutive equations (168b), which can be retrieved by pre-multiplying both sides of equation (179) by n_i. The other three, involving only stress components in $\mathcal{S}$, correspond to the so-called strong discontinuity conditions, which must be satisfied throughout $t \geqslant t_{SD}$. To obtain them in a more direct way, we rewrite the equation (179) in its matrix form, considering the orthonormal basis $\{\mathbf{n}, \mathbf{p}, \mathbf{q}\}$, with $\mathbf{p}$ and $\mathbf{q}$ tangent to $\mathcal{S}$, i.e.,

$$\begin{bmatrix} \Delta[\![u_n]\!] & \frac{1}{2}\Delta[\![u_p]\!] & \frac{1}{2}\Delta[\![u_q]\!] \\ \frac{1}{2}\Delta[\![u_p]\!] & 0 & 0 \\ \frac{1}{2}\Delta[\![u_q]\!] & 0 & 0 \end{bmatrix} = \frac{\Delta\alpha}{q^{\mathcal{S}}} \begin{bmatrix} \epsilon_{nn}^{\mathcal{S},ef} & \epsilon_{np}^{\mathcal{S},ef} & \epsilon_{nq}^{\mathcal{S},ef} \\ \epsilon_{pn}^{\mathcal{S},ef} & \epsilon_{pp}^{\mathcal{S},ef} & \epsilon_{pq}^{\mathcal{S},ef} \\ \epsilon_{qn}^{\mathcal{S},ef} & \epsilon_{qp}^{\mathcal{S},ef} & \epsilon_{qq}^{\mathcal{S},ef} \end{bmatrix} \tag{180}$$

from which it follows that, for $\mathcal{S}$ to actually correspond to a strong discontinuity line, one must have:

$$\epsilon^{ef}_{pp} = \epsilon^{ef}_{pq} = \epsilon^{ef}_{qq} = 0 \tag{181}$$

In other words, the strong discontinuity regime is immediately initiated after bifurcation only if these conditions are satisfied. As in general it is not the case, a bandwidth variable model, in which a transient step with weak discontinuities is adopted, is often necessary for the correct simulation of material failures. This model will be detailed in section 7.4. Before that, explicit expressions for the discrete softening modulus, H^*, are deduced in the next section, from the analysis of the energy consumed during the strong discontinuity regime.

7.3 Energy expended in the strong discontinuity regime

The power consumed, $\mathcal{P}$, during a quasi-static loading process in a solid domain Ω is given by:

$$\mathcal{P} = \int_\Omega \sigma_{ij}\dot{\epsilon}_{ij} d\Omega \tag{182}$$

Restricting the analysis to the period after the start of the strong discontinuity regime, i.e., $t \geqslant t_{SD}$, we can substitute equation (162) into equation (182), getting

$$\begin{aligned}\int_\Omega \sigma_{ij}\dot{\epsilon}_{ij} d\Omega &= \int_\Omega \sigma_{ij}\left[\dot{\bar{\epsilon}}_{ij} + \frac{\delta_\mathcal{S}}{2}([\![\dot{u}_i]\!]n_j + [\![\dot{u}_j]\!]n_i)\right] d\Omega \\ &= \int_{\Omega\setminus\mathcal{S}} \sigma^{\Omega\setminus\mathcal{S}}_{ij}\dot{\bar{\epsilon}}_{ij} d\Omega + \underbrace{\int_\mathcal{S} \sigma^{\mathcal{S}}_{ij}\left[\frac{1}{2}([\![\dot{u}_i]\!]n_j + [\![\dot{u}_j]\!]n_i)\right] d\mathcal{S}}_{\mathcal{P}_\mathcal{S}}\end{aligned} \tag{183}$$

where definition of $\dot{\bar{\epsilon}}_{ij}$ was given in equation (164) and $\mathcal{P}_\mathcal{S}$ is the power consumed in the development of the jump in the displacement field.

Considering equation (166a) and the symmetry of stress tensor, one can rewrite:

$$\mathcal{P}_\mathcal{S} = \int_\mathcal{S} t_i [\![\dot{u}_i]\!] d\mathcal{S} \tag{184}$$

In this way, the total energy consumed, from the beginning of the strong discontinuity regime until the total stress relief, is given by:

$$\mathcal{W}_\mathcal{S} = \int_{t_{SD}}^{t_\infty} \mathcal{P}_\mathcal{S} dt = \int_{t_{SD}}^{t_\infty}\int_\mathcal{S} t_i [\![\dot{u}_i]\!] d\mathcal{S} dt = \int_\mathcal{S}\left[\underbrace{\int_{t_{SD}}^{t_\infty} t_i [\![\dot{u}_i]\!] dt}_{G_{SD}}\right] d\mathcal{S} \tag{185}$$

where G_{SD} is the energy released in $\mathcal{S}$, per unit area, during the strong discontinuity regime. Assuming that the energy released during the transition in a weak discontinuity regime is small when compared to G_{SD}, this term can be understood as the fracture energy, G_f, usually adopted as a property of the material and whose value can be determined by standardized tests.

We now seek to rewrite the kernel of the integral in equation (184) in a more convenient form, taking into account the discrete damage model of the equations (168). Firstly, from equation (168e), we have:

$$\dot{\tau}_{\Delta[\![u]\!]} = \frac{1}{\tau_{\Delta[\![u]\!]}}(\Delta[\![u_i]\!] Q^e_{ij} [\![\dot{u}_j]\!]) \tag{186}$$

i.e.,

$$\Delta[\![u_i]\!] Q^e_{ij} [\![\dot{u}_j]\!] = \dot{\tau}_{\Delta[\![u]\!]}\tau_{\Delta[\![u]\!]} \tag{187}$$

Thus, post-multiplying $[\![\dot{u}_i]\!]$ in the constitutive equation (168b) – after applying equation (168c) – and considering the symmetry of Q^e_{ij}, in addition to the equivalence $q_{\mathcal{S}} = q^*(\Delta\alpha)$, one arrives to the following result:

$$t_i[\![\dot{u}_i]\!] = \Bigg[\underbrace{\frac{q_{\mathcal{S}}}{\Delta\alpha}\Delta[\![u_j]\!]Q^e_{ji}}_{t_i}\Bigg][\![\dot{u}_i]\!] = \frac{q_{\mathcal{S}}}{\Delta\alpha}(\dot{\tau}_{\Delta[\![u]\!]}\tau_{\Delta[\![u]\!]}) \tag{188}$$

Moreover, from equations (168e) and (168f), it is verified that dissipation occurs only if $\tau_{\Delta[\![u]\!]} = \Delta\alpha$ and $\dot{\tau}_{\Delta[\![u]\!]} = \dot{\alpha}$. Therefore, equation (188) is equivalent to

$$t_i[\![\dot{u}_i]\!] = q_{\mathcal{S}}\dot{\alpha} \tag{189}$$

Now, replacing equation (189) into the expression of G_{SD}, defined in equation (185), we obtain

$$G_{SD} = \int_{t_{SD}}^{t_\infty} q_{\mathcal{S}}\dot{\alpha}dt = \int_{t_{SD}}^{t_\infty} q_{\mathcal{S}}\frac{\dot{q}_{\mathcal{S}}}{H^*}dt = \int_{q_{SD}}^{0} q\frac{1}{H^*}dq \tag{190}$$

where the softening law discriminated in the equation (168g) was used. In the case $G_{SD} \approx G_f$, we have $q_{SD} \approx q_o = r_o = \dfrac{f_t}{\sqrt{E}}$, so that:

$$G_f = \int_{\frac{f_t}{\sqrt{E}}}^{0} q\frac{1}{H^*}dq \tag{191}$$

Finally, it is highlighted that different softening laws can be defined according to the structure of the discrete softening module. For example, linear softening is obtained from a constant H^*, while exponential softening requires an expression like $H^*(q) = A^*q$, where A^* is a constant . Thus, for each of these two cases, the solution of equation (191) results in:

i. Linear softening:

$$G_f = \frac{1}{H^*}\frac{q^2}{2}\Bigg|_{\frac{f_t}{\sqrt{E}}}^{0} = -\frac{1}{H^*}\left[\frac{f_t^2}{2E}\right] \Rightarrow H^* = -\frac{f_t^2}{2EG_f} \tag{192}$$

ii. Exponential softening:

$$G_f = \frac{1}{A^*}q\Bigg|_{\frac{f_t}{\sqrt{E}}}^{0} \Rightarrow A^* = -\frac{f_t}{G_f\ sqrtE}; \quad \therefore H^* = -\frac{f_t}{G_f\sqrt{E}}q \tag{193}$$

7.4 Variable bandwidth model

With the theoretical background presented until here, it is possible to distinguish between four steps that compose the fracture process in a solid body (in particular, the ones composed by quasi-brittle materials), as shown in Figure 25.

Each step is briefly described below:

I. **Elastic phase**: proportional stress-strain relation until the limit point $\mathbf{Y}$;

II. **Inelastic phase**: non linear behaviour with continuous strain and displacement fields. In this phase, the isotropic damage constitutive model summarized in equations (167) is directly applied and for each new strain state the bifurcation analysis, presented in section 6, is performed;

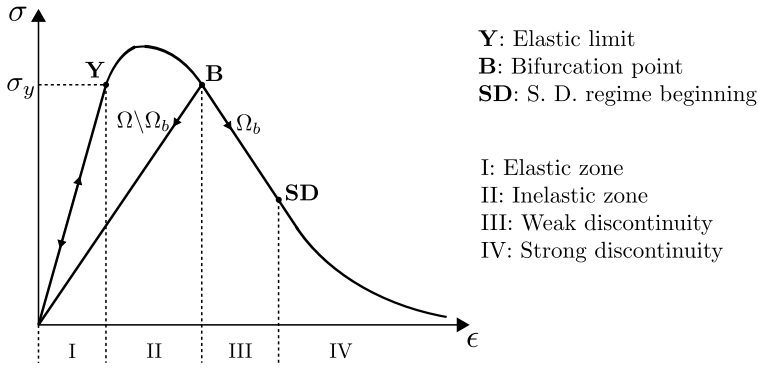

Figure 25: Fracture evolution process

III. **Weak discontinuity regime**: characterized by the presence of discontinuities in the strain field. The regularized kinematic equations presented in section 7.1.3 are adopted, with finite values for h, which can be interpreted as the localization bandwidth. As the loading process advances, its value reduces from h_B, on the bifurcation instant, $\mathbf{B}$, until a null value (numerically speaking, a small parameter, k) on the point $\mathbf{SD}$, which defines the beginning of the strong discontinuity regime;

IV. **Strong discontinuity regime**: characterized by discontinuities in the displacement field. the regularized kinematics is also used, with $h = k \approx 0$.

If on the bifurcation time (point $\mathbf{B}$) the strong discontinuity condition of equation (181) is also achieved, we have $\mathbf{B} \equiv \mathbf{SD}$ and step III above is suppressed. This is a typical case of brittle fracture.

The bandwidth evolution is governed by a pre-defined law. One can define, for example, a linear variation with the stress-like internal variable of the continuous constitutive model was considered, as illustrated in Figure 26, where $\bar{\beta}$ is an scalar value between 0 and 1.

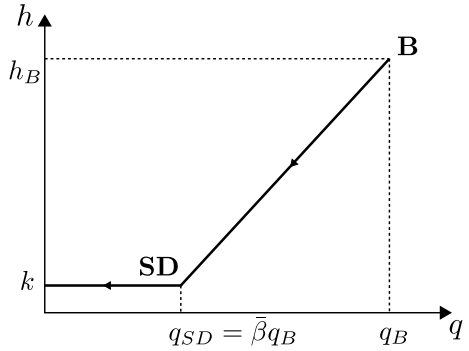

Figure 26: Bandwidth evolution law

Particularly, the initial width of the localization band, can be obtained from Eq. (177), i.e.,

$$h_B = \left| \frac{H(q_B)}{H^*(q_B)} \right| \tag{194}$$

From equations (167c), (167g) and (177), besides the specification of a bandwidth evolution law, the three steps of the inelastic loading differ basically by the expression of $q(r)$ and, consequently, of $D(r)$. Such expressions considering an exponential softening law are:

i. Continuum inelastic regime:

$$D(r) = 1 - \frac{q(r)}{r} = \begin{cases} 0 & \text{if } r \leqslant r_o \\ 1 - \dfrac{r_o}{r} e^{A(1-\frac{r}{r_o})} & \text{if } r > r_o \end{cases} \tag{195}$$

where A is a positive scalar constant. For example, the next expression presented in Oliver et al. [1990] can be adopted:

$$A = \left[\frac{G_f}{r_o^2 l^*} - \frac{1}{2} \right]^{-1} \tag{196}$$

in which l^* represents a length parameter associated to the numerical discretization size (the average of cells edges sizes in the BEM formulation used here).

ii. Weak discontinuity regime:

$$D(r) = 1 - \frac{b}{r} \left[-a + \left(\frac{b + a q_B}{q_B} \right) e^{b(r_B - r)} \right]^{-1} \quad (\text{for } r_B < r < r_{SD}) \tag{197}$$

where

$$a = -\frac{f_t R}{G_f \sqrt{E}}; \quad b = -\frac{f_t}{G_f \sqrt{E}} (k - R q_{SD}) \tag{198}$$

and r_B and r_{SD} are, respectively, the values of r on the bifurcation time and on the beginning of the strong discontinuity regime, this last one given by

$$r_{SD} = r_B - \frac{1}{b} \ln \left[\frac{q_B}{q_{SD}} \left(\frac{b + a q_{SD}}{b + a q_B} \right) \right] \tag{199}$$

iii. Strong discontinuity regime:

$$D(r) = 1 - \frac{q_{SD}}{r} e^{\frac{f_t k}{G_f \sqrt{E}} (r_{SD} - r)} \quad (\text{for} \quad r > r_{SD}) \tag{200}$$

More details about the deduction of above equations are presented in Peixoto et al. [2018].

8 Boundary integral equations with presence of discontinuities

To obtain the BIE when discontinuities – whether weak or strong – are present, the regularized kinematics presented in the section 7.1.3 can be used. However, for numerical reasons, it is important to reformulate it again, allowing the distribution of discontinuous surface effects over a finite (and arbitrary) region of the domain. Such a reformulation is presented initially. Then, starting from the differential formulation of the problem, the integral equations are obtained. Finally, the imposition of the equilibrium equation on the discontinuous interface, in its strong form, is highlighted as a necessary condition to complement the integral formulations.

8.1 Kinematic equations reformulation

Taking as a starting point Figure 24c, the reformulation of the kinematics with discontinuities starts with the definition of an arbitrary subdomain Ω_φ ($\subset \Omega$), around $\mathcal{S}$, as shown in Figure 27.

We also define a continuous function $\varphi(\mathbf{x})$, also arbitrary in Ω_φ, but satisfying the following conditions:

$$\varphi(\mathbf{x}) = \begin{cases} 0, & \text{for } \mathbf{x} \in \Omega^- \backslash \Omega_\varphi^- \\ 1, & \text{for } \mathbf{x} \in \Omega^+ \backslash \Omega_\varphi^+ \end{cases} \tag{201}$$

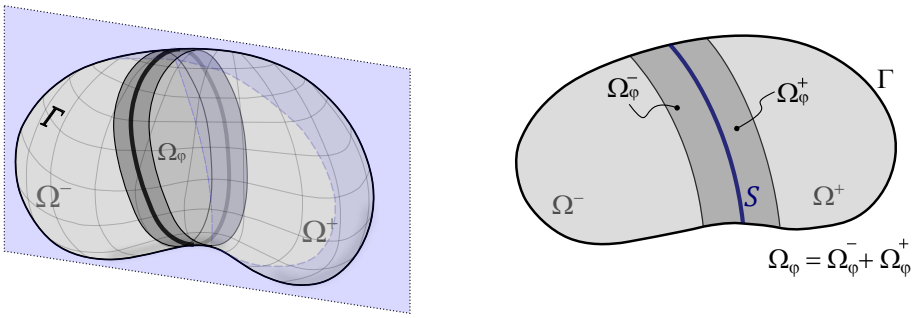

Figure 27: Arbitrary subdomain Ω_φ around the discontinuous surface.

Thus, equation (163) can be rewritten in the form:

$$\begin{aligned}\dot{u}_i(\mathbf{x},t) &= \underbrace{\dot{\bar{u}}_i(\mathbf{x},t) + \varphi(\mathbf{x})[\![\dot{u}_i]\!](\mathbf{x},t)}_{\dot{\hat{u}}_i(\mathbf{x},t)} + \underbrace{[\mathcal{H}_\mathcal{S}(\mathbf{x}) - \varphi(\mathbf{x})]}_{\mathcal{M}^\varphi_\mathcal{S}(\mathbf{x})}[\![\dot{u}_i]\!](\mathbf{x},t) \\ &= \dot{\hat{u}}_i(\mathbf{x},t) + \mathcal{M}^\varphi_\mathcal{S}(\mathbf{x})[\![\dot{u}_i]\!](\mathbf{x},t)\end{aligned} \tag{202}$$

where $\dot{\hat{u}}_i(\mathbf{x},t)$ are continuous functions and $\mathcal{M}^\varphi_\mathcal{S}(\mathbf{x})$ has null value for all $\mathbf{x}$ in Ω, except in subdomain Ω_φ. Note, therefore, that the displacement field (or velocity field) is composed of a regular portion, $\hat{u}_i(\mathbf{x},t)$, and another that contains the jump components, $\mathcal{M}^\varphi_\mathcal{S}(\mathbf{x})[\![u_i]\!](\mathbf{x},t)$, whose region of influence is Ω_φ.

It should also be noted, as described by Oliver [1996], that essential boundary conditions could not be imposed directly on the $\bar{u}_i$ or $[\![u_i]\!]$ parcels of the displacement field. However, with the reformulation defined in the equation (202), such conditions can be applied exclusively to the term $\hat{u}_i$, provided that $\Gamma_u \cap \Omega_\varphi = 0$.

Equation (164), in turn, takes the form:

$$\begin{aligned}\dot{\epsilon}_{ij}(\mathbf{x},t) &= \underbrace{\frac{1}{2}(\dot{\hat{u}}_{i,j} + \dot{\hat{u}}_{j,i})}_{\dot{\hat{\epsilon}}_{ij}} + \underbrace{\frac{\mathcal{M}^\varphi_\mathcal{S}}{2}([\![\dot{u}_{i,j}]\!] + [\![\dot{u}_{j,i}]\!]) - \frac{1}{2}(\varphi_{,i}\,[\![\dot{u}_j]\!] + \varphi_{,j}\,[\![\dot{u}_i]\!])}_{-\dot{\epsilon}^\varphi_{ij}} + \frac{\mu_\mathcal{S}}{2h}([\![\dot{u}_i]\!]n_j + [\![\dot{u}_j]\!]n_i) \\ &= \dot{\hat{\epsilon}}_{ij} - \dot{\epsilon}^\varphi_{ij} + \frac{\mu_\mathcal{S}}{2h}([\![\dot{u}_i]\!]n_j + [\![\dot{u}_j]\!]n_i)\end{aligned} \tag{203}$$

where $\hat{\epsilon}_{ij}$ is a regular portion of the strain field, ϵ^φ_{ij} has non-null values only in the subdomain Ω_φ and the last term is restricted to points on $\mathcal{S}$.

As in the case of equations (163) and (164), equations (202) and (203) are kinematically compatible only under strong discontinuity regime, i.e., when $\lim_{h\to 0}\left[\frac{\mu_\mathcal{S}(\mathbf{x})}{h}\right] = \delta_\mathcal{S}(\mathbf{x})$.

8.2 Boundary Value Problem formulations

The boundary value problem, considering the presence of a discontinuity surface $\mathcal{S}$, is fully defined through the following set of differential equations:

$$\dot{\sigma}_{ij,j} + \dot{b}_i = 0 \quad \text{in} \quad \Omega\backslash\mathcal{S} \quad \text{(internal equilibrium)} \tag{204a}$$

$$\dot{\sigma}^{+}_{ij} n_j - \dot{\sigma}^{-}_{ij} n_j = 0 \quad \text{on} \quad \mathcal{S} \quad \text{(external traction continuity)} \tag{204b}$$

$$\dot{\sigma}^{+}_{ij} n_j - \dot{\sigma}^{\mathcal{S}}_{ij} n_j = \dot{\sigma}^{-}_{ij} n_j - \dot{\sigma}^{\mathcal{S}}_{ij} n_j = 0 \quad \text{on} \quad \mathcal{S} \quad \text{(internal traction continuity)} \tag{204c}$$

$$\dot{\epsilon}_{ij} - \frac{1}{2}(\dot{u}_{i,j} + \dot{u}_{j,i}) = 0 \quad \text{in} \quad \Omega \quad \text{(kinematic compatibility)} \tag{204d}$$

$$\dot{\sigma}_{ij} = \dot{\sigma}^{\mathcal{S}}_{ij}(\dot{\epsilon}_{ij}) \quad \text{on} \quad \mathcal{S} \quad \text{(constitutive compatibility)} \tag{204e}$$

$$\dot{\sigma}_{ij} = \dot{\sigma}^{\Omega\backslash\mathcal{S}}_{ij}(\dot{\epsilon}_{ij}) = C_{ijkl}\dot{\epsilon}_{kl} \quad \text{in} \quad \Omega\backslash\mathcal{S} \quad \text{(constitutive compatibility)} \tag{204f}$$

$$\dot{\hat{u}}_i = \dot{\tilde{u}}_i \quad \text{in} \quad \Gamma_u \quad \text{(essential boundary conditions)} \tag{204g}$$

$$\dot{\sigma}_{ij} n_j = \dot{\tilde{t}}_i \quad \text{in} \quad \Gamma_\sigma \quad \text{(natural boundary conditions)} \tag{204h}$$

where $\sigma^{\mathcal{S}}_{ij}(\epsilon_{ij})$ represents an appropriate continuous constitutive relation, e.g., equations (167), and a linear elastic regime is considered for $\Omega\backslash\mathcal{S}$. Terms σ^{+}_{ij} and σ^{-}_{ij} refer, respectively, to the stress at Ω^{+} and Ω^{-}. The complementary equilibrium equations (204b) and (204c) are associated with the external and internal (to $\mathcal{S}$) traction continuity. Equation (204d) corresponds to (203).

Considering the arbitrariness of $\varphi(\mathbf{x})$ and a fixed orientation of the discontinuity surface after its establishment (material character of $\mathcal{S}$), the constitutive relations in equations (204e) and (204f), after applying equation (203), can be rewritten in the following forms:

$$\dot{\sigma}^{\mathcal{S}}_{ij}(\dot{\epsilon}_{ij}) = \dot{\sigma}^{\mathcal{S}}_{ij}(\dot{\hat{\epsilon}}_{ij}, [\![\dot{u}_i]\!], [\![\dot{u}_{i,j}]\!]) \tag{205}$$

$$\dot{\sigma}^{\Omega\backslash\mathcal{S}}_{ij}(\dot{\epsilon}_{ij}) = C_{ijkl}\dot{\epsilon}_{kl} = C_{ijkl}\left[\dot{\hat{\epsilon}}_{kl} - \dot{\epsilon}^{\varphi}_{kl}([\![\dot{u}_i]\!], [\![\dot{u}_{i,j}]\!])\right] \tag{206}$$

A first integral formulation of this problem can be obtained from the following weighted residual equation:

$$\int_{\Omega\backslash\mathcal{S}} (\dot{\sigma}^{\Omega\backslash\mathcal{S}}_{ij,j} + \dot{b}_i) u^*_i d\Omega + \int_{\mathcal{S}} n_j(\dot{\sigma}^{+}_{ij} - \dot{\sigma}^{-}_{ij}) u^*_i d\Gamma + \int_{\Gamma_\sigma} (\dot{\tilde{t}}_i - \dot{t}_i) u^*_i d\Gamma + \int_{\Gamma_u} (\dot{\hat{u}}_i - \dot{\tilde{u}}_i) t^*_i d\Gamma = 0 \tag{207}$$

where u^*_i and t^*_i represent arbitrary weighting fields.

Integrating the first term of equation (207) by parts, we obtain:

$$\int_{\Omega\backslash\mathcal{S}} \dot{\sigma}^{\Omega\backslash\mathcal{S}}_{ij,j} u^*_i d\Omega = \int_{\Gamma} \dot{t}_i u^*_i d\Gamma + \int_{\mathcal{S}} (\dot{\sigma}^{-}_{ij} - \dot{\sigma}^{+}_{ij}) n_j u^*_i d\Gamma - \int_{\Omega\backslash\mathcal{S}} \dot{\sigma}^{\Omega\backslash\mathcal{S}}_{ij} u^*_{i,j} d\Omega \tag{208}$$

and, substituting equation (208) into equation (207),

$$\int_{\Omega\backslash\mathcal{S}} \dot{\sigma}^{\Omega\backslash\mathcal{S}}_{ij} u^*_{i,j} d\Omega = \int_{\Omega\backslash\mathcal{S}} \dot{b}_i u^*_i d\Omega + \int_{\Gamma_\sigma} \dot{\tilde{t}}_i u^*_i d\Gamma + \int_{\Gamma_u} [(\dot{\hat{u}}_i - \dot{\tilde{u}}_i) t^*_i + \dot{t}_i u^*_i] d\Gamma \tag{209}$$

From equations (203) and (206) and considering the symmetries associated with the regime of small displacements in isotropic media, one can write:

$$\dot{\sigma}^{\Omega\backslash\mathcal{S}}_{ij} = C_{ijkl}\dot{\hat{u}}_{k,l} - C_{ijkl}\dot{\epsilon}^{\varphi}_{kl} \tag{210}$$

In this way, applying equation (210) to the kernel of the integral on the left side in equation (209), we obtain:

$$\int_{\Omega\backslash\mathcal{S}} \dot{\sigma}^{\Omega\backslash\mathcal{S}}_{ij} u^*_{i,j} d\Omega = \int_{\Gamma} \dot{\hat{u}}_i t^*_i d\Gamma - \int_{\Omega} \sigma^*_{ij,j} \dot{\hat{u}}_i d\Omega - \int_{\Omega} \sigma^*_{ij} \dot{\epsilon}^{\varphi}_{ij} d\Omega \tag{211}$$

and, finally, substituting equation (211) in equation (209), we arrive in the following result:

$$-\int_{\Omega}\sigma^{*}_{ij,j}\dot{\hat{u}}_i d\Omega = \int_{\Omega}\dot{b}_i u^{*}_i d\Omega + \int_{\Gamma}\dot{t}_i u^{*}_i d\Gamma - \int_{\Gamma}\dot{\hat{u}}_i t^{*}_i d\Gamma + \int_{\Omega}\sigma^{*}_{ij}\dot{\epsilon}^{\varphi}_{ij} d\Omega \tag{212}$$

The integral equations of interest are obtained next, through the particularization of the weighting fields.

8.3 Integral equations with discontinuities

If the solutions from the Kelvin's fundamental problem are adopted as the weighting fields in equation (212), similar equations as those presented in section 3 are obtained, regarding only the substitution of terms depicted in table 2.

Table 2: Terms correspondence for integral equations.

Continuum media	Presence of discontinuities
u_i	$\hat{u}_i$
ϵ_{ij}	$\hat{\epsilon}_{ij}$
ϵ^{o}_{ij}	ϵ^{φ}_{ij}

Thus, equations (67), (68) and (69) take the following forms:

$$\begin{aligned}\dot{\hat{u}}_i(\boldsymbol{\xi}) = \int_{\Gamma} u^{*}_{ij}(\boldsymbol{\xi},\mathbf{x})\dot{t}_j(\mathbf{x})\,d\Gamma - \int_{\Gamma} t^{*}_{ij}(\boldsymbol{\xi},\mathbf{x})\dot{\hat{u}}_j(\mathbf{x})\,d\Gamma + \int_{\Omega} u^{*}_{ij}(\boldsymbol{\xi},\mathbf{x})\dot{b}_j(\mathbf{x})\,d\Omega \\ + \int_{\Omega}\sigma^{*}_{ijk}(\boldsymbol{\xi},\mathbf{x})\dot{\epsilon}^{\varphi}_{jk}(\mathbf{x})\,d\Omega\end{aligned} \tag{213}$$

$$\begin{aligned}c_{ij}(\boldsymbol{\xi})\dot{\hat{u}}_j(\boldsymbol{\xi}) = \int_{\Gamma} u^{*}_{ij}(\boldsymbol{\xi},\mathbf{x})\dot{t}_j(\mathbf{x})\,d\Gamma - \int_{\Gamma} t^{*}_{ij}(\boldsymbol{\xi},\mathbf{x})\dot{\hat{u}}_j(\mathbf{x})\,d\Gamma \\ + \int_{\Omega} u^{*}_{ij}(\boldsymbol{\xi},\mathbf{x})\dot{b}_j(\mathbf{x})\,d\Omega + \int_{\Omega}\sigma^{*}_{ijk}(\boldsymbol{\xi},\mathbf{x})\dot{\epsilon}^{\varphi}_{jk}(\mathbf{x})\,d\Omega\end{aligned} \tag{214}$$

$$\begin{aligned}\dot{\hat{\epsilon}}_{ij}(\boldsymbol{\xi}) = \int_{\Gamma} u^{*}_{ijk}(\boldsymbol{\xi},\mathbf{x})\dot{t}_k(\mathbf{x})\,d\Gamma - \int_{\Gamma} t^{*}_{ijk}(\boldsymbol{\xi},\mathbf{x})\dot{\hat{u}}_k(\mathbf{x})\,d\Gamma + \int_{\Omega} u^{*}_{ijk}(\boldsymbol{\xi},\mathbf{x})\dot{b}_k(\mathbf{x})\,d\Gamma \\ + \int_{\Omega}\sigma^{*}_{ijkl}(\boldsymbol{\xi},\mathbf{x})\dot{\epsilon}^{\varphi}_{kl}(\mathbf{x})\,d\Omega + F^{\epsilon\epsilon}_{ijkl}\dot{\epsilon}^{\varphi}_{kl}(\boldsymbol{\xi})\end{aligned} \tag{215}$$

8.4 Equilibrium equation on the discontinuity surface

Differently from what happens with conventional continuous solids, the integral formulations considering the presence of discontinuities do not completely define the boundary value problem represented by the equations (204). In fact, a simple inspection of equation (207) indicates that the condition of traction external continuity – equation (204b) – is implicitly satisfied, however, the same does not occur with equation (204c). Therefore, the condition of internal continuity must be imposed separately. As in Oliver et al. [2003], this is done by taking the strong form of the equation.

Noting that equation (204c) corresponds to (166b), one can work with its corresponding instantaneous version: equation (166a). Thus, considering equations (205) and (206), we obtain:

$$f_i = \left\{C_{ijkl}\left[\hat{\epsilon}_{kl} - \epsilon^{\varphi}_{kl}([\![u_i]\!], [\![u_{i,j}]\!])\right] - \sigma^{\mathcal{S}}_{ij}(\epsilon_{ij})\right\} n_j = 0 \tag{216}$$

where ϵ_{ij} is given by the instantaneous version of equation (203) which, for points on $\mathcal{S}$, corresponds to

$$\epsilon_{ij} = \hat{\epsilon}_{ij} - \epsilon^{\varphi}_{ij} + \frac{1}{2h}([\![u_i]\!] n_j + [\![u_j]\!] n_i) \tag{217}$$

Equation (216) is called the interface equilibrium equation and, in the context of the BEM, discussed in the next section, its numerical solution is obtained by adopting cells with embedded discontinuities, providing the components of the displacement jumps, $[\![u_i]\!]$, needed to calculate ϵ^{φ}_{ij}. As will become clear, these components are assumed to be constants within a cell, resulting in null gradient tensors, i.e., $[\![u_{i,j}]\!] = 0$. Thus, for a given regular strain, $\hat{\epsilon}_{ij}$, and considering equation (217), equation (216) has as unknowns only the components $[\![u_i]\!]$, i.e., one can write $f_i \equiv f_i([\![u_i]\!]) = 0$. In this format, its solution can be obtained by Newton's method after its linearisation.

Thus, a regularized constitutive equation, relating stresses to regular strains, $\hat{\epsilon}_{ij}$, can be defined using equation (206):

$$\tilde{\sigma}_{ij}(\hat{\epsilon}_{ij}) = \sigma^{\Omega\setminus\mathcal{S}}_{ij}\left(\hat{\epsilon}_{ij} - \epsilon^{\varphi}_{ij}\big([\![u_i]\!](\hat{\epsilon}_{ij})\big)\right) = C_{ijkl}(\hat{\epsilon}_{kl} - \epsilon^{\varphi}_{kl}) \tag{218}$$

where $[\![u_i]\!](\hat{\epsilon}_{ij})$ represents the solution of equation (216).

9 A BEM Formulation for Problems with discontinuities

Discretization of the boundary equations (213) to (215), follows the same procedures already discussed in section 4. The same can be said about the solution strategy presented there. In this way, only the main special aspects, regarding the analysis involving discontinuities, are described here. Such main aspects are: cells with embedded discontinuity, displacement jump evaluation and the numerical counterpart of the regularized constitutive equation (218).

9.1 Cells with embedded discontinuity

Subdomain Ω_{φ}, illustrated in Figure 27, needs to be discretized by new concept of internal cells, called as cells with embedded discontinuity, which are now described. Furthermore, regions under inelastic behaviour, but still in the pre-bifurcation phase, must also be divided into standard cells, as illustrated in Figure 28a.

In cells with embedded discontinuity, only one collocation point is commonly adopted, so that the initial strains are considered constant in its interior. Thus, for such cells, typically represented in Figure 28b, one can write, for $\mathbf{x} \in \Omega_c$,

$$\begin{Bmatrix} \dot{\epsilon}^{\varphi}_{11}(\mathbf{x}) \\ \dot{\epsilon}^{\varphi}_{22}(\mathbf{x}) \\ \dot{\epsilon}^{\varphi}_{12}(\mathbf{x}) \end{Bmatrix} \approx \begin{Bmatrix} \dot{\epsilon}^{\varphi,c}_{11} \\ \dot{\epsilon}^{\varphi,c}_{22} \\ \dot{\epsilon}^{\varphi,c}_{12} \end{Bmatrix} = \{\dot{\epsilon}^{\varphi,c}\} \text{ (for 2D)}, \quad \begin{Bmatrix} \dot{\epsilon}^{\varphi}_{11}(\mathbf{x}) \\ \dot{\epsilon}^{\varphi}_{22}(\mathbf{x}) \\ \dot{\epsilon}^{\varphi}_{33}(\mathbf{x}) \\ \dot{\epsilon}^{\varphi}_{12}(\mathbf{x}) \\ \dot{\epsilon}^{\varphi}_{13}(\mathbf{x}) \\ \dot{\epsilon}^{\varphi}_{23}(\mathbf{x}) \end{Bmatrix} \approx \begin{Bmatrix} \dot{\epsilon}^{\varphi,c}_{11} \\ \dot{\epsilon}^{\varphi,c}_{22} \\ \dot{\epsilon}^{\varphi,c}_{33} \\ \dot{\epsilon}^{\varphi,c}_{12} \\ \dot{\epsilon}^{\varphi,c}_{13} \\ \dot{\epsilon}^{\varphi,c}_{23} \end{Bmatrix} = \left\{\dot{\epsilon}^{\varphi,c}\right\} \text{ (for 3D)}, \tag{219}$$

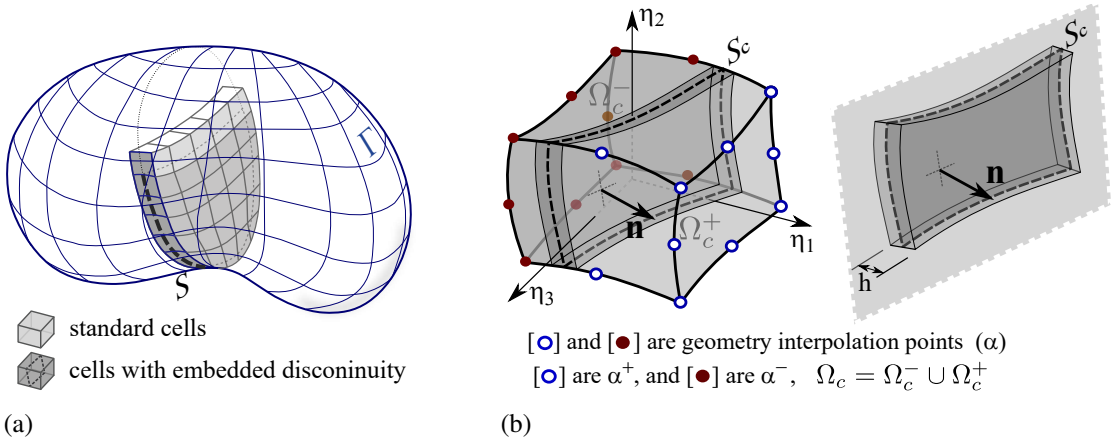

Figure 28: (a) Solid with region divided into cells, (b) Cell with embedded strong discontinuity

whereas, in the pre-bifurcation phase (in which ϵ_{ij}^{φ} is replaced by ϵ_{ij}^{o}) and in the case of plane strain state, a fourth term must be added to this vector: $\dot{\epsilon}_{33}^{o}(\mathbf{x}) = \dot{\epsilon}_{33}^{o,c}$, since the out-of-plane component σ_{i33}^{*} is not necessarily null. In the post-bifurcation steps, this fourth term is naturally null.

On the other hand, the cell geometry is parameterized through conventional linear or quadratic shape functions:

$$X_j(\eta_1,\eta_2) \approx M^{\alpha}(\eta_1,\eta_2)X_j^{\alpha} \text{ (for 2D)}, \quad X_j(\eta_1,\eta_2,\eta_3) \approx M^{\alpha}(\eta_1,\eta_2,\eta_3)X_j^{\alpha} \text{ (for 3D)}, \tag{220}$$

where the index α refers to the cell's geometry interpolation points (indicated in Figure 28b – in which quadratic shape functions are considered) and η_i are natural coordinates, such that $\eta_i \in [-1,+1]$.

The geometry interpolation functions can also be used to define the function $\varphi(\mathbf{x})$ inside a cell with embedded discontinuity, since the conditions of equation (201) are fully satisfied from the choice:

$$\varphi(\mathbf{x}(\eta_1,\eta_2)) = \sum_{\alpha^+} M^{\alpha^+}(\eta_1,\eta_2) \text{ (for 2D)}, \quad \varphi(\mathbf{x}(\eta_1,\eta_2,\eta_3)) = \sum_{\alpha^+} M^{\alpha^+}(\eta_1,\eta_2,\eta_3) \text{ (for 3D)}, \tag{221}$$

where the summation is performed over the interpolation functions associated with the cell's points located on the Ω_c^+ side of the cell. For example, in Figure 28b, the points associated to α^- or α^+ are indicated.

Within a cell with embedded discontinuity, it is further assumed that the jump components in the displacements are constant, so that, for plane problems

$$\begin{cases} [\![u_i]\!](\mathbf{x}) \approx [\![u_i^c]\!] = \begin{Bmatrix} [\![u_1^c]\!] \\ [\![u_2^c]\!] \end{Bmatrix} = \{[\![u^c]\!]\}, & \text{para } \mathbf{x} \in \Omega_c \\ [\![u_{i,j}]\!] = 0, & \text{para } \mathbf{x} \in \Omega_c \end{cases} \tag{222}$$

analogously for three-dimensional problems.

In the next subsection, the way to obtain these components is detailed, based on the numerical solution of the equation (216).

9.2 Displacement jump evaluation

The components of the displacement jump inside a cell with embedded discontinuity are obtained through the numerical solution of the interface equilibrium equation. For this, it is necessary to

determine the gradient of the regularizing function, $\varphi(\mathbf{x})$, which can be done from equation (221), i.e.,

$$\varphi_{,i} = \frac{\partial \varphi}{\partial \eta_k}\frac{\partial \eta_k}{\partial x_i} = \left(\frac{\partial M^\alpha}{\partial \eta_k}x_i^\alpha\right)^{-1}\frac{\partial \varphi}{\partial \eta_k} = \left(\frac{\partial M^\alpha}{\partial \eta_k}X_i^\alpha\right)^{-1}\left[\frac{\partial}{\partial \eta_k}\left(\sum_{\alpha^+} M^{\alpha^+}\right)\right] \tag{223}$$

Rewriting in a matrix form and applying to the collocation point:

$$\begin{aligned}\{\nabla\varphi(\boldsymbol{\xi}^c)\} &= [J(\eta_1^{\xi_c},\eta_2^{\xi_c})]^{-1}\{\nabla_\eta\varphi(\eta_1^{\xi_c},\eta_2^{\xi_c})\} \text{ (for 2D), and,}\\ \{\nabla\varphi(\boldsymbol{\xi}^c)\} &= [J(\eta_1^{\xi_c},\eta_2^{\xi_c},\eta_3^{\xi_c})]^{-1}\{\nabla_\eta\varphi(\eta_1^{\xi_c},\eta_2^{\xi_c},\eta_3^{\xi_c})\} \text{ (for 3D),}\end{aligned} \tag{224}$$

where $\eta_i^{\xi_c}$ refer to the natural coordinates of the cell's collocation point, $\{\nabla_\eta\varphi(\eta_1^{\xi_c},\eta_2^{\xi_c})\}$ (or $\{\nabla_\eta\varphi(\eta_1^{\xi_c},\eta_2^{\xi_c})\}$) correspond to the vector defined by the term in square brackets in equation (223) and matrix $[J(\eta_1^{\xi_c},\eta_2^{\xi_c},\eta_3^{\xi_c})]$ for plane problems is given by

$$[J(\eta_1,\eta_2)] = \begin{bmatrix}\dfrac{\partial M^1(\eta_1,\eta_2)}{\partial \eta_1} & \cdots & \dfrac{\partial M^{n_c}(\eta_1,\eta_2)}{\partial \eta_1}\\ \dfrac{\partial M^1(\eta_1,\eta_2)}{\partial \eta_2} & \cdots & \dfrac{\partial M^{n_c}(\eta_1,\eta_2)}{\partial \eta_2}\end{bmatrix}\begin{bmatrix}X_1^1 & X_2^1\\ \vdots & \vdots\\ X_1^{n_c} & X_2^{n_c}\end{bmatrix} \tag{225}$$

in which n_c represents the number of geometry interpolation points for the cell. Similar expression can be easily extended to three-dimensional problems.

Returning now to equation (203) and taking into account equation (222), it can be noted that, for three-dimensional problems,

$$\{\epsilon^{\varphi,c}\} = \begin{bmatrix}\varphi_{,1}(\boldsymbol{\xi}^c) & 0 & 0\\ 0 & \varphi_{,2}(\boldsymbol{\xi}^c) & 0\\ 0 & 0 & \varphi_{,3}(\boldsymbol{\xi}^c)\\ \frac{1}{2}\varphi_{,2}(\boldsymbol{\xi}^c) & \frac{1}{2}\varphi_{,1}(\boldsymbol{\xi}^c) & 0\\ \frac{1}{2}\varphi_{,3}(\boldsymbol{\xi}^c) & 0 & \frac{1}{2}\varphi_{,1}(\boldsymbol{\xi}^c)\\ 0 & \frac{1}{2}\varphi_{,3}(\boldsymbol{\xi}^c) & \frac{1}{2}\varphi_{,2}(\boldsymbol{\xi}^c)\end{bmatrix}\begin{Bmatrix}[\![u_1^c]\!]\\ [\![u_2^c]\!]\\ [\![u_3^c]\!]\end{Bmatrix} = [\nabla^s\varphi]\{[\![u^c]\!]\} \tag{226}$$

and, for two-dimensional problems,

$$\{\epsilon^{\varphi,c}\} = \begin{bmatrix}\varphi_{,1}(\boldsymbol{\xi}^c) & 0\\ 0 & \varphi_{,2}(\boldsymbol{\xi}^c)\\ \frac{1}{2}\varphi_{,2}(\boldsymbol{\xi}^c) & \frac{1}{2}\varphi_{,1}(\boldsymbol{\xi}^c)\end{bmatrix}\begin{Bmatrix}[\![u_1^c]\!]\\ [\![u_2^c]\!]\end{Bmatrix} = [\nabla^s\varphi]\{[\![u^c]\!]\} \tag{227}$$

Thus, using equations (217), (222) and (227) (or(226)), the following matrix form is obtained for equation (216):

$$\{f\} = [\bar{N}^c]^T\big([C]\{\hat{\epsilon}^c\} - [C][\nabla^s\varphi]\{[\![u^c]\!]\} - \{\sigma^{\mathcal{S}}(\{\hat{\epsilon}^c\} - [\nabla^s\varphi]\{[\![u^c]\!]\} + \frac{1}{h}[N^c]\{[\![u^c]\!]\})\}\big) = \{0\} \tag{228}$$

where $[C]$ is the elastic linear constitutive matrix, corresponding to the tensor C_{ijkl}, and

$$[\bar{N}^c] = \begin{bmatrix}n_1 & 0 & 0\\ 0 & n_2 & 0\\ 0 & 0 & n_3\\ n_2 & n_1 & 0\\ n_3 & 0 & n_1\\ 0 & n_3 & n_2\end{bmatrix};\quad [N^c] = \begin{bmatrix}n_1 & 0 & 0\\ 0 & n_2 & 0\\ 0 & 0 & n_3\\ \frac{1}{2}n_2 & \frac{1}{2}n_1 & 0\\ \frac{1}{2}n_3 & 0 & \frac{1}{2}n_1\\ 0 & \frac{1}{2}n_3 & \frac{1}{2}n_2\end{bmatrix} \tag{229}$$

for three-dimensional problems, while for two-dimensional problems

$$[\bar{N}^c] = \begin{bmatrix} n_1 & 0 \\ 0 & n_2 \\ n_2 & n_1 \end{bmatrix}; \quad [N^c] = \begin{bmatrix} n_1 & 0 \\ 0 & n_2 \\ \frac{1}{2}n_2 & \frac{1}{2}n_1 \end{bmatrix} \tag{230}$$

For a given state of regular strains, $\{\hat{\epsilon}^c\}$, equation (228) can then be solved from its linearisation, i.e.,

$$\{f\}_{j-1} + \left[\frac{\partial\{f\}}{\partial\{[\![u^c]\!]\}}\right]_{j-1} \{\delta[\![u^c]\!]\}_j \approx 0 \tag{231}$$

where j is an iterative index, $\{\delta[\![u^c]\!]\}_j = \{[\![u^c]\!]\}_j - \{[\![u^c]\!]\}_{j-1}$ and

$$\left[\frac{\partial\{f\}}{\partial\{[\![u^c]\!]\}}\right]_{j-1} = [\bar{N}^c]^T \left[-[C][\nabla^s\varphi] - \left[\frac{\partial\sigma^{\mathcal{S}}}{\partial\epsilon}\right]_{j-1} \left[\frac{1}{h}[N^c] - [\nabla^s\varphi]\right]\right] \tag{232}$$

It is emphasized here that vector $\{\sigma^{\mathcal{S}}(\cdot)\}$, present in equation (228), corresponds to the stress provided by the constitutive model adopted to represent the effects of the discontinuity. For example, such stresses can be given by equation (167b), with the damage variable being provided by one of the equations: (197) or (200), depending on the discontinuity regime (weak or strong). Term $\left[\frac{\partial\sigma^{\mathcal{S}}}{\partial\epsilon}\right]$, present in the equation (232), is the matrix form of the tangent operator defined, for example, in equation (62).

The complete algorithm to evaluate the displacement jump inside a cell is:

i. Set $j = 0$ and $\{[\![u^c]\!]\}_0$ with the final values of the last displacement jump components evaluation;

ii. $j = j + 1$;

iii. If $j >$ maximum number of iterations specified, the process is interrupted;

iv. Calculate $\{f\}_{j-1}$ and $\left[\frac{\partial\{f\}}{\partial\{[\![u^c]\!]\}}\right]_{j-1}$, respectively from equations (228) and (232);

v. Solve equation (231), $\left[\frac{\partial\{f\}}{\partial\{[\![u^c]\!]\}}\right]_{j-1} \{\delta[\![u^c]\!]\}_j = -\{f\}_{j-1}$, for $\{\delta[\![u^c]\!]\}_j$;

vi. Actualize $\{[\![u^c]\!]\}_j = \{[\![u^c]\!]\}_{j-1} + \{\delta[\![u^c]\!]\}_j$;

vii. If $\frac{\| \{\delta[\![u^c]\!]\}_j \|}{\| \{[\![u^c]\!]\}_j \|} >$ TOL, where TOL is a pre-defined scalar tolerance, return to step (ii). Else:

viii. Return with the result $\{[\![u^c]\!]\} = \{[\![u^c]\!]\}_j$.

9.3 Regularized constitutive equation

Through equation (226) or (227), one can also write the matrix form of the regularized constitutive equation (218) for a cell with discontinuity, i.e.,

$$\{\tilde{\sigma}(\hat{\epsilon}^c)\} = [C](\{\hat{\epsilon}^c\} - \{\epsilon^{\varphi,c}\}) = [C](\{\hat{\epsilon}^c\} - [\nabla^s\varphi]\{[\![u^c]\!]\}) \tag{233}$$

The stresses provided by this equation are necessary for the non linear solution strategy, for the post-bifurcation steps. In addition to them, one must define a tangent operator for the regularized constitutive equation, which can be done by taking its derivative:

$$\left[\frac{\partial\tilde{\sigma}}{\partial\hat{\epsilon}^c}\right] = [C]\left([I] - [\nabla^s\varphi]\left[\frac{\partial\{f\}}{\partial\{[\![u^c]\!]\}}\right]^{-1} [\bar{N}^c]^T \left([C] - \left[\frac{\partial\sigma^{\mathcal{S}}}{\partial\epsilon}\right]\right)\right) \tag{234}$$

9.4 Solution strategy

The algorithm for a complete analysis involving discontinuities, follows exactly the same steps as listed in section 4.2.1. The only exceptions are in steps (vii) and (xiii) for post-bifurcation phases, as described below:

vii. The tangent matrix $[\partial\sigma/\partial\epsilon]$ present in equation (135) is substituted by equation (234) during evaluation of $[D]^i_{j-1}$;

xiii. To evaluate the stress inside a cell with discontinuity, firstly the displacement jumps are calculated, as described in the algorithm at the end of section 9.2. Then, such result is applied to equation (233).

10 Examples of Non Linear Problems with discontinuities

This section presents numerical analyses of problems where occur the presence of discontinuity – like analysis of crack propagation in quasi-brittle materials – to illustrate the application of the formulation and algorithms discussed in the last sections. The first two examples are concrete fracture experiments available in the literature, that consider mixed-mode crack propagation: the first presented by Arrea and Ingraffea [1982], and the second by Gálvez et al. [1998]. They were modeled under plane stress assumption, with the CSDA. The third example consider a prismatic bar under simple tension, with a circular corner notch, where a three-dimensional model containing cells with embedded strong discontinuity was used. For all examples, the control method adopted to drive the incremental-iterative procedure in the non linear analyses, considered a convergence tolerance of 10^{-4}.

10.1 Example 1: Arrea and Ingraffea four point bending of a notched beam

The four point bending of a concrete notched beam, experimentally studied by Arrea and Ingraffea [1982], was analyzed in this example to present the capability of the formulation for the treatment of mixed-mode fracture problems. Geometry, loads, boundary conditions and material properties are presented in Figure 29, together with the approximate crack path observed in the experiments. As non linear analysis control method, the vertical displacement of the right point in the notch mouth (point A in fig. 29), was considered.

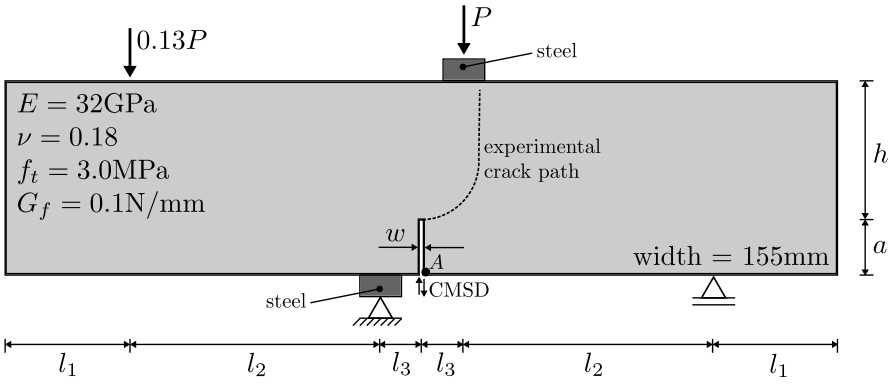

$l_1 = 203\text{mm}$, $l_2 = 397\text{mm}$, $l_3 = 61\text{mm}$, $h = 224\text{mm}$, $a = 82\text{mm}$, $w = 5\text{mm}$

Figure 29: Example 1 – Arrea and Ingraffea experiment: four point bending of a notched concrete beam.

The boundary was divided by 642 linear elements and a initial square cell with diagonal of 1.6 mm was introduced at the tip of the initial notch, such that, the origin of the discontinuity line is imposed in the midpoint of that cell edge on the notch.

Initially, this cell works in elastic regime. Once the bifurcation condition is reached, the discontinuity activation occurs, and a new cell is generated in elastic regime, and this process is repeated through the analysis. The discontinuity tracking algorithm used, starts with a cell of 0.7 mm side length, and with a growth factor of cell size $\beta = 1.001$, until a maximum crack segment size of 8 mm.

This example consider analysis with strong discontinuity regime is imposed directly after the end of the elastic regime, and also, analysis with variable bandwidth model. The final mesh achieved with the variable bandwidth model is presented in Figure 30, in which 72 new cells were generated. The final mesh for the analysis with direct strong discontinuity is quite similar. The curve of load P in function of the Crack Mouth Sliding Displacement (CMSD) of the original notch is presented in Figure 31. The numerical results are plotted over the empirical envelopment taken from the reference, showing a good accuracy.

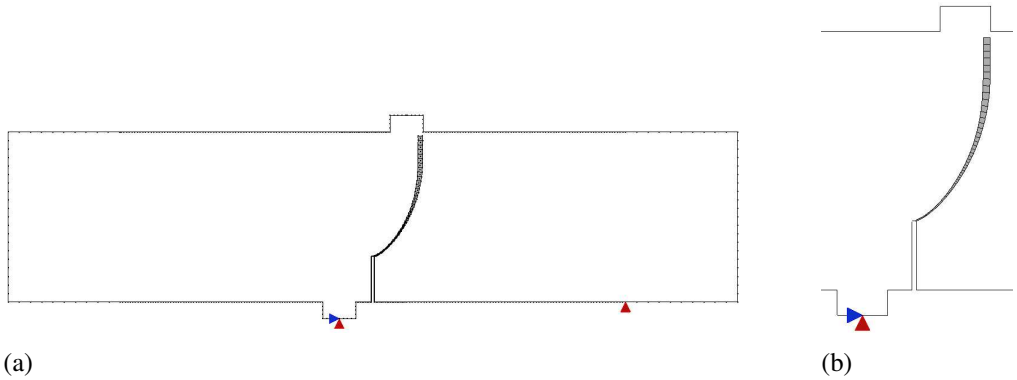

Figure 30: Example 1 - Final mesh: (a) Total mesh, (b) Detail

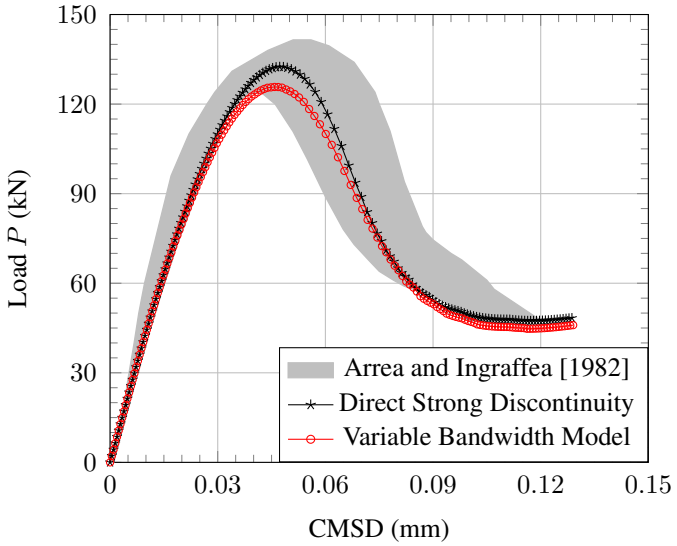

Figure 31: Example 1 - Crack mouth sliding displacement equilibrium path

10.2 Example 2: Gálvez et al. three and four point bending

Other shear tests, resulting in mixed-mode fracture patterns of a pre-notched concrete beam, reported by Gálvez et al. [1998], were also analysed with the numerical formulation with CSDA. The problem description is represented in Figure 32.

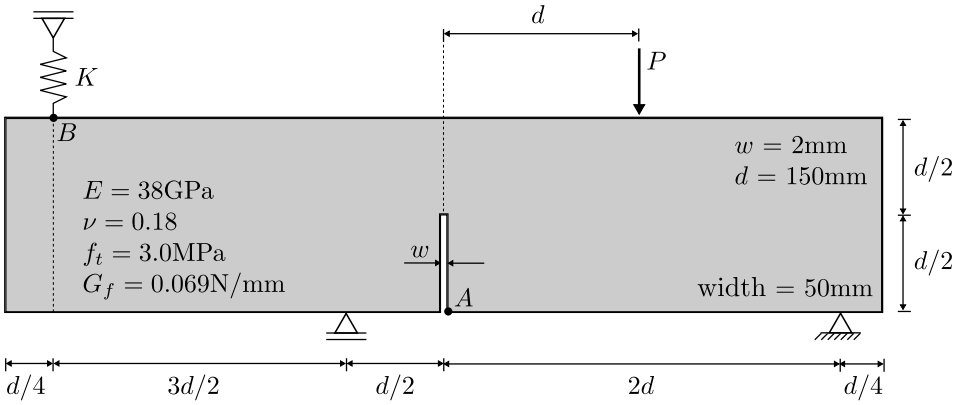

Figure 32: Example 2 – Gálvez et al. experiment data

Two cases were considered: three and four point bending. In the first one, point B in Figure 32 is free (K = 0), while in the second, the vertical displacement of such point was constrained (K = ∞). Each analysis is individually described next.

10.2.1 Three point bending

The non linear procedure was controlled by fixed increments of the vertical displacement of point B.

Problem boundary was divided by 607 linear elements and a initial square cell, with diagonal of 1.2 mm, was placed at the notch tip. The tracking algorithm was used, however with no variation of cells sizes ($\beta = 1.0$). The final mesh, where 92 new cells were generated, is shown in Figure 33.

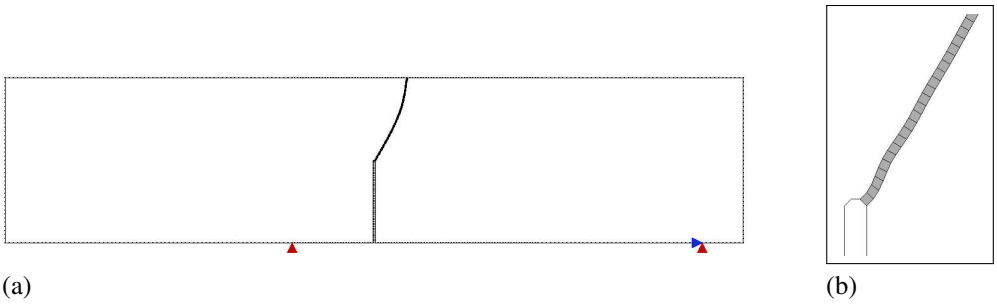

Figure 33: Example 2 - Final mesh: (a) Complete mesh, (b) Detail

Results for the external load P in function of point B vertical displacement and of the crack mouth opening displacement (CMOD) are presented in Figure 34, for the analysis with variable bandwidth model. Moreover, the numerical crack path is plotted in Figure 35. All these results are compared, in the mentioned figures, with experimental data.

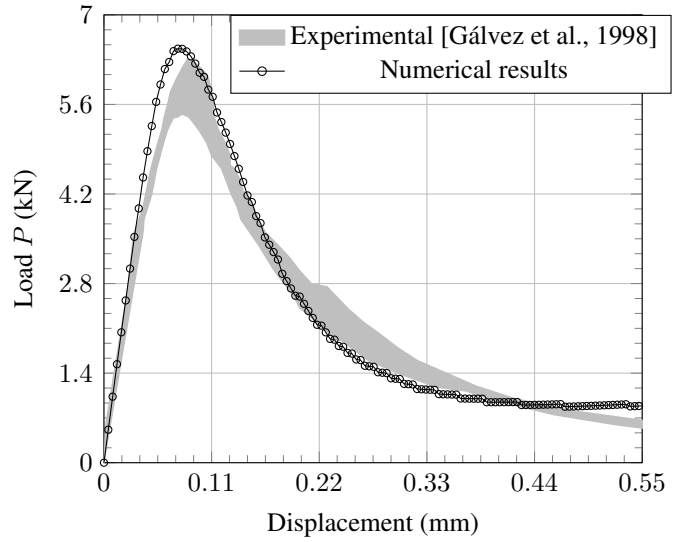

(a)

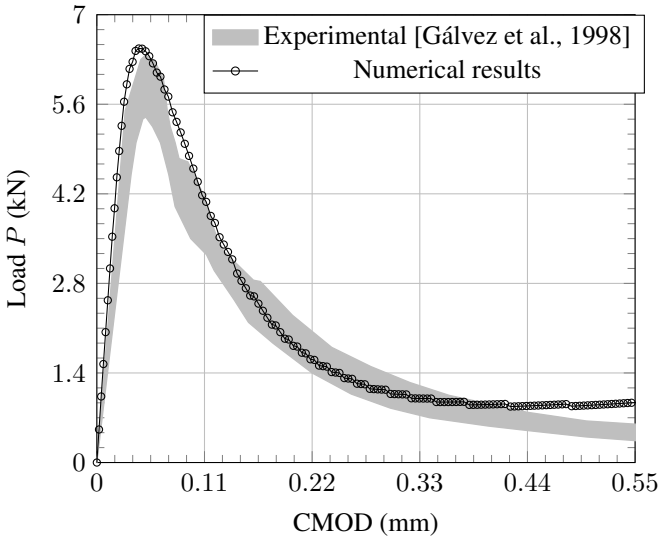

(b)

Figure 34: Example 2 - Results for three point bending: (a) Point B vertical displacement, (b) Crack mouth opening displacement

10.2.2 Four point bending

In the four point bending case of Gálvez et al. [1998] experiment, the vertical displacement component of point A (see Fig. 32) was used to control the non linear increments.

The boundary discretization was the same of the three point bending case, i.e., 607 linear elements. The initial cell was again squared, however with a diagonal of 0.6 mm. The generated cells had their sizes incremented by the adoption of $\beta = 1.001$ in the tracking algorithm. Such increment was suspended when a new discontinuity segment exceeded 0.75 mm length. The final mesh is shown in Figure 36, in which 188 additional cells were generated.

To compare the numerical and experimental results, a curve of the applied load P versus the loaded point vertical displacement is presented in Figure 37, while the crack path is plotted in Figure 38.

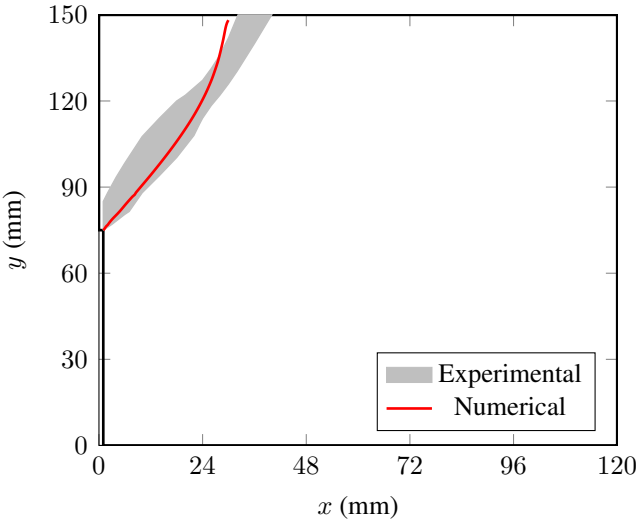

Figure 35: Example 2 - Results for three point bending crack path [Gálvez et al., 1998]

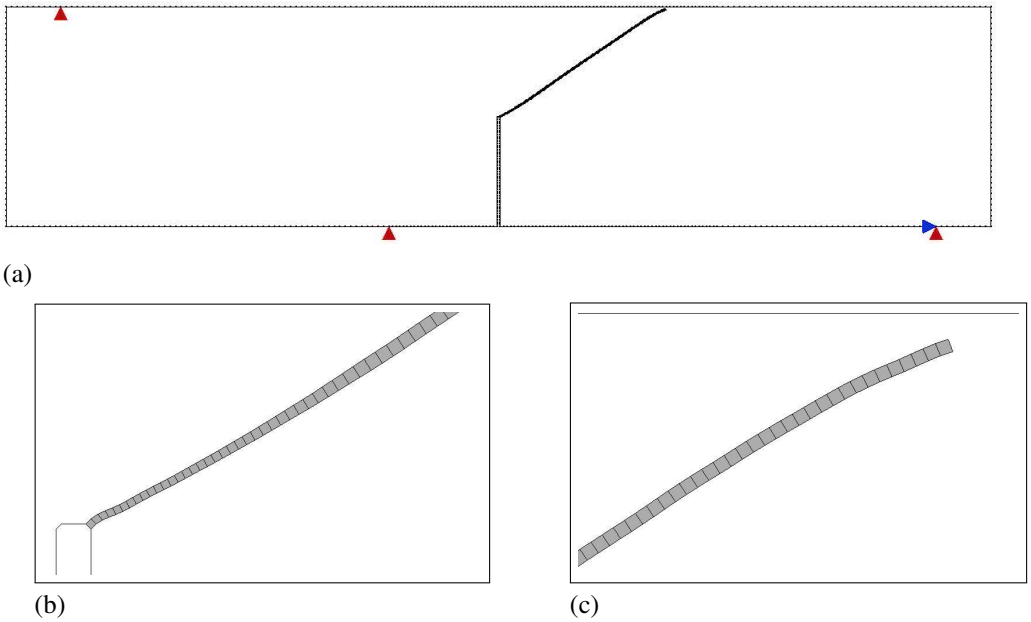

Figure 36: Example 2 - Final mesh for simulation of four point bending [Gálvez et al., 1998]: (a) Complete mesh, (b) First cell detail, (c) Final cells detail.

10.3 Example 3: Prismatic bar with a circular corner notch

A prismatic bar under simple tension, with a circular corner notch is considered in this example. Dimensions and material properties are presented in Figure 39. The failure surface is supposed to occur at the horizontal notch plane highlighted, with the discontinuity fracture surface spreading from the interior notch border. Quadrilateral boundary elements were used, and hexahedral cells with embedded uniform strong discontinuity were applied for the discretization of specific regions of the solids, where cracks were expected to propagate. Strong discontinuity regime is imposed directly after the end of the elastic regime. Direct displacement control method was adopted to

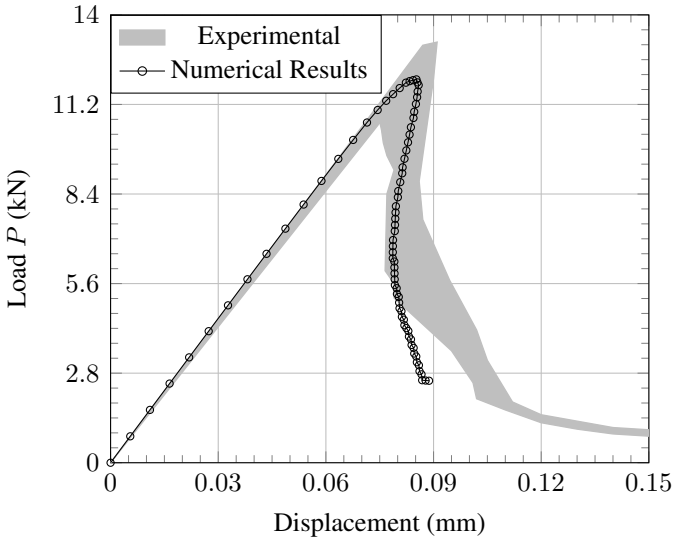

Figure 37: Exemplo 2 - Results for four point bending: Loaded point vertical displacement

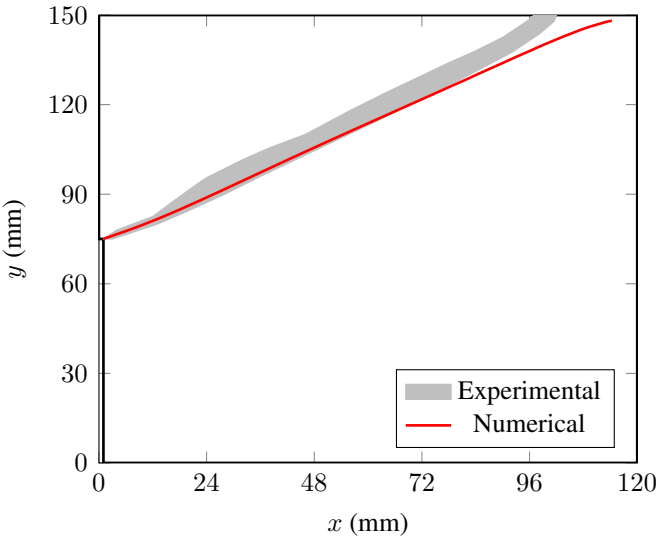

Figure 38: Exemplo 2 - Results for four point bending: Crack path

drive the incremental-iterative procedure of the non linear analyses.

Two meshes, with different refinements, were considered as shown in Figure 40. Displacement control of the corner point A (figure 39) was adopted for the non linear analysis progress. Results for the displacement equilibrium path of point A and an intermediate point B are plotted in Figure 41. The reference critical fracture stress σ_{fcrit}, shown in Figure 41, was achieved as a particular case of the stress-intensity solution for a quarter-elliptical corner crack, given by Anderson [2005].

The equilibrium path present a peak stress a little under the reference critical fracture stress. The increase in mesh refinement provides an accurate representation of the unload behaviour. Also, from the results for point B (not a control node) it is possible to note a typical snap-back of the equilibrium path. At this point neighbourhood, the discontinuity is activated only when the unload stress is around 0.136 MPa. The unloading branches of all equilibrium paths present a non

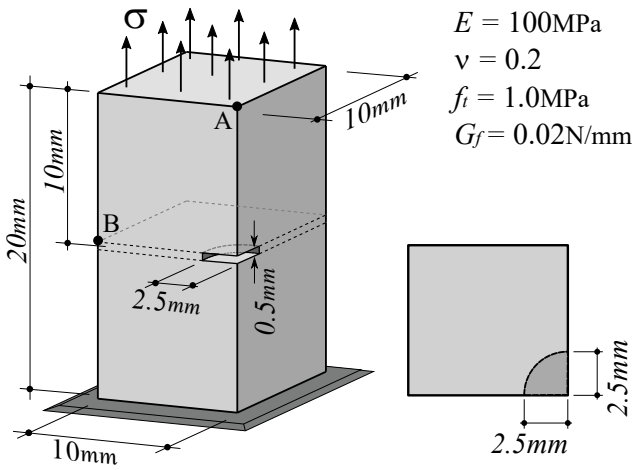

Figure 39: Example 3 - Prismatic bar under simple tension, with a circular corner notch - dimensions and material properties

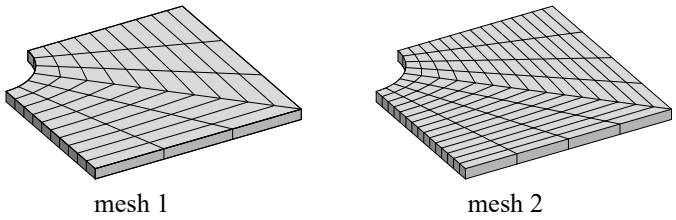

Figure 40: Example 3 - Cells distribution for mesh 1 and mesh 2

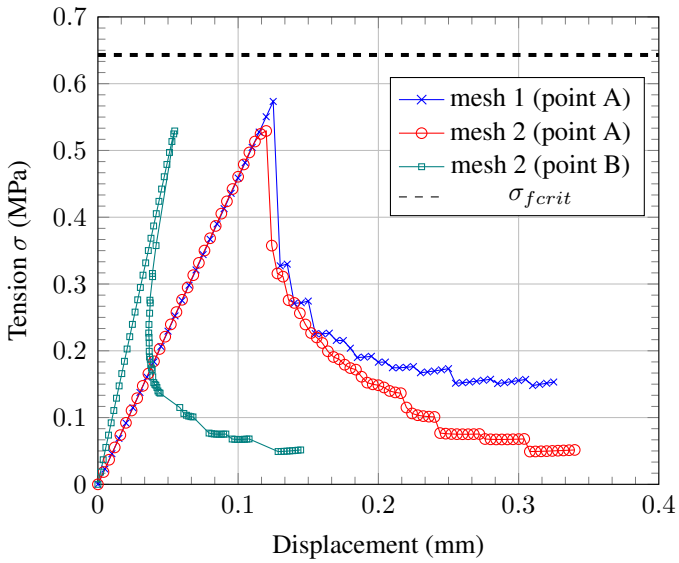

Figure 41: Example 3 - Displacement equilibrium path for control point A, for point B, and the reference critical fracture stress σ_{fcrit}.

smooth curve. This can be explained by the gradual activation of discontinuity at the cells on the fracture plane, in different load steps, schematically presented in Figure 42.

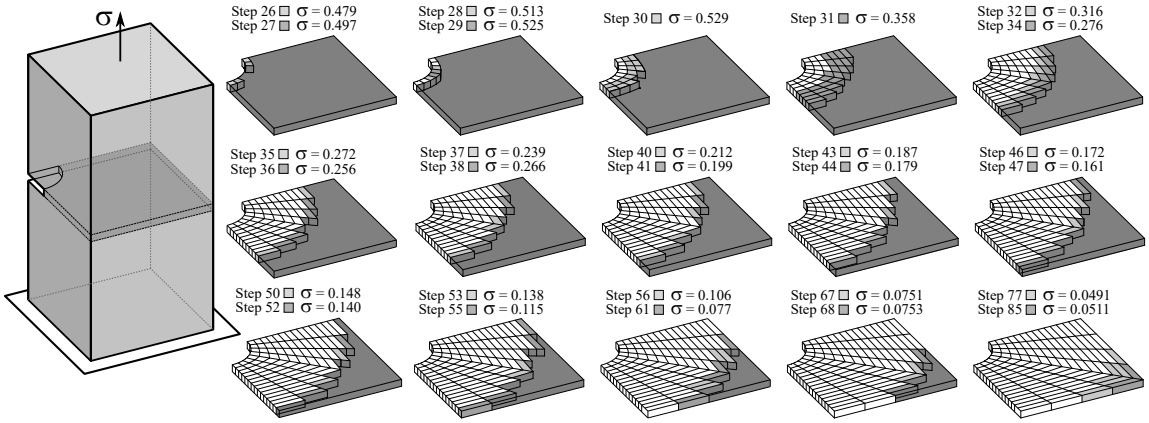

Figure 42: Example 3 - Gradual activation of discontinuity at the crack plane

11 Final Remarks

This chapter has presented the Boundary Element Method as a versatile technique for dealing with damage modeling analysis, both for continuum medium and in the presence of discontinuity.

The non linear constitutive modelling, with elastoplastic or elasto-degrading models were associated with the implicit BEM formulation for physically non linear problems. The solution strategy was detailed in a general algorithm applicable to different control methods.

For dealing with problems with discontinuity in the strain or displacement fields, the CSDA was introduced with a variable bandwidth model, together with a review in the boundary element equations. The integral equations with discontinuity and the equilibrium equation on the discontinuity surface allowed the evaluation of displacement jumps that occur in the non linear analysis. Algorithms for the evaluation of displacement jumps and strategy solution were presented.

The techniques presented in this chapter requires the discretization of the region of the domain where dissipation effects occur, using cells. Conventional cells were used for the continuum non linear analysis, while, in the possible presence of discontinuities there were needed the use of cells with embedded discontinuity, presented in a section, with its particularities.

The results for some problems presented, showed the potential of the application of BEM in the analysis of physically non linear problems, using a minimum of domain discretization.

Acknowledgements

Acknowledgements are optional, at the discretion of the chapter co-authors.

12 References

M. H. Aliabadi. *The boundary element method – Aplications in solids and structures*. John Wiley and Sons, Chichester, West Sussex, UK, 2002.

T. L. Anderson. *Fracture Mechanics – Fundamentals and applications*. Taylor & Francis Group, third edition, 2005.

M. Arrea and A. R. Ingraffea. Mixed-mode crack propagation in mortar and concrete. Technical report, 81-13, Department of Structural Engineering, Cornell University, Ithaca, USA, 1982.

J. L. Batoz and G. Dhatt. Incremental displacement algorithms for nonlinear problems. *International Journal for Numerical Methods in Engineering*, 14:1262–1267, 1979.

G. Beer, I. Smith, and C. Duenser. *The Boundary Element Method with Programming: For Engineers and Scientists*. SpringerWienNewYork, 2008.

A. Benallal, C. A. Fudoli, and W. S. Venturini. An implicit BEM formulation for gradient plasticity and localization phenomena. *International Journal for Numerical Methods in Engineering*, 53: 1853–1869, 2002.

A. S. Botta, W. S. Venturini, and A. Benallal. BEM applied to damage models emphasizing localization and associated regularization techniques. *Engineering Analysis with Boundary Elements*, 29(8):814–827, 2005.

C. A. Brebbia, J. C. F. Telles, and L. C. Wrobel. *Boundary element techniques – Theory and applications in engineering*. Springer-Verlag, Berlin, 1984.

H. D. Bui. Some remarks about the formulation of three-dimensional thermoelastoplastic problems by integral equations. *International Journal of Solids and Structures*, 14:935–939, 1978.

I. Carol, E. Rizzi, and K. Willam. A unified theory of elastic degradation and damage based on a loading surface. *International Journal of Solids and Structures*, 31(20):2835–2865, 1994.

Z. Chen and H. L. Schreyer. A numerical solution scheme for softening problems involving total strain control. *Computers & Structures*, 37(6):1043–1050, 1990.

C. Comi and U. Perego. Fracture energy based bi-dissipative damage model for concrete. *International Journal of Solids and Structures*, 38(36):6427–6454, 2001.

M. A. Crisfield. A fast incremental-iteractive solution procedure that handles snap-through. *Computers & Structures*, 13:55–62, 1981.

M. A. Crisfield. An arc length method including line searches and acelerations. *International Journal for Numerical Methods in Engineering*, 19:1269–1289, 1983.

E. A. de Souza Neto, D. Peric, and D. R. J. Owen. *Computational Methods For Plasticity: Theory and Application*. Wiley, Chichester, West Sussex, UK, 2006.

U. Eberwien, C. Duenser, and W. Moser. Efficient calculation of internal results in 2d elasticity BEM. *Engineering Analysis with Boundary Elements*, 29:447–453, 2005.

J. C. Gálvez, M. Elices, G. V. Guinea, and J. Planas. Mixed mode fracture of concrete under proportional and nonproportional loading. *International Journal of Fracture*, 94:267–284, 1998.

X.-W. Gao and T. G. Davies. An effective boundary element algorithm for 2D and 3D elastoplastic problems. *International Journal of Solids and Structures*, 37:4987–5008, 2000.

X. W. Gao and T. G. Davies. *Boundary element programming in mechanics*. Cambridge University Press, Cambridge, 2002.

R. García, J. Flórez-López, and M. Cerrolaza. A boundary element formulation for a class of non-local damage models. *International Journal of Solids and Structures*, 36(24):3617–3638, 1999.

M. Guiggiani and P. Casalini. Direct computation of Cauchy principal value integrals in advanced boundary elements. *International Journal for Numerical Methods in Engineering*, 24:1711–1720, 1987.

M. Guiggiani and A. Gigante. A general algorithm for multidimensional cauchy principal value integrals in the boundary element method. *The American Society of Mechanical Engineers*, 57: 906–915, 1990.

U. Herding and G. Kuhn. A field boundary element formulation for damage mechanics. *Engineering Analysis with Boundary Elements*, 18(2):137–147, 1996.

R. Hill. *The mathematical theory of plasticity*. Oxford University Press, 1950.

Q. Huang. Boundary element method: an introduction. Technical report, Department of Mechanical Engineering – Vanderbilt University, USA, 1993.

L. M. Kachanov. Time rupture process under creep conditions (in russian). *Izr. ARad. Nauk SSSR otd Tekh. Nauk.*, 8:26–31, 1958. Cited by Carol et al. [1994].

J. C. Lachat and J. O. Watson. Effective numerical treatment of boundary integral equations – A formulation for three dimensional elastostatics. *International Journal for Numerical Methods in Engineering*, 10:991–1005, 1976.

J. Lemaitre and J. L. Chaboche. *Mechanics of Solid Materials*. Cambridge University Press, Cambridge, UK, 1990.

F.-B. Lin, G. Yan, Z. P. Bažant, and F. Ding. Non-local strain softening model of quasi-brittle materials using boundary element method. *Engineering Analysis with Boundary Elements*, 26: 417– 424, 2002.

O. L. Manzoli and W. S. Venturini. Uma formulação do MEC para simulação numérica de descontinuidades fortes. *Revista Internacional de Métodos Numéricos para Cálculo y Diseño en Ingeniería*, 20(3):215–234, 2004.

O. L. Manzoli and W. S. Venturini. An implicit BEM formulation to model strong discontinuities. *Computational Mechanics*, 40:901–909, 2007.

O. L. Manzoli, R. A. Pedrini, and W. S. Venturini. Strong discontinuity analysis in solid mechanics using boundary element method. In E. J. Spountzakis and M. H. Aliabadi, editors, *Avances in Boundary Element Techniques X*, pages 323–329, Athens, Greece, 2009.

J. Mazars and J. Lemaitre. Application of continuous damage mechanics to strain and fracture behavior of concrete. *Application of Fracture Mechanics to Cementitious Composites. NATO Advanced Research Workshop*, 47:375–378, September 1984.

A. Mendelson. Boundary-integral methods in elasticity and plasticity. Technical report, TN-D-7418, National Aeronautics and Space Administration, NASA, USA, 1973.

S. Mukherjee. Corrected boundary-integral equations in planar thermoelastoplasticity. *International Journal of Solids and Structures*, 13:331–335, 1977.

J. Oliver. Modelling strong discontinuities in solid mechanics via strain softening constitutive equations. Part 1: Fundamentals. *International Journal for Numerical Methods in Engineering*, 39:3575–3600, 1996.

J. Oliver. On the discrete constitutive models induced by strong discontinuity kinematics and continuum constitutive equations. *International Journal of Solids and Structures*, 37:7207–7229, 2000.

J. Oliver, M. Cervera, S. Oller, and J. Lubliner. Isotropic damage models and smeared crack analysis of concrete. In *SCI-C Computer Aided Analysis and Design of Concrete Structures*, pages 945–957, 1990.

J. Oliver, M. Cervera, and O. Manzoli. On the use of strain-softening models for the simulation of strong discontinuities in solids. In R. de Borst and E. van der Giessen, editors, *Material instabilities in solids*, chapter 8, pages 107–123. John Wiley & Sons, Chichester, 1998.

J. Oliver, M. Cervera, and O. Manzoli. Strong discontinuities and continuum plasticity models: the strong discontinuity approach. *International Journal of Plasticity*, 15:319–351, 1999.

J. Oliver, A. E. Huespe, and E. Samaniego. A study on finite elements for capturing strong discontinuities. *International Journal for Numerical Methods in Engineering*, 56:2135–2161, 2003.

J. Oliver, A. E. Huespe, S. Blanco, and D. L. Linero. Stability and robustness issues in numerical modeling of material failure with the strong discontinuity approach. *Computer Methods in Applied Mechanics and Engineering*, 195:7093–7114, 2006.

R. G. Peixoto, F. E. S. Anacleto, G. O. Ribeiro, R. L. S. Pitangueira, and S. S. Penna. A solution strategy for non-linear implicit BEM formulation using a unified constitutive framework. *Engineering Analysis with Boundary Elements*, 64:295–310, 2016.

R. G. Peixoto, G. O. Ribeiro, R. L. S. Pitangueira, and S. S. Penna. The strong discontinuity approach as a limit case of strain localization in the implicit BEM formulation. *Engineering Analysis with Boundary Elements*, 80:127–141, 2017.

R. G. Peixoto, G. O. Ribeiro, and R. L. S. Pitangueira. A boundary element method formulation for quasi-brittle material fracture analysis using the continuum strong discontinuity approach. *Engineering Fracture Mechanics*, 202:47–74, 2018.

P. E. Petersson. Crack growth and development of fracture zones in plain concrete and similar materials. TVBM-1006. Technical report, Division of Building Materials, Lund Institute of Technology, Lund, Sweden, 1981.

A. Portela, M. H. Aliabadi, and D. P. Rooke. The dual boundary element method: effective implementation for cracked problems. *International Journal for Numerical Methods in Engineering*, 33:1269–1287, 1992.

S. Rajgelj, C. Amadio, and A. Nappi. Application of damage mechanics concepts to the boundary element method. In C. A. Brebbia and M. S. Ingber, editors, *Proceedings of the Seventh International Conference on Boundary Element Technology (BETECH 92)*, pages 617–634, Springer, Dordrecht., 1992.

P. C. Riccardella. An implementation of the boundary-integral technique for planar problems in elasticity and elasto-plasticity. Technical report, SM-73-10, Department of Mechanical Engineering, Carnegie Institute of Technology, Carnegie-Mellon University, Pittsburgh, USA, 1973.

J. R. Rice and J. W. Rudnicki. A note on some features of the theory of localization of deformation. *International Journal of Solids and Structures*, 16:597–605, 1980.

E. Riks. The application of Newton's method to the problem of elastic stability. *Journal of Applied Mechanics*, 39:1060–1066, 1972.

E. Riks. An incremental approach to the solution of snapping and buckling problems. *International Journal of Solids and Structures*, 15:529–551, 1979.

J. C. Simo and T. J. R. Hughes. *Computational Ineslaticity*. Springer-Verlag, Nova York, USA, 1998.

J. C. Simo and J. W. Ju. Strain- and stress-based continuum damage models - i. formulation. *International Journal of Solids and Structures*, 23(7):821–840, 1987.

J. C. Simo, J. Oliver, and F. Armero. An analysis of strong discontinuities induced by strain-softening in rate-independent inelastic solids. *Computational Mechanics*, 12:277–296, 1993.

J. Sládek, V. Sládek, and Z. P. Bažant. Non-local boundary integral formulation for softening damage. *International Journal for Numerical Methods in Engineering*, 57:103–116, 2003.

J. Swedlow and T. Cruse. Formulation of boundary integral equations for three-dimensional elasto-plastic flow. *International Journal of Solids and Structures*, 7(12):1673–1683, 1971.

J. C. F. Telles. *The boundary element method applied to inelastic problems*. Springer-Verlag, Berlin, 1983.

J. C. F. Telles and C. A. Brebbia. On the application of the boundary element method to plasticity. *Applied Mathematical Modelling*, 3:466–470, 1979.

J. C. F. Telles and J. A. M. Carrer. Implicit procedures for the solution of elastoplastic problems by the boundary element method. *Mathematical and Computer Modelling*, 15:303–311, 1991.

P. S. Theocaris and E. Marketos. Elastic-plastic analysis of perforated thin strips of a strain-hardening material. *Journal of Mechanics and Physics of Solids*, 12:377–390, 1964.

E. van der Giessen and R. de Borst. Introduction to material instabilities in solids. In R. de Borst and E. van der Giessen, editors, *Material instabilities in solids*, chapter 1. John Wiley & Sons, Chichester, 1998.

Y.-B. Yang and M.-S. Shieh. Solution method for nonlinear problems with multiple critical points. *AIAA Journal*, 28:2110–2116, 1990.

A Particular non linear constitutive models

Particular constitutive models, associated with the general equations presented in section 2.3, are presented here. As an example of the elastic-plastic class, the von Mises associative isotropic model is detailed, while for the elastic-degrading class, several isotropic damage models are presented.

A.1 Elastoplastic von Mises associative isotropic model

The elastoplastic von Mises yield criterion defines a loading function of the type

$$F(\sigma_{ij}, q) = \sqrt{3J_2(s_{ij})} + q(r) - \sigma_Y \tag{235}$$

where,

$$s_{ij} = \sigma_{ij} - \frac{1}{3}\sigma_{kk}\delta_{ij} \quad \text{and} \quad J_2(s_{ij}) = \frac{1}{2}s_{ij}s_{ij}, \tag{236}$$

σ_Y is the original material's yield stress and q is a scalar stress-like internal variable, thermodynamically conjugated to the scalar strain-like variable, r, by the hardening-softening modulus:

$$\dot{q} = -H(r)\dot{r} \tag{237}$$

Particularly, the strain-like hardening-softening internal variable is the so called equivalent plastic strain, defined by

$$r(t) = \int_0^t \parallel \dot{\epsilon}^p_{ij}(\tau) \parallel d\tau \tag{238}$$

in which the variable t is associated to time.

The first term in the right side of equation (235) is known as von Mises equivalent stress, while the second and third terms, represent the current yield limit.

Equation (237) makes the role of the hardening-softening law of equation (43), since, from equations (46-b) and (235),

$$H = -\frac{\partial q}{\partial \epsilon^p_{ij}} m_{ij} \tag{239}$$

and thus, using equation (42),

$$\dot{q} = -\dot{\lambda}h = \frac{\partial q}{\partial \epsilon^p_{ij}}\dot{\epsilon}^p_{ij} = \frac{\partial q}{\partial \epsilon^p_{ij}} m_{ij}\dot{\lambda} = -H\dot{\lambda} \quad \Rightarrow \quad h = H, \quad \dot{r} = \dot{\lambda} \tag{240}$$

Such law is a material property. For example, a linear hardening is defined by taking $H(r)$ as a constant (positive for hardening and negative for softening).

Moreover, as the model is associative,

$$m_{ij} = n_{ij} = \frac{\partial F}{\partial \sigma_{ij}} = \sqrt{\frac{3}{2}}\frac{s_{ij}}{\sqrt{s_{kl}s_{kl}}} = \sqrt{\frac{3}{2}}\frac{s_{ij}}{\parallel s_{ij} \parallel} \tag{241}$$

Now, to rewrite the loading function gradients and the hardening-softening modulus in a strain-based formulation, equations (50) may be used to give

$$\bar{m}_{ij} = -\bar{n}_{ij} = -\sqrt{6}\mu\frac{s_{ij}}{\parallel s_{ij} \parallel} \tag{242}$$

$$\bar{H} = -q'(r) + 3\mu \tag{243}$$

where, μ is the shear modulus, defined in equation (11).

Thus, applying equations (242) and (243) to equation (49), the appropriate tangential stiffness operator is directly obtained.

It is worthy to mention that the development made in this subsection is valid for three-dimensional and plane strain problems, but not for plane stress case, for which an operator is commonly applied to account for the constraint of zero out-of-plane stress (see, for example, references Simo and Hughes [1998] or de Souza Neto et al. [2006]).

A.2 Isotropic damage models

A simple isotropic damage model can be characterized by a single scalar damage variable, D, which defines the relation between initial and current secant stiffness, in the spirit of the original damage interpretation by Kachanov [1958], i.e.,

$$C^s_{ijkl} = (1 - D)C_{ijkl}, \qquad D \in [0, 1] \tag{244}$$

The loading function, in the strain space, can be written in the following generalized form

$$\bar{F}(\epsilon_{ij}, r) \equiv \bar{F}(\epsilon_{ij}, D) = \phi(\epsilon_{ij}) - r(D) \tag{245}$$

where $\phi(\epsilon_{ij})$ is called as equivalent strain and $r(D)$ is the (scalar) strain-like variable and represents the current limit value of this equivalent strain for elastic behaviour.

For the hardening-softening law, the following generic assumptions are made

$$\dot{r} = -\dot{\lambda}\bar{h}, \quad \bar{h} = -\frac{\partial r}{\partial D} \quad \Rightarrow \quad \dot{D} = \dot{\lambda} \tag{246}$$

Thus, using equations (244) and (246), equations (64-b) and (64-a) assume the respective forms

$$\bar{M}_{ijkl} = \frac{\partial C^s_{ijkl}}{\partial D} = -C_{ijkl} \tag{247}$$

$$\bar{m}_{ij} = \bar{M}_{ijkl}\epsilon_{kl} = -C_{ijkl}\epsilon_{kl} \tag{248}$$

Moreover, from equations (64-c) and (245),

$$\bar{n}_{ij} = \frac{\partial \phi}{\partial \epsilon_{ij}} \tag{249}$$

Different constitutive models can be defined here simply by changing the definition of the equivalent strain. Some examples are presented in table 3.

Table 3: Particular parameters for isotropic damage models.

Model	$\phi(\epsilon_{ij})$	$\bar{n}_{kl}$
Mazars and Lemaitre [1984]	$\sqrt{\epsilon_{ij}\epsilon_{ij}}$	$\frac{\epsilon_{kl}}{\phi(\epsilon_{ij})}$
Simo and Ju [1987]	$\sqrt{\epsilon_{ij}C_{ijkl}\epsilon_{kl}}$	$\frac{\epsilon_{ij}C_{ijkl}}{\phi(\epsilon_{ij})}$
Oliver et al. [1990]	$\sqrt{\epsilon^+_{ij}C_{ijkl}\epsilon^+_{kl}}$	$\frac{\epsilon^+_{ij}C_{ijkl}}{\phi(\epsilon_{ij})}$
Oliver et al. [2006]	$\sqrt{\epsilon^+_{ij}C_{ijkl}\epsilon_{kl}}$	$\frac{\epsilon^+_{ij}C_{ijkl}}{\phi(\epsilon_{ij})}$
Lemaitre and Chaboche [1990]	$\sqrt{\frac{1}{E}\epsilon_{ij}C_{ijkl}\epsilon_{kl}}$	$\frac{1}{E}\frac{\epsilon_{ij}C_{ijkl}}{\phi(\epsilon_{ij})}$

Particularly, for Oliver et al. [1990] constitutive model,

$$\epsilon^+_{ij} = \langle\epsilon_{ij}\rangle = \sum_{k=1}^{n_{dim}} \langle\epsilon_k\rangle \hat{p}_k \otimes \hat{p}_k \tag{250}$$

where n_{dim} is the problem's dimension, ϵ_k represents the k-th principal strain, $\hat{p}_k$ is the unit vector in the corresponding principal direction and $\langle \epsilon_k \rangle = (|\epsilon_k| + \epsilon_k)/2$.

Finally, the hardening-softening modulus is given from equation (64-d), using equations (245) and (246), i.e.,

$$\bar{H} = \frac{\partial r}{\partial D} \tag{251}$$

or, as during damage loading, $r = \phi$,

$$\bar{H}^{-1} = \left[\frac{\partial r}{\partial D} \right]^{-1} = \frac{\partial D}{\partial \phi} \tag{252}$$

and an expression for evaluation of D is usually postulated as a function of the equivalent strain.

The tangent operator is then obtained by substitution of equations (244), (248), (249) and (252) into equation (63).